ADAPTING MODULAR STRUCTURES FOR HEALTHCARE APPLICATIONS

by

Mu'taz Suleiman

A thesis

Submitted to the Faculty of Graduate Studies

in partial fulfilment of the requirements for the

Degree of Master of Science

in

Civil Engineering

Supervisor

Dr. Ahmed Elshaer, P.Eng.

Assistant Professor- Dept. of Civil Engineering

Lakehead University

Thunder Bay, ON

April 2022

Author's Declaration Page

I hereby declare that I am the sole author of this thesis. This is a true copy of the thesis, including any required final revisions, as accepted by my examiners. Chapter 3 of this thesis has been published in Sustainability-MDPI as part of the Special Issue titled "Innovation Materials and Structural Optimization for Resilient Infrastructure." Chapter 4 has been accepted as a conference paper at the Canadian Society of Civil Engineering Conference 2022 – Structural Speciality. I understand that this thesis may be made electronically available to the public.

Abstract

COVID-19 has highlighted many vital factors to consider when it comes to the healthcare systems. Some challenges such as personnel, equipment, and space demands. Personnel demand can be met by calling retired doctors and nurses and doctors from different specializations to participate in administering to COVID-19 patients. As for the equipment, more equipment can be purchased to accommodate the increasing number of patients. While for the space demand, this requires adapting innovative solutions in healthcare applications to ensure faster delivery and better infection control. Modular Construction (MC) can offer an adequate solution to this arising challenge. MC relies on using componentized, panelized, or volumetric units produced off-site and then transported to the site to form various configurations. They can utilize different materials (e.g., steel, concrete, composites) as they have significant advantages in project adaptability. Since healthcare space requires prompt delivery, modular structures can excel in this aspect since they provide a safer working environment, less material wastage, and sustainability. However, using such modular structures as isolation rooms alone is insufficient, as the ventilation system plays a crucial role in infection control. Another factor to consider when designing a layout of the modular structure is the load development on various surfaces within the layout and how this can impact the overall structural performance and cost of the project. Therefore, the objective of this thesis is to assess the ventilation system performance by altering the flow rates (i.e., air change per hour (ACH)) and the placements of the inlet and outlet of the ventilation system, using numerical modelling (e.g., computational fluid dynamics (CFD)). This is done by utilizing the Lagrangian physics model to inject aerosols in a modular room, simulate a cough, then assess how the ventilation system impacts the aerosol particles' destination. Results were validated against full-scale experimental testing and demonstrated that CFD models could accurately simulate aerosols translation within a modular room. Since low-rise modular buildings typically have an irregular layout, this will result in a complex wind load distribution on different modules depending on their location. Therefore, an assessment of an existing low-rise modular field-hospital layout has been examined in CFD to evaluate wind load developed on modules in different locations (i.e., corner, edge, and internal) to determine the critical locations where load intensities are high. The results have been validated with experimental wind tunnel tests available in the literature. The results of this thesis showed that, as the ACH rate increases, the aerosols removal rate also increases, given a direct flow field is established between the inlet and the outlet. In addition, inlet and outlet

placement is essential, as it dictates the aerosol removal performance from the room. Therefore, considering a shorter path for aerosols to travel helps reduce contaminants within the room. As for the wind load evaluation, the thesis discusses that the module's location within the layout significantly impacts the loads that the module experiences. Corner modules tend to experience the most critical forces, since they have more prominent exposure to wind pressures. In addition, this highlights the need to perform wind load evaluation when adopting a large number of modules in the project, since categorization can effectively reduce the project’s cost.

Acknowledgments

As modest as this work is, I express my deepest gratitude to Allah (the almighty) for the countless blessings he bestowed upon me. I pray that he accepts me to serve him and be a faithful follower of Prophet Mohammed who always encouraged us to strive for knowledge.

I am grateful to my supervisor, Dr. Ahmed Elshaer, who expressed confidence in me and paved the path of knowledge and made it attainable. He was the main reason I have continued my graduate education, as his ways of teaching are enchanting. I wish to reach his level of scientific knowledge and success, as he always demonstrated his care and interest in new projects and challenges. As the proverb goes “He who taught me a letter, owns me” and I am sincerely thankful for all his support throughout my journey.

I would like to express my gratitude to my parents, my father, Ahmad, and my mother, Azizeh, for their continuous prayers and support. I would also like to thank my brothers, Munther and Motasem, and my sister, Farah, for believing in me. This wouldn’t have been done without their persistence and courage.

I would like to also thank BOLT Tridel for their continuous financial support throughout my post-secondary education journey, which enabled me to focus on my studies and achieve my goals.

Table of Contents

List of Tables

List of Equations

List of Figures

List of Symbols

ρ	Density
U	Three velocity components (u, v, w)
T	Temperature
Y_i	Species fraction
J_i	Diffusion flux
μ	Viscosity
k	Turbulence kinematic energy
ε	Turbulence dissipation
p	Pressure
∇	Divergence
τ	Deviatoric stress tensor
m_p	Particle's mass
v_p	Instantaneous particle velocity
F_s	Resultant of the forces that act on the surface
F_b	Resultant of the forces that act on the body
F_d	Drag force
F_p	Pressure gradient force
F_{vm}	Virtual mass force
F_g	Gravity force
F_u	User-defined body force
F_c	Contac force
F_{Co}	Coulomb force
C_d	Drag coefficient of the particle

v_s	Particle slip velocity which is $v_s = v - v_p$, where v is the instantaneous velocity of the continuous phase
A_p	The projected area of the particle
Re_p	Particle Reynolds number
D_p	Particle diameter
V_p	Volume of particle
∇p_{static}	The gradient of the static pressure
g	Gravitational acceleration vector
$r_p(t)$	Instantaneous position vector

Chapter 1 Introduction

1.1 Background

Recently, an identified corona virus (COVID-19) has caused a global pandemic. This family of viruses is considered highly contagious and leads to respiratory illnesses (WHO, 2020). As of March 2022, the total number of COVID-19 cases in Canada has exceeded 3 million patients, and 1.1 million are in Ontario (Government of Canada, 2022). The vigorous spread of this virus has led to increased infections within close contact since viruses and pathogens are carried by airborne particles generated from sneezing or coughing (WHO, 2020). With the increasing number of cases, healthcare systems have been suffering from the growing demand for intensive care units (ICUs). They have been facing many challenges, such as a shortage of doctors and nurses to oversee COVID-19 patients, a limited supply of medical care equipment, and the space required to provide the care needed for patients. The latter is where modular structures can offer an adequate solution. Modular structures have been attracting significant attention from the construction industry. They provide many advantages over conventional structures due to their more accessible transportation, safer construction process, and less material wastage. The modular construction (MC) technique refers to prefabricated structural components produced off-site and then transported and assembled on-site to form various types of structures (Smith et al., 2010). MC provides improved efficiency in the construction process and ensures the quality of structures since the production takes place within a controlled environment. Different materials (i.e., steel, concrete, timber, and composite) can be utilized to form different structures (i.e., low-rise, high-rise, and bridges), proving their adaptability to projects' scopes and objectives. When it comes to modular structures, three different types can be utilized depending on the project, which are componentized, panelized, and volumetric modules (Smith et al., 2010). This thesis focuses on the space problem, as it tackles this problem from two aspects. First, an assessment of the ventilation system, which is done by injecting aerosols into the room and by altering different factors (i.e., ACH rate and ventilation system placement), the aerosols' destination is impacted. This provides an understanding of how each factor impacts the outcome. Second, the structural planning aspects of the modular buildings, through simulating wind to obtain loads developed on modules within a layout. This enables the understanding of how the location of modules impacts the wind loads they experience and provide a recommendation on the different aspects

to consider when adopting a modular building, based on the critical forces developed on their surfaces and their locations within the layout.

1.2 Research Objectives

Due to the increasing demand for ICU beds, studying modular structures to provide an appropriate solution to this problem is crucial. As previous studies have demonstrated the different aspects of modular structures and their applications, the need to assess them for the medical use case is limited, as it is vital to quantitively describe various factors impacting the design of modular structures, from the structural aspect and the interior ventilation system performance, since they will be used in a sensitive environment. While the ventilation assessment is an important aspect of the design of the modular structures, the need to assess for structural is also important since the modular building layout for healthcare applications focuses on increasing the perimeter area, thus creating an irregular layout, and since wind loads are dynamic and depend on the structural layout, it is important to be able to perform the assessments. This is achieved through the pursuit of the following objectives:

1. Investigate different factors when planning and designing modular buildings to serve as field hospitals.
2. Assess the main factors impacting the ventilation system performance.
3. Examining a modular building layout adopted in a previous case study and performing wind load evaluation using CFD under different wind angles of attack.
4. Obtaining force-time history plots, identifying critical forces developed on modules, correlating them to the location tested.

1.3 Organization of Thesis

This thesis aims to investigate different factors when planning and designing modular buildings constructed to serve as field hospitals. The planning for the placements of the ventilations system and the adopted ACH rate are altered to understand the impact of these factors. As for the forces developed on surfaces, they provide the designers with an understanding of how the location of modules impacts the intensity of the developed forces. Accordingly, **Chapter 1** (this chapter) provides a general introduction to healthcare system challenges and a brief description of the modular structures. **Chapter 2** presents a literature review that overviews previous experimental and analytical works on modelling multiphase flow. In addition, different advancements in the

structural aspects of modular buildings involve optimization and utilization of new emerging materials and methods. **Chapter 3** investigates the propagation of mouth-generated aerosols within a modular hospital room. This is done by studying different parameters such as the ACH rate and the ventilation system placements. Detailed CFD models were developed to perform the assessment. The models were validated with a full-scale experimental study presented in the literature to assess the accuracy of the numerical methods adopted. The study highlights key factors impacting the translation of particles within a modular hospital room, leading to better infection control within the modular unit. **Chapter 4** studies the layout of a modular building adopted in the literature to evaluate the wind loads developed on various selected modules. The modules were selected based on their location in the layout (e.g., corner, edge, and internal). The numerical models were validated with wind tunnel experimental results available in the literature. The study adapted the physics models utilized in the validation to assess the layout performance. The results highlight the importance of the location within the layout on the wind load development on the various modules, demonstrating that different locations within the layout will experience different wind loads highlighting critical locations. Therefore, module categorization based on loads can be utilized in the project's planning stages, which can be more efficient for large projects. **Chapter 5** concludes the thesis by summarizing the conclusions and recommendations for future studies involving modular structural applications.

Chapter 2 Literature Review

2.1 Introduction

Modular construction (MC) is considered one of the innovative techniques adopted in the construction industry. It provides faster delivery, more reliable structures, and a safer construction process compared to conventional methods (Smith et al., 2010). Modular buildings consist of various components, panels, and volumetric units formed to produce a structure. This highlights their adaptability to the project since they can be used for different applications (e.g., residential, commercial, and medical) (Smith et al., 2010). Thus, it is suitable to utilize such a technique to provide the healthcare system with the required space to serve COVID-19 patients in a timely manner. Chapter 2 (this chapter) provides a literature review of various studies concerned with ventilation systems, aerosols modelling, wind load evaluation, and recent advancements in volumetric modular structures.

2.2 Ventilation Systems and Aerosols Modelling

This section provides an overview of the available and emerging studies about ventilation systems and aerosols modelling. First, an overview of the ventilation system is presented and discussed, outlining the main parameters controlling the performance of the ventilation system. This is followed by an overview of studies available on aerosols modelling and critical factors impacting their dispersion.

2.2.1 Ventilation System and Space Overview

Understanding the implementation of appropriate ventilation systems is essential to controlling the spread of aerosols. There have been many studies investigating the ventilation systems requirement and guidelines. For example, (Curry, 1990) reviewed the use of isolation rooms, highlighting the guidelines, regulations, and designs adopted to ensure proper operation. The study highlights measures to reduce the risk of infectious diseases and provides comprehensive details about the engineering controls that can take place to control the spread. While there are many engineering controls to provide an appropriate design, another aspect plays a more significant role, which is the administrative controls (or work practice), since the design can be well handled. Still, the mechanical elements of the isolation rooms will deteriorate over time, deeming them ineffective. For example, the filtration system can clog with dust and lint, causing the ventilation system to become weak against infection control. Therefore, periodic testing and assessment are

required to ensure effective operations. Since the transmission of the disease is mainly taking place through coughing or sneezing, particles carrying the disease need to be controlled. The ventilation system takes effect since it works on the dilution and removal of those particles by supplying the room with fresh air, which decreases the likelihood of transmission. The ventilation system alone is not sufficient to guarantee infection control. Therefore, respiratory protection is required even in state-of-the-art isolation rooms. The intensity of ventilation is referred to as the ACH rate, which can be used to estimate the time needed to remove infectious particles, as well as the volume of air being exchanged. As for air mixing, the better the mixing, the more effective the dilution and the more efficient particles removal are for air mixing. Stagnation and short-circuiting are to be avoided when designing the ventilation system. Stagnation occurs when part of the room is not receiving a clean supply of air, thus leaving the infectious particles in that spot without experiencing dilution. As for short-circuiting, it refers to when the ventilation system inlet and outlet are placed too close to each other, thus leading the clean supply air to leave the isolation room without dilution or mixing with the contaminants. As for the flow direction, clean supply air should be placed near staff (i.e., entrance) and directed towards the outlet with an uninterrupted flow field near the patient to reduce transmission and ensure the containment of the contaminants within the isolation room. In addition, (Hyttinen et al., 2011) reviewed the experimental studies adopted in studying airborne infection isolation rooms. The review found that the guidelines for the design of ventilation systems are highly variable in different countries. In addition, the focus of the recent studies has been the use of mixing-type ventilations through the control of ACH rates. As for emerging studies, the use of auxiliary devices, such as room-air cleaners and ultraviolet germicidal irradiation systems, has been examined and proved to enhance control efficiency. The use of a temporary negative pressure isolation system demonstrated suitable containment of contaminants, given that an appropriate flow pattern is created. Thus, the design of the room to reduce leakage is an effective method when considering the design for isolation purposes, to reduce energy consumption and increase the dilution process. Furthermore, (Beggs et al., 2008) carried out an extensive review and analysis of guidelines in the United Kingdom and the United States governing the design of ventilation systems for hospital wards and multi-bed rooms. CFD was utilized to evaluate the effectiveness of various ventilation strategies in removing airborne pathogens from ward spaces. A room with various locations of ventilation grilles is shown in Figure 2.1. Diffuser A is located near the lower part of the room; as for diffuser B, it is located

near the higher part of the room; as for diffuser C, it is located at the ceiling. E is the source of the aerosols.

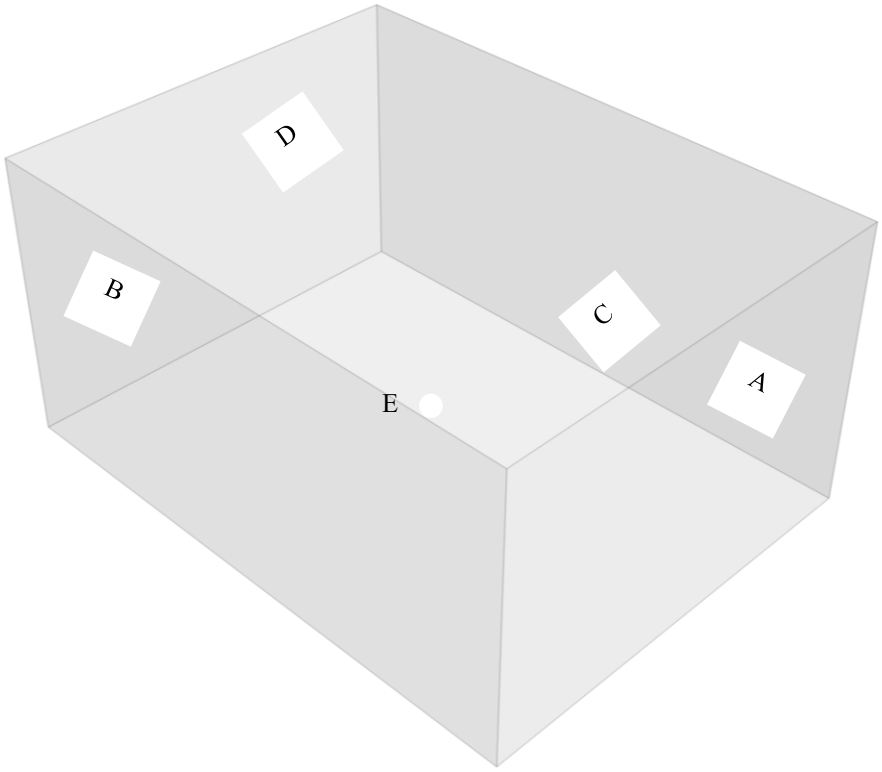

Figure 2.1 Proposed ventilation locations (A, B, C, and D) and E is the aerosol source (Adopted from Beggs et al., 2008)

Three different ventilation regimes are considered in this case. First, diffuser A is the supply, and diffuser B is the outlet. As for the second regime, diffuser B is the supply, and diffuser A is the outlet. As for the third regime, diffuser D is the supply, and diffuser C is the outlet. The results demonstrated lower aerosol particle concentration in the ward in the case of having the supply and outlet diffusers at the ceiling, as shown in Figure 2.2.

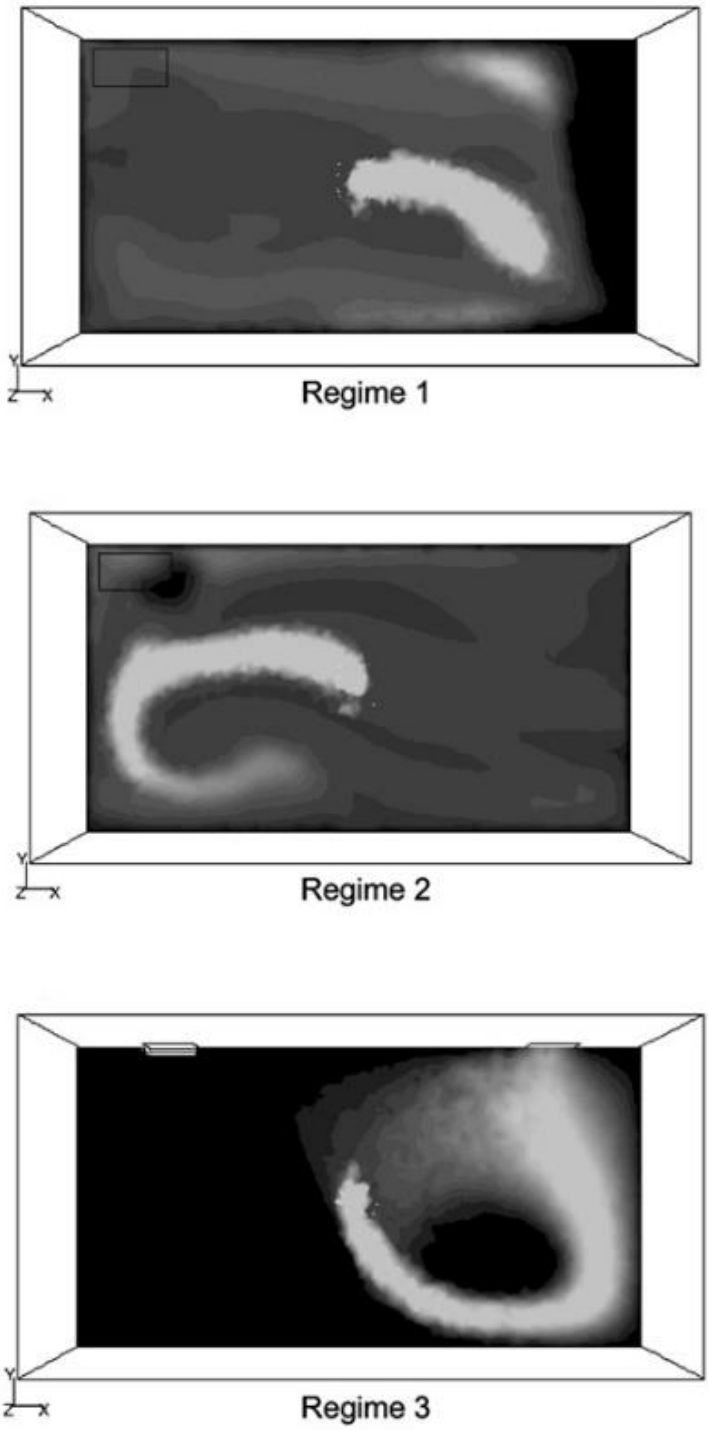

Figure 2.2 Aerosol concentration contour plots (Beggs et al., 2008)

Additionally, (Gbadamosi et al., 2020) conducted a study on the isolation space creation measures for COVID-19 patients, considering different spaces, including self-isolation at home, isolation at regular hospitals, epidemic hospitals, retrofitted buildings, temporary mobile cabins, and newly

constructed temporary hospitals for COVID-19. The study relies on a mixed-method approach, which utilizes secondary quantitative data and a qualitative literature review on COVID-19 to propose a solution to the space problem. The study found that the most effective methods of controlling the spread are isolation in temporary mobile cabins and newbuild COVID-19 hospitals. While this solves the space problem that healthcare systems face, other critical aspects need to be considered for this approach, including healthcare staff and medical equipment shortages. This highlights the use of modular buildings as field hospitals in such a pandemic.

2.2.2 Ventilation Systems CFD Applications

There have been many studies concerned with ventilation system assessment using CFD. (Ren et al., 2021) examined three different ventilation systems placements within a double-patient ward, through CFD numerical modelling using OpenFOAM software. The study focused on different particles diameters (i.e., $3\ \mu m, 6\ \mu m, 12\ \mu m, 20\ \mu m, 45\ \mu m, and\ 175\ \mu m$) injected using Eulerian-Lagrangian model. The ACH rate remains at 12.3. Three different ventilation systems are examined; first, the outlet and the inlet are located on the same sidewall; second, the outlet and the inlet are located on the opposite sidewall; and finally, one inlet is located on the ceiling, and two outlets are located on the sidewall, as shown in Figure 2.3. The study found that the particles smaller than $20\ \mu m$ tend to be removed by the ventilation system, while particles larger than $45\ \mu m$ land on near surfaces; thus, suggesting the placement of the outlet near the landing zone of those larger particles.

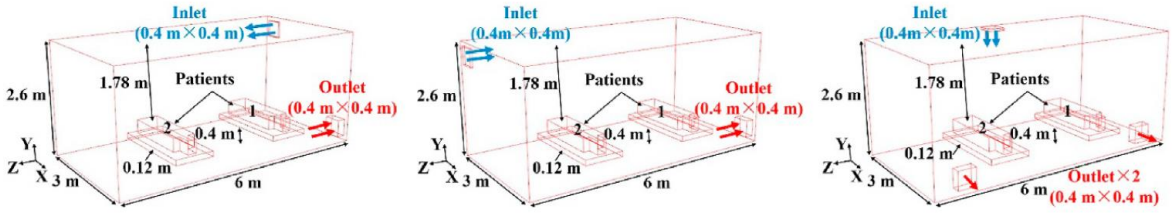

(a) Ventilation strategy I (b) Ventilation strategy II (c) Ventilation strategy III

Figure 2.3 Different ventilation strategies (Ren et al., 2021)

On the other hand, (Anghel et al., 2020) examined the source of the particles within a hospital ward using ANSYS Fluent, considering three different scenarios. First, the infected patient coughs on the right side of the unit, second, the infected patient is located on the left side of the unit, and

finally, the infected person is in the middle of the unit, as shown in Figure 2.4. The study found that scenario II causes respiratory droplets are spreading more than in the other two scenarios. Thus, suggesting the utilization of increased air supply while maintaining a constant flow.

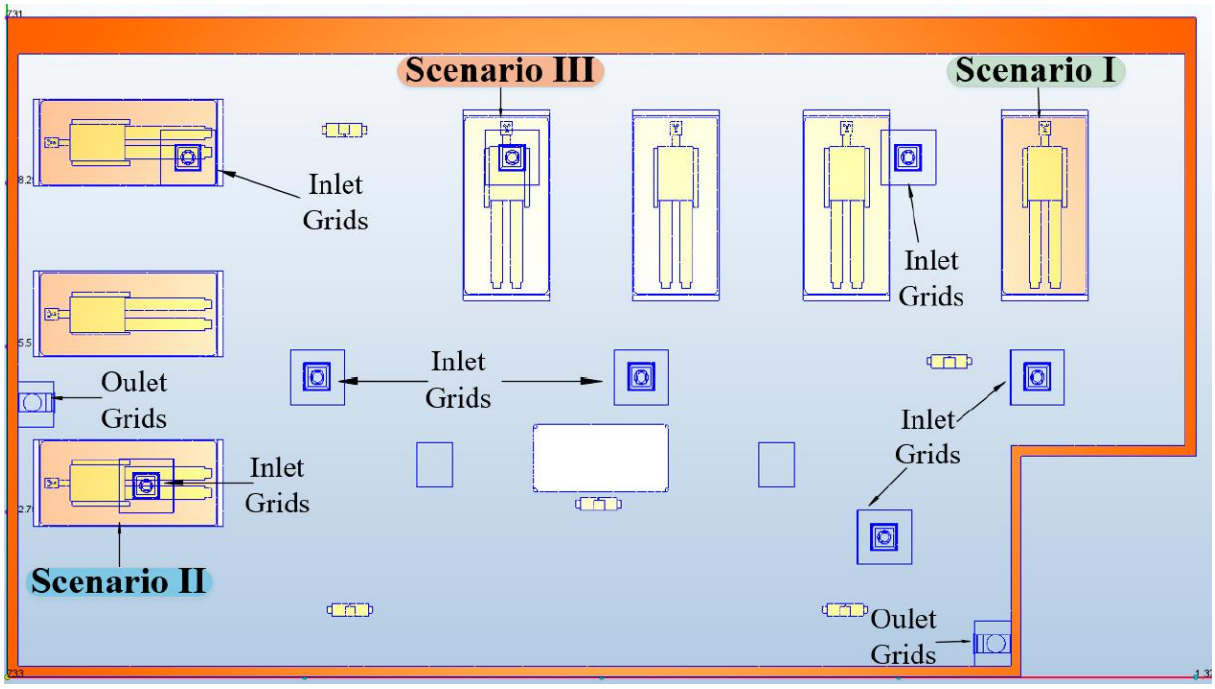

Figure 2.4 Three different scenarios (Anghel et al., 2020)

(Ahmadzadeh et al., 2020) investigated the effect of the ventilation system on the transmission of droplets generated when talking or sneezing by a person with a viral respiratory infection such as COVID-19 in a classroom, as shown in Figure 2.5. Considering two different conditions, first, the teacher is speaking in the classroom, and second, a student in the classroom coughs under various conditions (e.g., window open) using CFD. Particles were modelled using Euler-Lagrangian and using ANSYS Fluent to perform the simulations. The study found that airborne pathogens are significantly reduced when the infected person is close to the air-conditioning and an open window. As for the worst-performing case was found to be when the cough source was in the corner of the classroom.

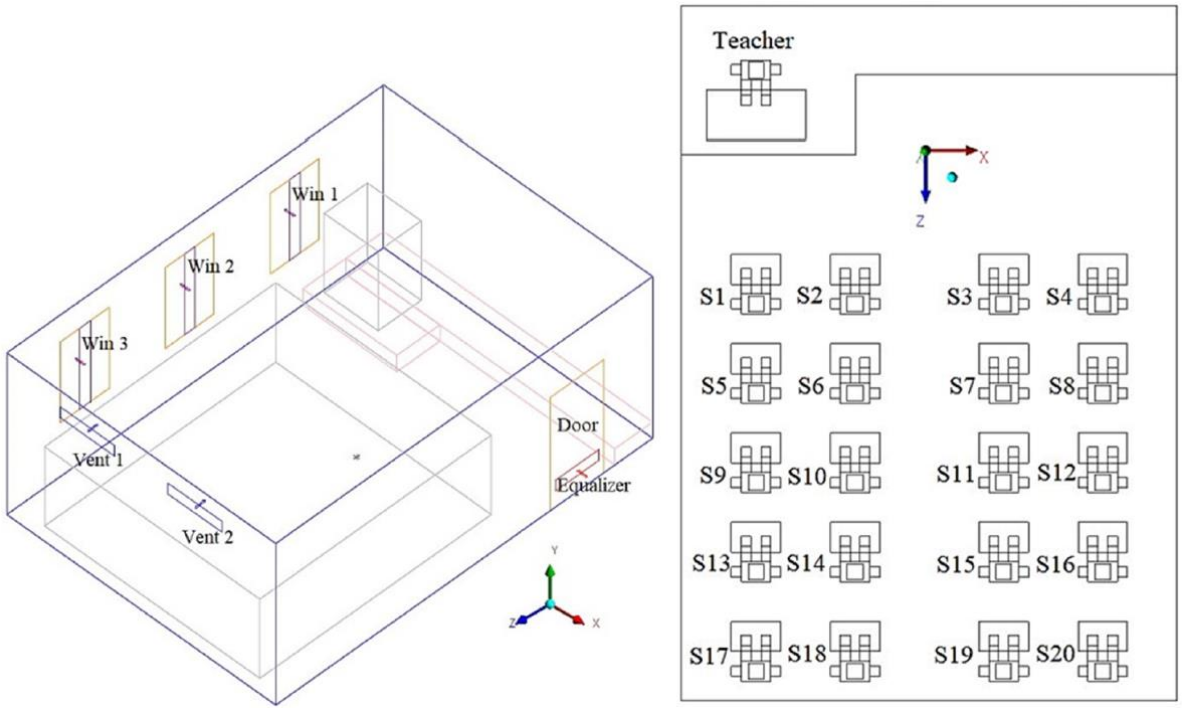

Figure 2.5 Classroom setup (Ahmadzadeh et al., 2020)

It was noted that there are many parameters impacting the translation of the droplet. Ventilation systems are the critical factor in the destination of the droplets. Thus, the need to assess the impact of the inlet and outlet placement as well as the ACH rate for the geometry is considered in this thesis.

2.2.3 Aerosol Modelling Overview

Experimental testing has been widely used to model particle flows. While there are many ways to conduct such experiments, technology limitations (e.g., ability to capture small particles, and speed) have limited such experiments. Recently, modern technological advancements have emerged and are currently utilized experimentally and numerically. For example, (Zhu et al., 2006) examined the transport characteristics of saliva droplets produced by coughing in a calm indoor environment. The study investigated the use of an experimental and CFD analysis to understand how the particle's trajectory is affected. The study includes the coughs of three subjects. Using particle image velocimetry, as shown in Figure 2.6.

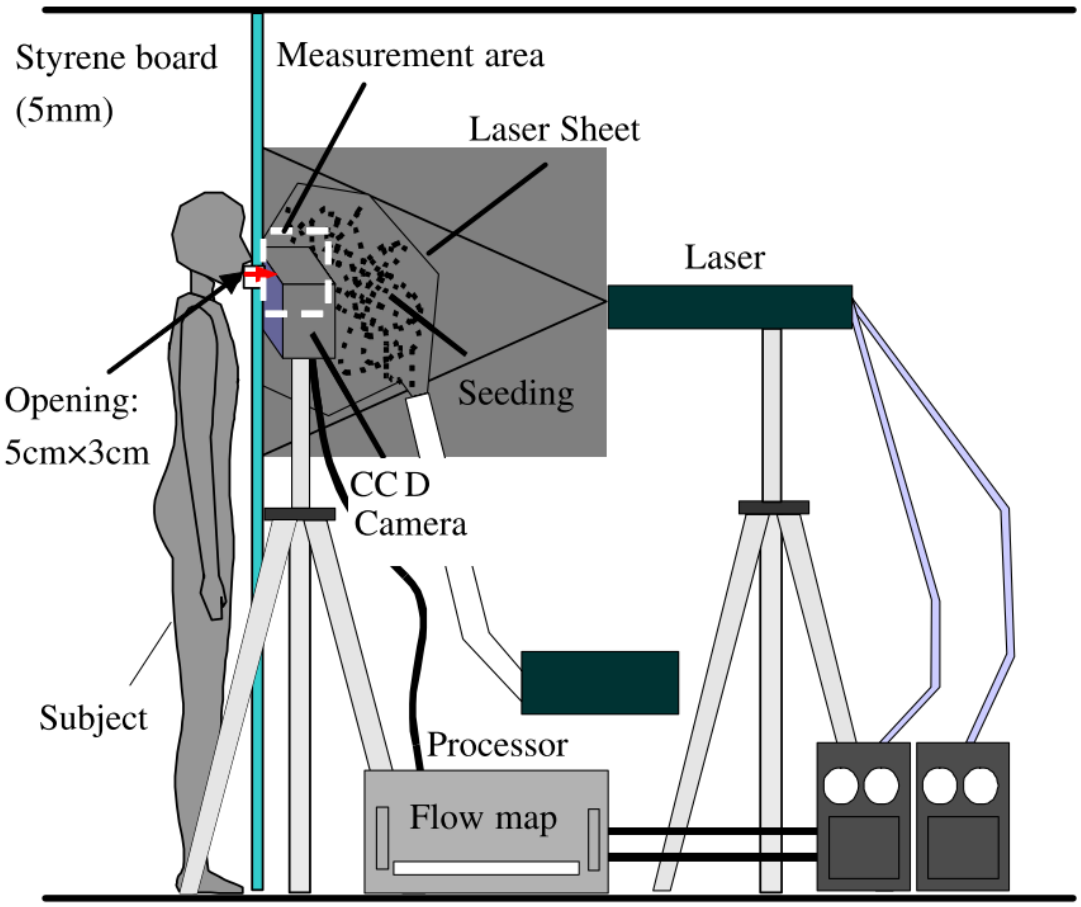

Figure 2.6 Particle image velocimetry (Zhu et al., 2006)

The latter study found that more than 6.7 mg of saliva is produced, and particles reach an average velocity of 11.2 m/s. It was also found that saliva particles can travel further than 2 m in an empty space. The study utilized the Lagrangian model in the dispersion of saliva droplets with different diameters. It was found that droplets of a diameter of 30 μm or smaller are not affected by gravity or inertia but by the flow field of the space they are in due to their smaller size. In comparison, droplets of sizes $50 - 200$ μm are affected by gravity, but they fall as the flow field weakens. As for droplets of size 300 μm or larger, they are affected by both gravity and inertia but will fall eventually due to their larger diameter. The analytical results demonstrate that droplet transport is significantly impacted by the spatial relationship between the ventilation system placement and the source of the cough. In contrast, (Lindsley et al., 2012) conducted a study about the quantity and size distribution of cough-generated aerosols produced by influenza patients during and after the illness. The study was conducted using a laser aerosols particle spectrometer, as shown in

Figure 2.7, capable of capturing a size range of $0.35 - 10\ \mu m$. Nine subjects were considered in this study. The study found that the average cough aerosol volume with influenza is $38.3 \times 10^{-12} L$. As for the average cough volume after recovery, it was determined to be $26.4 \times 10^{-12} L$. In addition, when the subjects had influenza, an average of 63% of each subject's cough aerosol particle volume in the detection range was in the respirable size fraction, highlighting that these particles could reach the alveolar region of the lungs if inhaled by another person.

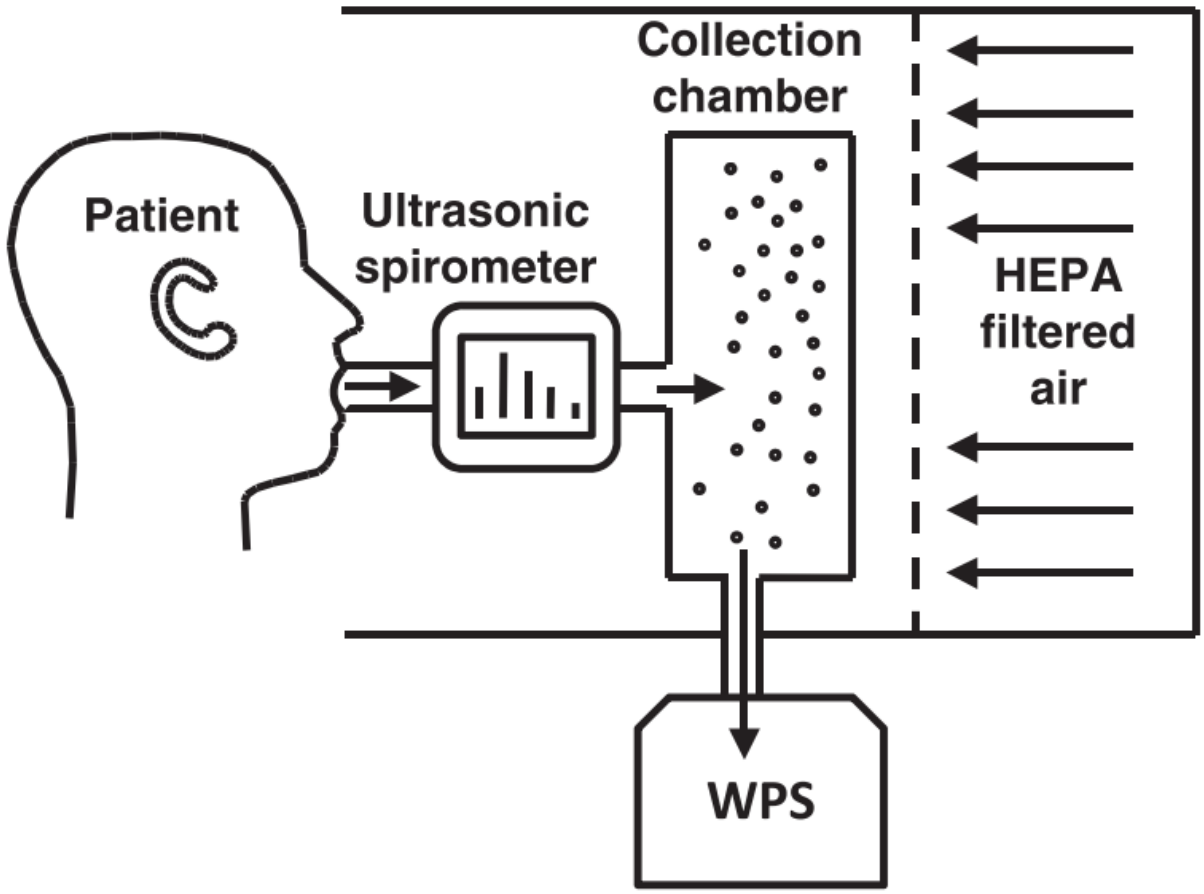

Figure 2.7 Cough aerosol particle measurement system (Lindsley et al., 2012)

The dispersion of expiratory airborne droplets in a model single patient hospital recovery room with stratified air ventilation was investigated by (Aliabadi, 2013). The focus of the study was to examine low-energy ventilation systems for adoption in hospital rooms, providing better air quality. This study consists of three parts. First, the use of air-assist internally mixing atomizer to

generate a poly-disperse distribution of droplets to assess the ventilation and near-field droplet size, velocity, and diffusivity in radial and axial directions for steady and transient atomization experimentally has been conducted. The second part is the use of the atomizer to inject droplets into a mock-up patient recovery room with an underfloor air distribution ventilation system to examine the far-field size-resolved concentration measurements representative of a receiver experimentally. Thirdly, the study examined the use of CFD to predict airborne droplet exposure under different cases in the far-field experiments. The study determined that the underfloor air distribution system's performance in removing injection particles depends on critical factors, such as momentum, the direction of injection, occupant location, and ACH rate. In addition, the dispersion of droplets depends on the droplets' size since smaller droplets tend to disperse more quickly than larger ones. It was also found that stratification alone is insufficient to reduce exposure to airborne droplets. Instead, a higher ACH rate with sufficient dilution may be a better approach.

2.2.4 Aerosol Modelling using CFD

Many studies have focused on performing experimental testing to study the characteristics of a cough, which helped understand some parameters that aid in designing numerical simulations. This enabled the use of numerical modelling to perform various tests to further understand how the cough aerosols propagate. For example, a study done by (Gupta et al., 2009) examined how airborne disease transmission occurs by characterizing the flow dynamics of a cough since coughing is one of the prime sources of airborne diseases. It has high velocity and a large quantity of droplets ejection. Using experimental testing and CFD modelling, the study determined that the flow rate at which the cough is ejected can be represented as a combination of gamma probability distribution functions. In contrast, a sequential cough of two single coughs showed higher concertation of particles in the first cough than in the second cough. As for the travel distance of the aerosols, (Blocken et al., 2020) conducted an aerodynamic study focusing on assessing the $1.5\,m$ distance of social distancing. The study of micro-droplets emitted from one person to another through coughing, sneezing, or exhaling is essential to understand how the social distancing rule impacts the droplets transfer. The setting in this case, when two subjects are walking or running in specific configurations, as for the social distancing rule, is accounting for when the two subjects are standing still, not considering the effects of aerodynamics; therefore,

the impact of external wind is deemed to be absent in this study. The study was conducted using CFD simulations and based on three different configurations, side by side running, inline, and staggered, as shown in Figure 2.8. The study concluded that the trailing person's most significant exposure to droplets is when the tailing person is in line behind the leading person (i.e., positioned in the slipstream). It was also found that the exposure to droplets increases when the distance between the leading person and the trailing person decreases. The study recommends $1.5\,m$ distance when the walking or running in the slipstream is taking a staggered configuration or side-by-side configurations or keeping a more significant distance that increases with the walking or running speed.

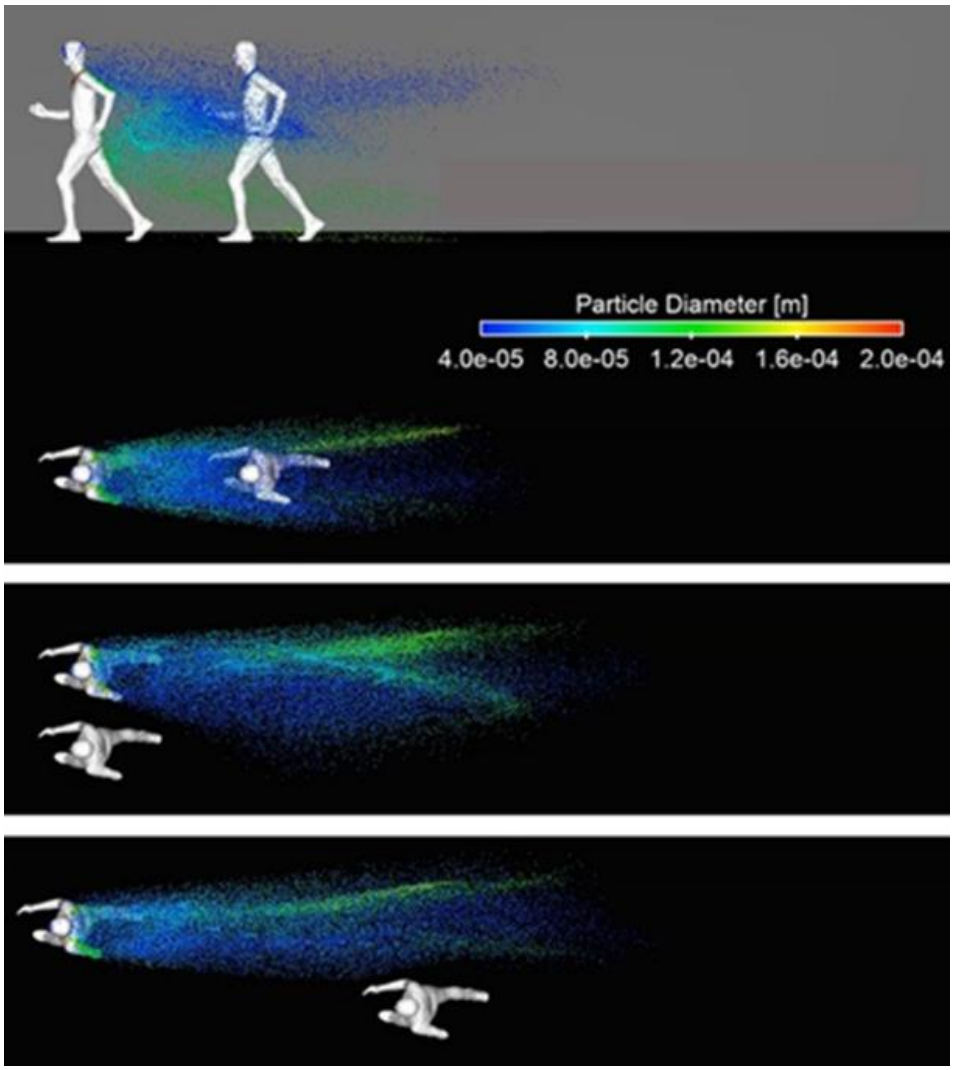

Figure 2.8 Droplet spreading when running at 14.4 km/h in the different configurations studied (Blocken et al., 2020)

Another study by (B. Zhang et al., 2020) investigated the transport and trajectory of cough-induced bimodal aerosol in an air-conditioned space. The study focuses on ventilation's influence and the nearby human breathing zone. An experimental system consisting of an air-conditioned room with various inlets and outlets, a cough simulator, and a receiver was constructed to validate the CFD model. The CFD model was established as a transient three-dimensional multiphase multicomponent Eulerian-Lagrangian model. The results demonstrated a good agreement between the experimental and CFD. The study concluded that aerosol source location and ambient air movement could be crucial factors of aerosol trajectory in direct or indirect influence. This paper

is utilized in the validation and will be described in detail in the next chapter. As for the governing equations to model the trajectory of particles within space, three-dimensional, transient, turbulent multiphase flow using the Eulerian-Lagrangian frame. The principal governing equations concerned with performing such simulations are summarized in Table 1. In addition, Lagrangian modelling depends on various physics models summarized in Table 2. Many important factors impact the solution of such models. Thus, the need to assess the models used for the application is essential.

Table 1 Major governing equations

Model	Representative Equation
Continuity	$\frac{\partial}{\partial t}(\rho Y_i) + \nabla.(\rho \mathrm{UY_i}) = -\nabla.J_i$
Momentum	$\frac{\partial}{\partial t}(\rho U) + \nabla.(\rho \mathrm{UU}) = -\nabla \mathrm{p} + \nabla.\tau$
Energy	$\frac{\partial}{\partial t}(\rho E) + \nabla.[\mathrm{U}(\rho \mathrm{E} + \mathrm{p})] = \nabla.[k\nabla \mathrm{T} - \sum_i h_i J_i + (\tau.U)]$
Equation of state	$p = \rho RT$
Species conservation	$\sum Y_i = 1$
Diffusion flux	$J_i = -\rho D_{i,m} \nabla Y_i$
Turbulent viscosity	$\mu_T = C_\mu \bar{\rho} \frac{k^2}{\varepsilon}$
Turbulence k	$\frac{\partial}{\partial t}(\rho k) + \nabla.(\rho \mathrm{kU}) = \nabla.\left[\left(\mu + \frac{\mu_t}{\sigma_k}\right)\nabla k\right] + G_k + G_b - \rho\varepsilon - Y_M$
Turbulence ε	$\frac{\partial}{\partial t}(\rho \varepsilon) + \nabla.(\rho \varepsilon U) = \nabla.\left[\left(\mu + \frac{\mu_t}{\sigma_k}\right)\nabla \varepsilon\right] + C_{1\varepsilon}\frac{\varepsilon}{k}(G_k + C_{3\varepsilon}G_b) - C_{2\varepsilon}\rho\frac{\varepsilon^2}{k}$

Table 2 Major governing Lagrangian phase models

Conservation of linear momentum	$m_p \frac{d_{v_p}}{d_t} = F_s + F_b$ $F_s = F_d + F_p + F_{vm}$ $F_b = F_g + F_{MRF} + F_u + F_c + F_{Co}$
Drag force	$F_d = \frac{1}{2} C_d \rho A_p \lvert v_s \rvert v_s$
Drag coefficient (Schiller-Naumann correlation)	$C_d = \begin{cases} \frac{24}{Re_p}\left(1 + 0.15 Re_p^{0.687}\right) & Re_p \leq 10^3 \\ 0.44 & Re_p > 10^3 \end{cases}$ $Re_p = \frac{\rho \lvert v_s \rvert D_p}{\mu}$
Pressure gradient force	$F_p = -V_p \nabla p_{static}$
Gravity force	$F_g = m_p g$
Particle position and velocity	$\frac{dr_p}{dt} = v_p$

2.3 Wind Load Evaluation and Modular Structures

This section provides an overview of the use of Large-Eddy Simulation (LES) to perform wind load evaluations, as well as an overview of the recent advancements in modular structures. First, an overview of the techniques used to perform wind load evaluations is presented and discussed, followed by an overview of the emerging technologies concerning modular structures.

2.3.1 Wind Load Evaluation

Wind load is a governing load for various structures, which highlights the importance of adopting high-fidelity techniques when evaluating their impact while designing structures (e.g., modular structures). Wind load evaluations have seen significant advancement over the years, which highlights the role of wind loads when it comes to designing structures. With the advancement of modular structures, the complexity of understanding such structures requires the utilization of various tools (e.g., full-scale tests, wind tunnels, and CFD). For example, (Ho et al., 1992) explored the low building wind load variability with application to codes. The study utilized wind tunnel testing to assess the wind code specifications based on data from wind tunnel tests on isolated buildings in idealized homogenous upstream terrains. In addition, the study reports preliminary results of systematic wind tunnel testing, specially designed to account for the effects of realistic surroundings on wind loads for various building shapes. The study found that the major contributor to the highly variable wind loads is the peak coefficients $C_p C_g$With a coefficient of variation in order of 0.6. Another contributor to this variation is the dynamic reference pressure. More data is required to understand the appropriately and better describe this parameter. Additionally, (Ho et al., 2005) examined the contribution of the University of Western in support of Texas Tech University and the United States National Institute of Standards and Technology to create an aerodynamic database for low building design. The paper describes the background necessary to understand the testing configurations, basic models, and wind simulation. Parametric comparisons are performed to obtain basic quality checks. Parameters such as roof slope, building height, and building plan dimension show that data obtained within the study are consistent with the expected aerodynamic behaviour. Comparison with full-scale data shows that wind tunnel tests match the full-scale well but cannot reproduce the largest of the peak point suctions near roof edges. This study is adopted in the validation process for the CFD simulation and will be described in more detail in the next chapter. As for the study of CFD applications on low-rise buildings, (Ricci et al.,

2017) conducted LES on a low-rise building to evaluate wind loads and assess the structural response. The study focuses on the comparison between wind tunnel tests and CFD analysis, using pressure distribution as well as dynamic structural analysis. The study found that the mean pressure coefficient can accurately be predicted by LES, unlike the standard deviation, as it can be less accurate, and this is mainly observed at the edges, as shown in Figure 2.9.

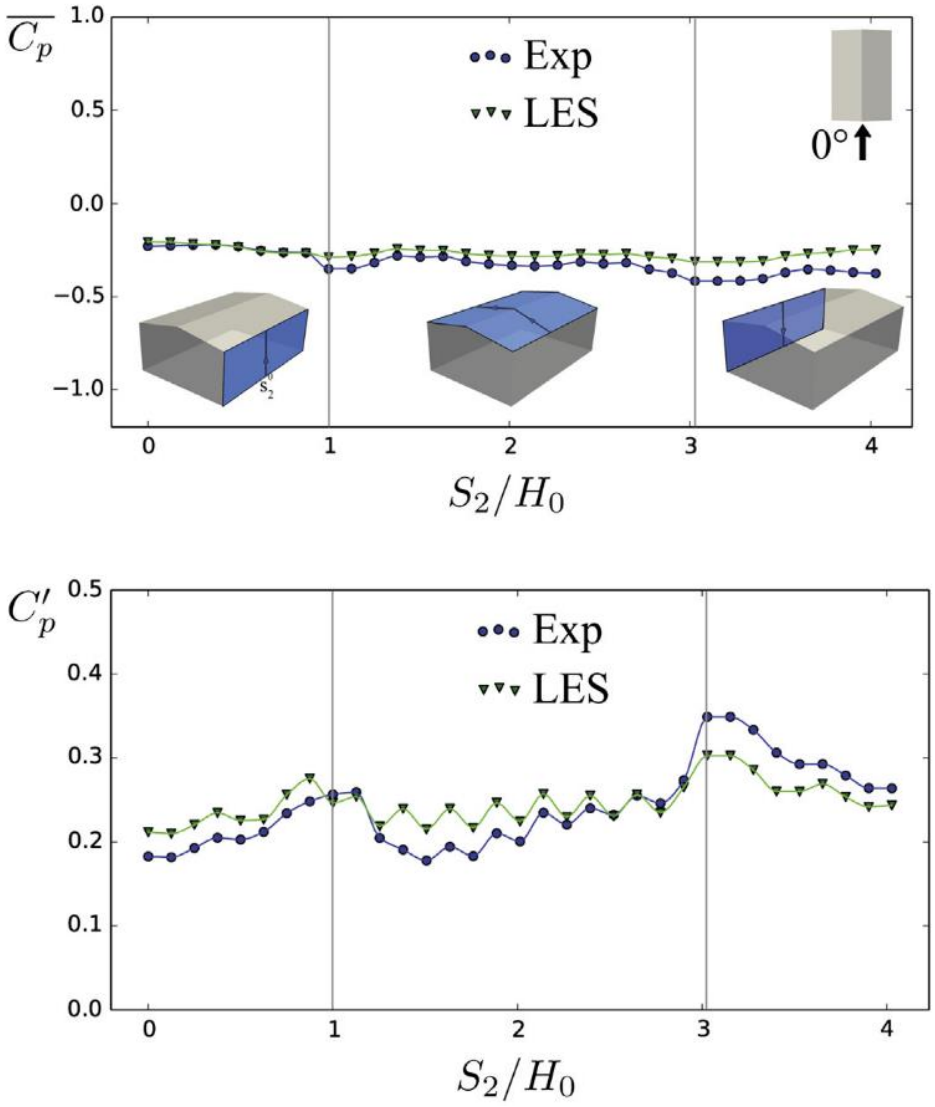

Figure 2.9 Mean pressure coefficient and standard deviation (Ricci et al., 2017)

Since many factors impact the wind loads developed on structures, including the distribution of the surrounding structures, a study done by (Elshaer et al., 2017) examined the effect of urban development on the variations in wind load on buildings. With the changes in urban topology,

planning a building placement in a dense metropolitan is crucial since the structure can experience different flow mechanisms, such as wake effects and channelling. These flow mechanisms are impacted by the surrounding structures' shape, height, and location, which are dynamically changing with new developments. The study examines two cases. First, having the building surrounded by generic surrounding configurations of different heights. Secondly, the building environment of the Financial District, Toronto, is adopted and examined for three different development stages. The study found that the change in urban development can have different impacts on the structural and non-structural elements. As the urban development becomes denser, the fluctuations in wind pressures increased. The increased volatility can lead to increased pressure on cladding components, which poses a higher risk. LES has been utilized to perform wind simulations over the years. Still, there are many factors to consider when performing such simulations, such as the consideration of the inflow generation to be able to introduce the matching turbulence. When it comes to utilizing LES to perform wind simulations, the need to accurately generate inflow turbulence is crucial to performing high-fidelity simulations. There are three main families of techniques used to generate turbulence in LES, which are precursor database, recycling method, and synthetic turbulence. The precursor technique has been adopted widely in wind engineering applications, but it has drawbacks since it consists of two stages and can be computationally expensive. As for the recycling method, it is similar to the precursor method but requires the terrain characteristics to be known and accurately implemented. As for the synthetic techniques, there are mainly two types, the weighted amplitude wave superposition method, which satisfies the turbulent velocity field of targeted power and cross-spectra, but it is not dependent on the grid discretization; thus, it doesn't satisfy the continuity equation. As for the second type, it is referred to as random flow generation. This technique has been developed repeatedly to account for atmospheric boundary layer conditions and improve its accuracy. Among the efforts exerted towards improving the accuracy of inflow generators, (Aboshosha et al., 2015) proposed a technique of turbulent inflow generation that can be used as inflow boundary conditions when conducting large-eddy simulations of lower atmospheric boundary layers. With this development, the production of accurate inflow generation is improved with the introduction of consistent discrete random flow generation (CDRFG), as it works on the bases of synthesizing random divergent-free turbulent velocities, as shown in Figure 2.10.

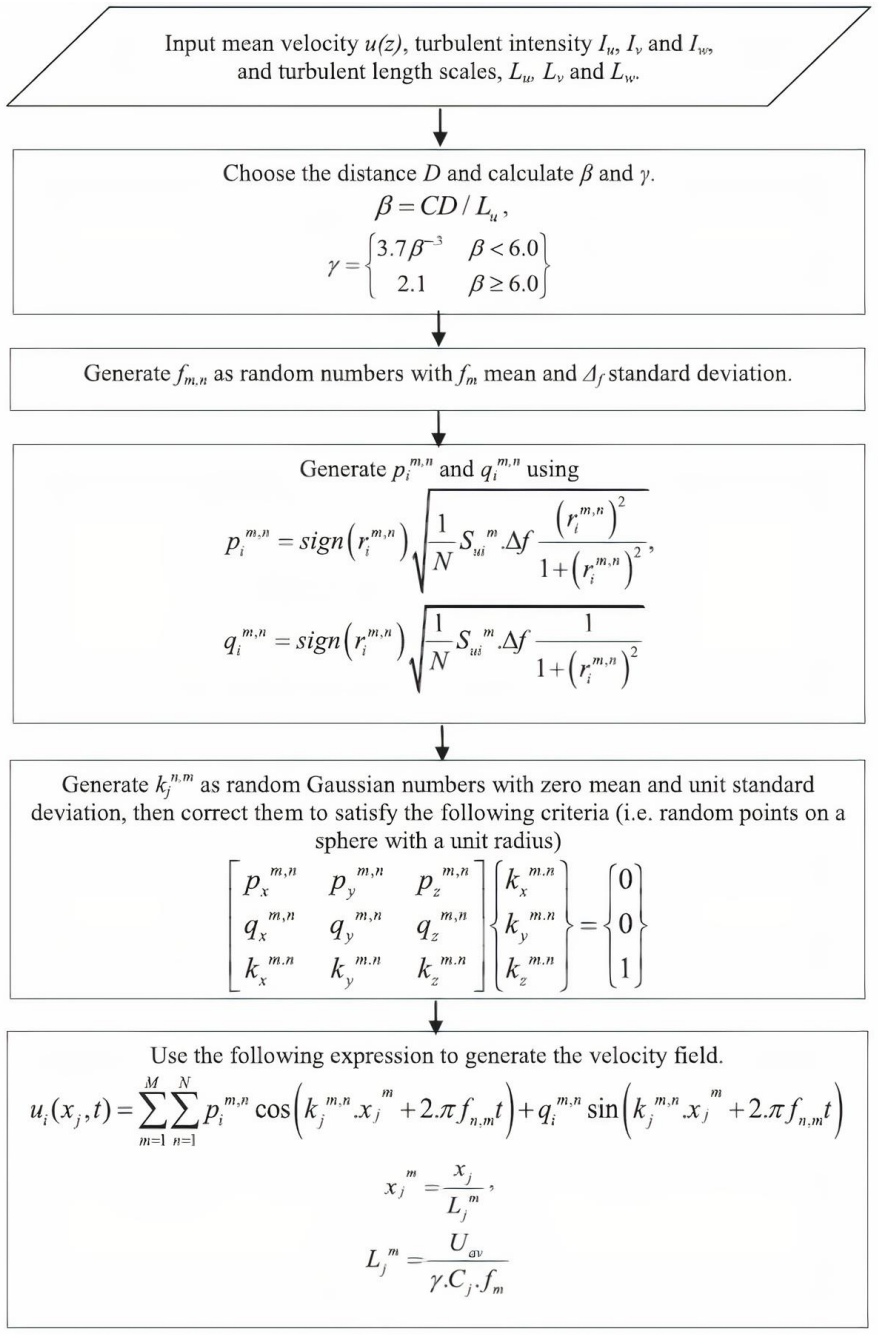

Figure 2.10 CDRFG flowchart ((Aboshosha et al., 2015)

The latter technique maintains the turbulent spectra and coherency function, which are critical to appropriately simulate interactions of turbulent atmospheric boundary layers flow. The study found that previous inflow generators lack accuracy when it comes to modelling the target spectra and coherency. It was found that CDRFG maintains consistent spectra and coherency. This has

been validated with previous studies, numerically and experimentally, demonstrating this technique's applicability when conducting large-eddy simulations. Thus, this thesis has adopted it as the flow generation technique in Chapter 4.

In addition, (Elshaer et al., 2016) performed an LES simulation to evaluate wind-induced responses for an isolated and surrounded building. The study utilized the CDRFG technique for flow generation, as it satisfies turbulence spectra and coherency, which increases the fidelity of the simulation. In addition, results were compared to the wind tunnel data from the literature to assess the accuracy of the inflow generation. Figure 2.11 shows (a) wind profile, (b) turbulence intensities, and (c) length scales measured from both wind tunnel tests and CFD.

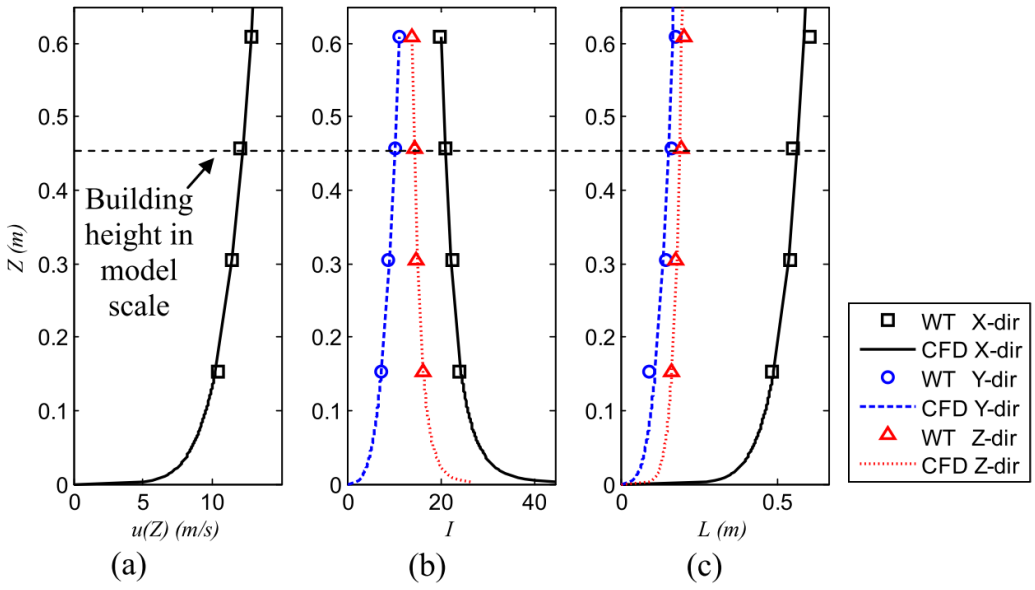

Figure 2.11 Profiles measured from the wind tunnel, and CFD (Elshaer et al., 2016)

The study found that there is a good agreement in the pressure measurements compared to the boundary layer wind tunnel. Thus, deeming the utilization of LES and CDRFG to be more accurate when estimating the pressure distribution on the structure, which supports the adoption of the latter technique in this thesis for wind load evaluation on modular buildings (Chapter 4).

2.3.2 Modular Structures

Many studies have covered various aspects of modular structures, including materials, connections, and applications. For example, (Lawson et al., 2008) investigated the robustness of light steel frames and modular construction. Various forms of construction adopting lightweight steel and modular technologies are reviewed. The study focuses on the accidental actions that can impact the structural stability using a scenario-based approach, and selective modules are removed, as shown in Figure 2.12. As for the horizontal and vertical forces developed in the connections between the modules, they can be calculated explicitly. The study was conducted using a series of stressed skin tests on modular structures, which is when the upper module is supported by the lower module, and the vertical support to one edge of the lower module was removed. The study determined that modules could span as deep beams with one longitudinal support removed with minimal displacements, indicating the robustness of the torsional stiffness of the volumetric module.

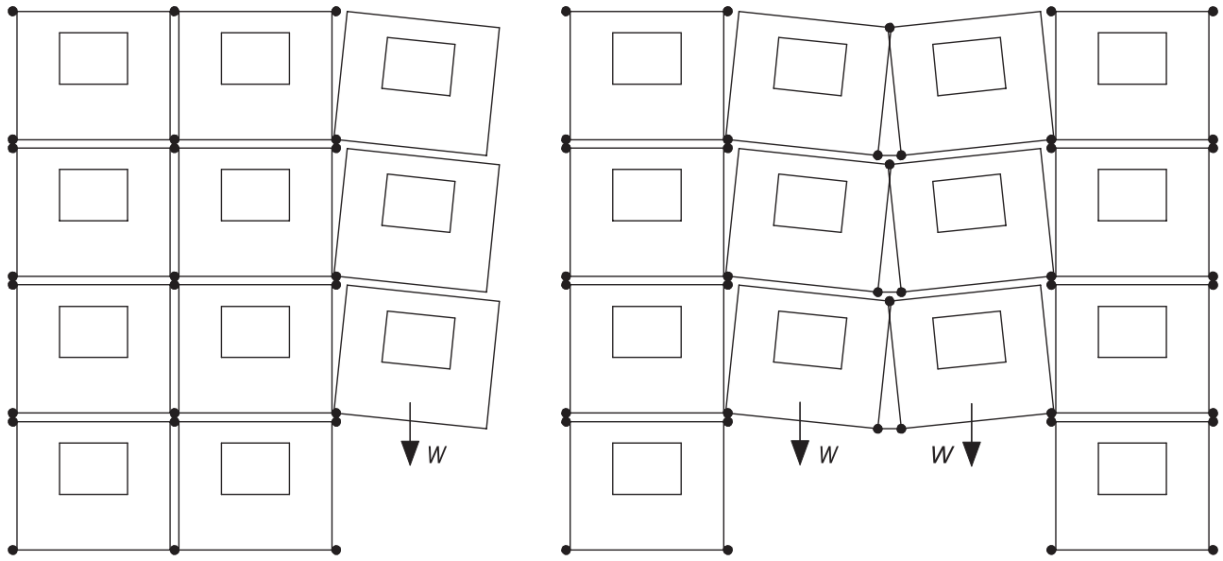

Figure 2.12 Robustness scenarios in modular construction (Lawson et al., 2008)

Another study by (Lacey et al., 2018) examined modular steel buildings' performance consisting of stacked module assemblies. A case study of a six-storey modular apartment building, as shown in Figure 2.13, located in Port Hedland, Western Australia, was examined to assess the performance through equivalent static and fluctuating wind loads, in accordance with the

Australian Standard 1170.2, to understand the influence of inter-module connection stiffness on the structural performance using finite element modelling (FEM).

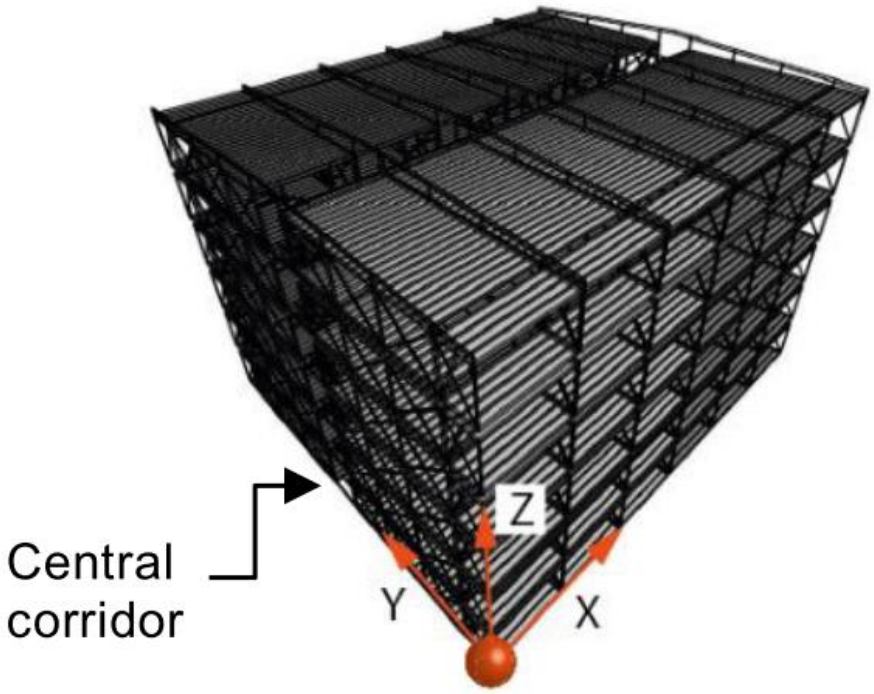

Figure 2.13 Numerical model layout (Lacey et al., 2018)

The study concluded that variations in the fundamental period depend mainly on the frame type, height, and inter-connection stiffness. As for the case study, the inter-storey drift ratio primarily depends on the vertical connection translational stiffness in the along wind direction, with the ratio decreasing as the stiffness of the connection increases. Along this line of research, (Peng et al., 2021) investigated corner-supported modular buildings under wind actions. The study proposes a novel design of a corner-supported steel-concrete composite module, as shown in Figure 2.14. Parameters such as strength and stiffness are of interest to improve. These improvements are achieved using concrete-filled steel tubular (CFST) columns, laminated double beams, and integrated concrete slabs. The structural integrity is enhanced through the designs of tenon-connected inter-module connections, in addition to beam-to-beam bolt connections. The study revealed an average increase of 21% in elastic stiffness and 33% in capacity under lateral loads compared to steel hollow sections (SHS).

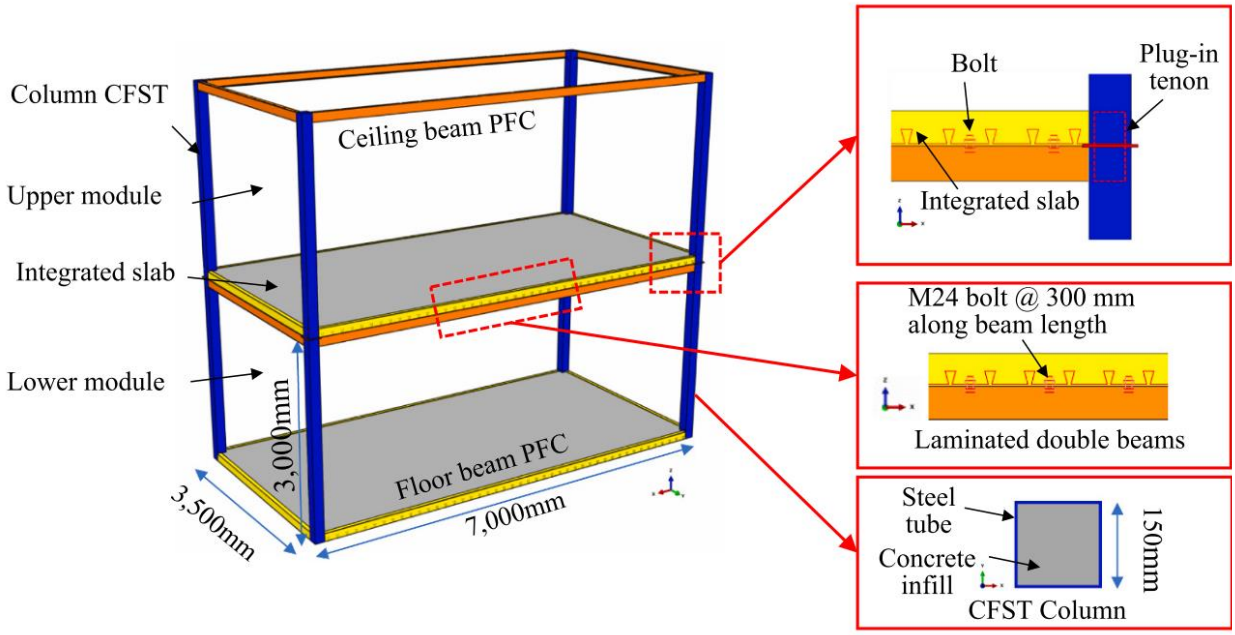

Figure 2.14 Corner-supported steel-concrete composite modules (Peng et al., 2021)

Using finite element analysis modelling ABAQUS, two approaches are adopted, the simplified method (SM) and the detailed method (DM), to demonstrate how CFST can be modelled. The detailed method contains sophisticated, realistic details that can simulate interactions between each structural component, which produces more accurate predictions which can be useful for the design of a single structural component. As for the simplified method, it is developed to save computational costs while still capable of predicting the load-displacement curves and the failure modes of the modular buildings. The proposed design of CFST columns demonstrated increased lateral resistance compared to SHS, as shown in Figure 2.15.

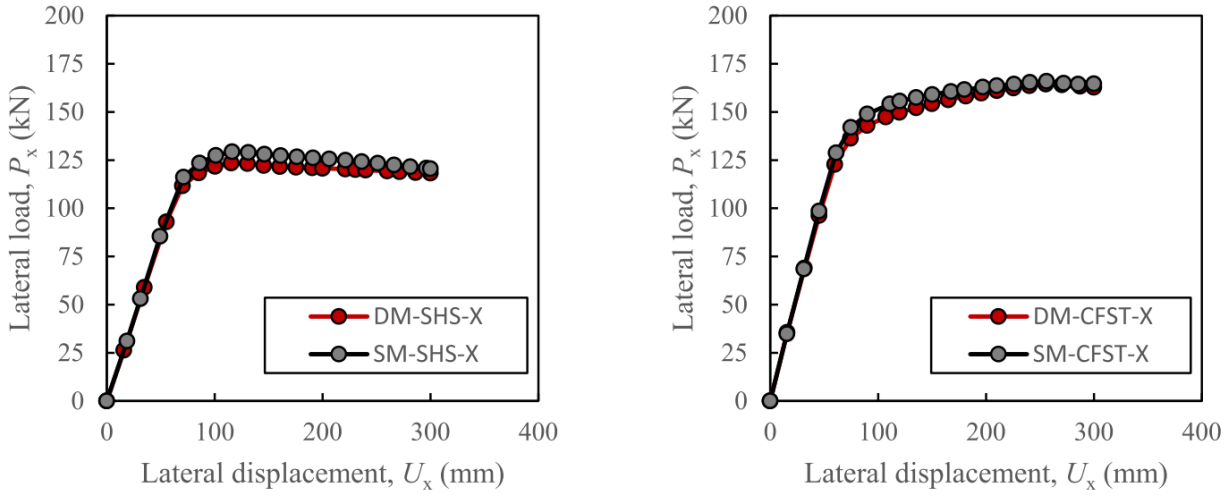

Figure 2.15 Lateral resistance for CFST and SHS using detailed and simplified methods adopted in FEM model (Peng et al., 2021)

Also, (J. F. Zhang et al., 2020) studied the mechanical properties of full-scale assembled light steel modular buildings consisting of a bottom frame and a top frame connected with columns and high-strength bolts, as shown in Figure 2.16. The results were performed using FEM (i.e., ABAQUS). Deformation in both full-scale and FEM was compared, as shown in Figure 2.17. The load-displacements graphs were then plotted for column 2 (C2) and column 3 (C3) at the top end point (a) and mid-height point of columns (b), as shown in Figure 2.18.

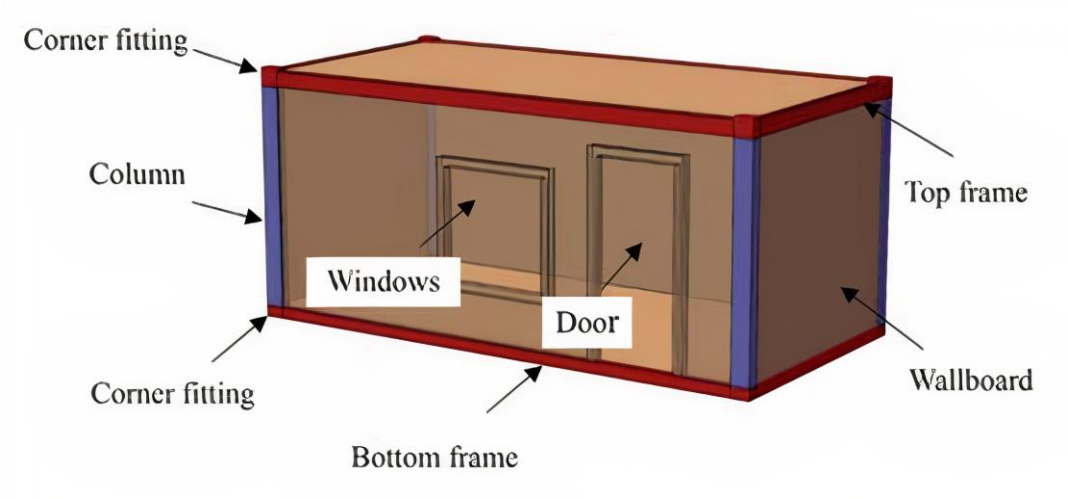

Figure 2.16 Assembled-type light steel module (J. F. Zhang et al., 2020)

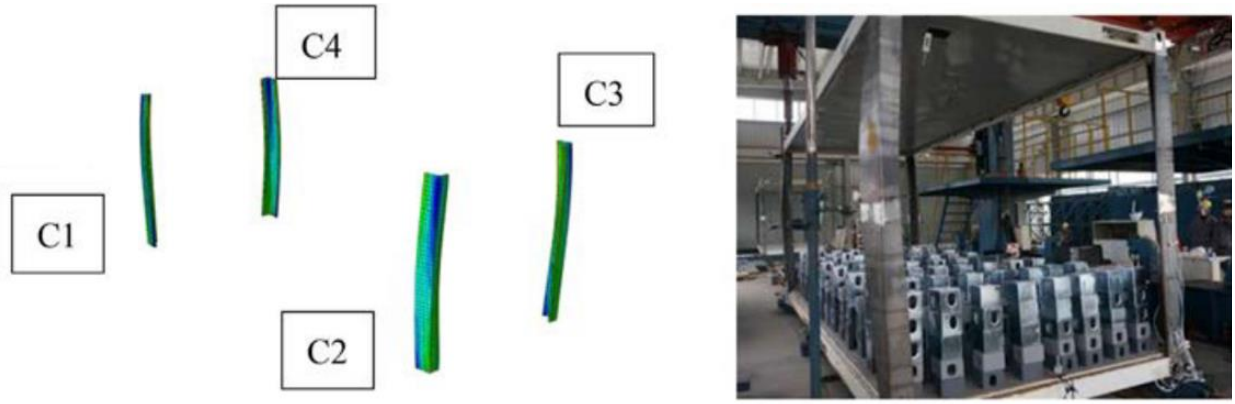

Figure 2.17 Deformation in four columns in FEM and full-scale (J. F. Zhang et al., 2020)

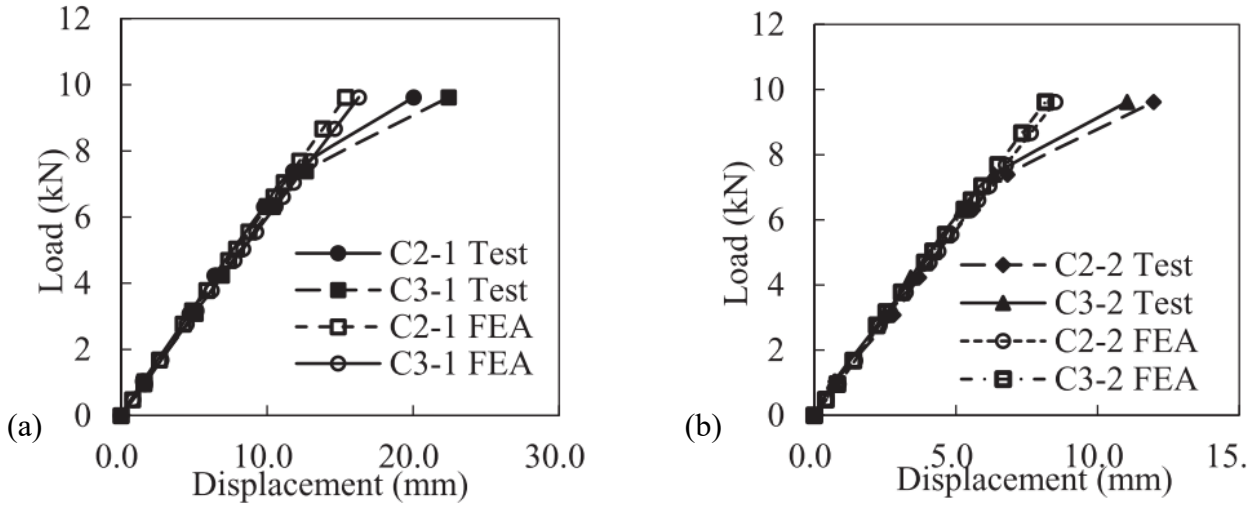

Figure 2.18 Load displacement of C2 and C3 (a) at the top end of the column (b) at the mid-point (J. F. Zhang et al., 2020)

Through the vertical bearing capacity test and horizontal stiffness test, the study found that the assembled-type light steel module failed due to the excessive flexural-torsional buckling of the four columns. The bottom frame remained in the elastic stage, indicating good deformation capacity and weak rigidity. As for the horizontal stiffness, the module had a weak horizontal stiffness under horizontal load, and deformation was still in the elastic stage. A study conducted

by (Wang et al., 2021) investigated the seismic performance of assembled-type light steel modules based on joint stiffness analysis. The study was performed using quasi-static loading, and through full-scale experimental, as shown in Figure 2.19, and FEM, a stiffness analysis of intra-modular and inter-modular connections was performed. In Figure 2.19, the labels refer to the following: 1. Reaction wall; 2. Horizontal hydraulic jack and force transducer; 3. Hinged support; 4. Pedestal; 5. Top frame; 6. Bottom frame; 7. Ceiling beam; 8. Floor beam; 9. Column; 10. Intra-modular connection; 11. Inter-modular connection.

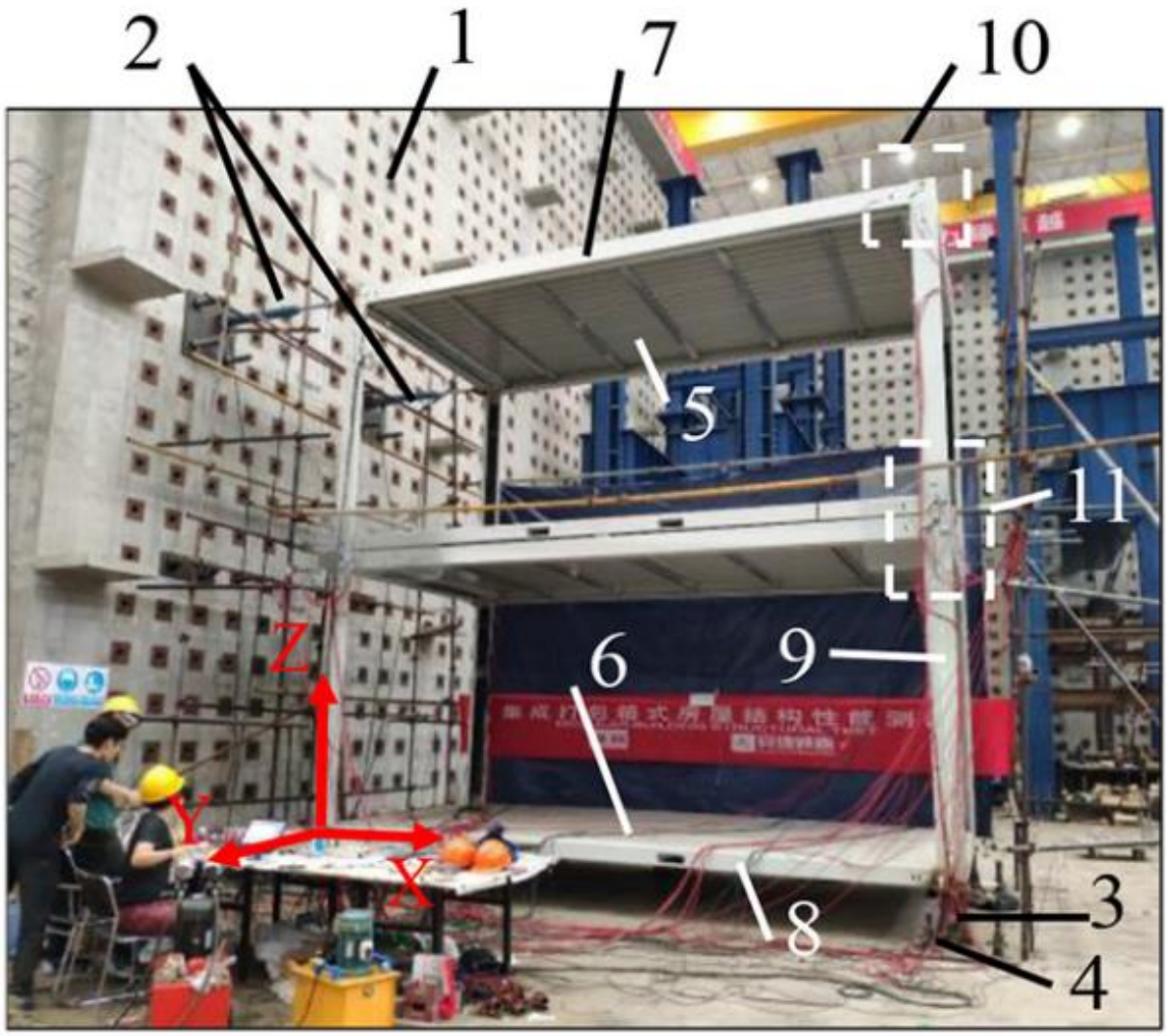

Figure 2.19 Full-scale test setup (Wang et al., 2021)

The study found that the weld fractures at the connection between the ceiling beam and corner fitting near the loading end decrease the bearing capacity, highlighting the importance of connection design. In addition, the holes in the corner fittings have an insignificant effect on the initial rotational stiffness of the unit's intra-modular connection but will still reduce the bearing capacity. As for the intra-modular connection, based on the calculations according to Eurocode 3, the connection appears to be semi-rigid, which should be considered when performing analysis. On the other hand, (Gatheeshgar et al., 2020) investigated the use of cold-formed steel in the applications of modular buildings. The application adopted in the paper was to further optimize and enhance the usability of cold-formed steel sections based on various aspects, such as weight reduction, access space, transportation restrictions, and structural, fire, and energy performances. Incorporating cold-formed steel members with slotted webs can address such problems. The study utilized an optimization technique referred to as particle swarm optimization to reduce material usage while maintaining the performance of the sections. Results were then analyzed further using the finite element method. Three different sections were considered in this study to determine the effect of optimization on their performance, which are the lipped channel section, folded-flange section, and super-sigma section, as shown in Figure 2.20.

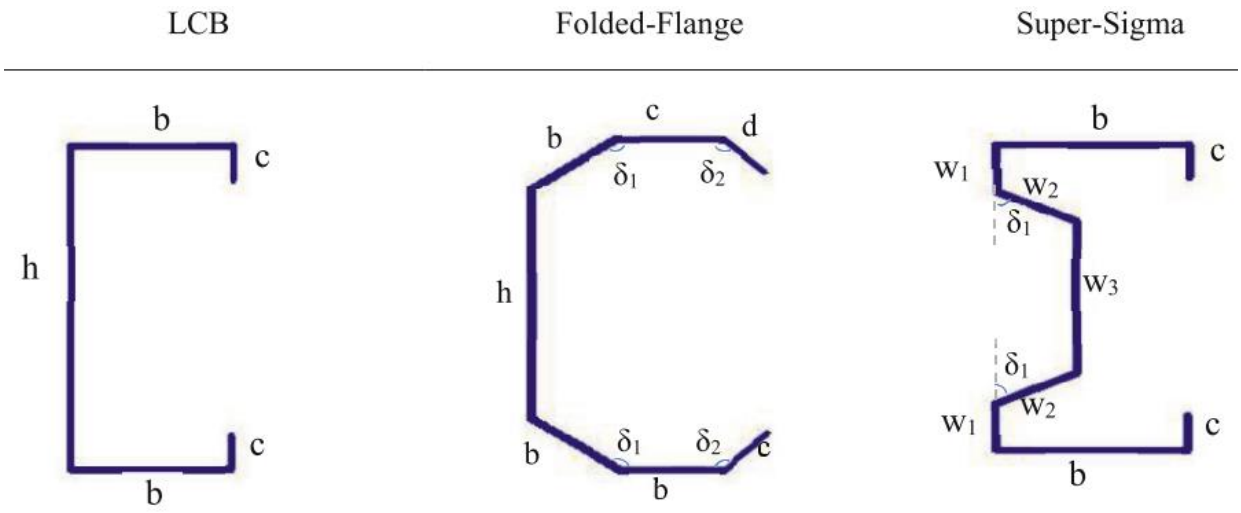

Figure 2.20 Selected sections for optimization (Gatheeshgar et al., 2020)

The study found that the flexural capacity of the optimized sections improved by 30%, 60%, and 65% for the lipped channel, folded-flange, and super sigma, respectively, in comparison to the conventional cold-formed steel sections. A study conducted by (N.Usefi et al., 2021) examined the

utilization of hybrid-cold formed steel frames in comparison to ordinary moment-resisting frames. The study focuses on the structural performance and sustainability of the frames, which is achieved through quantitative and qualitative analyses that outline both systems' advantages and disadvantages. The study found that hybrid-cold form steel frames perform structurally better in storey shear and drift. In addition, hybrid-cold form steel frames have less impact on the environment in comparison to the ordinary moment-resisting steel frames. This can be attributed to the less materials used in the construction, which also leads to increased cost savings of up to 23% in comparison to the ordinary moment-resisting frames. The stability of structures is critical to understand; therefore, (Z. Chen et al., 2021) explored the multidirectional stability and response of prefabricated volumetric modular steel construction. The study summarizes essential factors impacting the structural stability and performance of multi-storey prefabricated volumetric modular steel buildings. Several factors influencing structural performance, such as connections, stability systems, and configurations, are discussed to enhance the understanding of these factors on the overall structural performance. The study found that prefabricated volumetric modular steel buildings can be utilized in low-rise and mid-rise structures since they provide cost-effective, faster, safer, and eco-sustainable solutions in comparison to the conventional methods. In addition, multidirectional stability in these applications is well understood, in contrast to the high-rise applications, as there are many technical challenges facing the utilizations, such as the response of lateral force resisting systems on structural and non-structural components, which can result in poor connection design, since high-rise structures are typically designed to be flexible. The impact of having flexible structures on structural and non-structural components is essential. (Hwan Doh et al., 2017) investigated the use of an innovative steel bracket connection to determine the shear loading, ultimate resistance, and failure modes in modular building applications, as shown in Figure 2.21. The study was conducted through experimental testing and finite element modelling. The study focused on parameters such as the bolthole dimensions and spacing to better understand their impact on the structural behaviours of the steel bracket connection.

Figure 2.21 Steel connection assembled (Hwan Doh et al., 2017)

As for the steel bracket connection, it consisted of a hollow cube steel section with dimensions of $370\ mm \times 370\ mm \times 370\ mm$ with a wall thickness of $15\ mm$, as shown in Figure 2.22. Six faces on the cube, including a plain face, two faces with rectangular cut-outs utilized for assembly, two faces with four boltholes and a rectangular cut-out for access, one face with four boltholes, and one larger hole in the center for transportation purposes. The bracket connection utilized Q235B steel, which is a commonly used material in the Chinese steel industry. The material property is shown in Table 3.

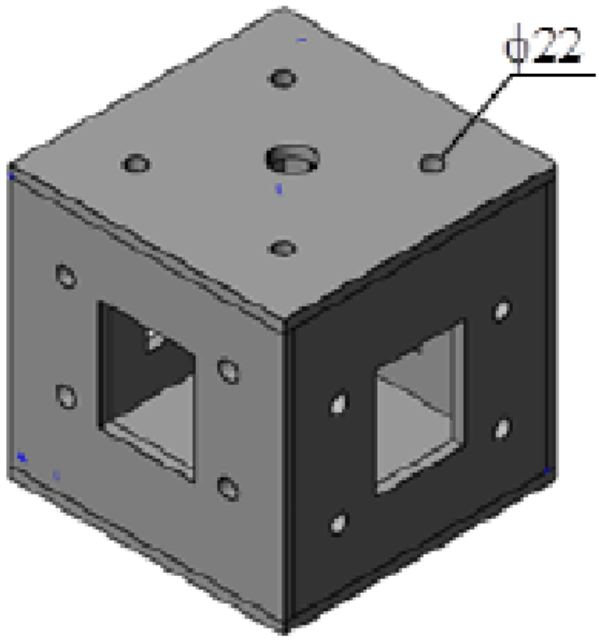

Figure 2.22 Steel bracket connection (Hwan Doh et al., 2017)

Table 3 Q325B steel properties (Hwan Doh et al., 2017)

Yield strength	$235\ MPa$
Ultimate strength	$375 - 460\ MPa$
Density	$7.85\ g/cm^3$
Modulus of elasticity	$200 - 210\ GPa$
Poisson's ratio	$0.25 - 0.33$
Elongation	26%

The study found that the steel bracket connection failed in a ductile manner, with no evidence of plate failure. The connection failure was due to the exceedance of the bolt tensile capacity. Further analysis is required to optimize this connection.

On the other hand, (Godbole et al., 2018) conducted a study on the dynamic loading that occurs on the modules during transportation to investigate the vehicular vibrations on the truck-trailer, which may cause damage to the components attached to the unit. The study focuses on different parameters such as the level of loading on the vehicle, location of the centre mass, suspension setup of the truck-trailer, and the amount of damping of the vibrating parts. This is done through modelling the road roughness as a stationary Gaussian process to obtain the acceleration response spectrum. The study found that components should be designed to withstand $32\ m/s^2$ of vertical acceleration in both directions, in addition to the gravitational acceleration, in order to be able to withstand the acceleration the truck experiences. Cost analysis is an essential when it comes to planning construction, thus, (Lopez and Froese, 2016) performed a cost and benefits analysis of panelized and modular prefabricated homes. The study's objective was to provide a framework of the advantages and disadvantages of the panelized and modular construction techniques to build single-family homes with similar characteristics. Panelized homes identified advantages when it comes to transportation, equipment, machinery, and insulation technology. In contrast, modularized homes excelled in quality control and on-site work and trades. The study found that modular homes are marginally more cost-effective in the case study analyzed with the circumstances considered, thus, proving the possibility of evaluating the cost-effectiveness of different construction techniques. (Kamali and Hewage, 2016) investigated the environmental performance of modular buildings throughout their lifecycle. The study compares modular and conventional construction techniques to outline both methods' challenges and benefits. The study found that, on average, modular buildings provide a better lifecycle performance since they have advantages when it comes to energy performance. More advantages of modular buildings are outlined in Table 4.

Table 4 Summarizing advantages and disadvantages of modular buildings (Kamali and Hewage, 2016)

	Parameters	Description
Advantages	Time	• Continuous construction work • It is not dependent on the weather
	Cost	• Less site overhead and congestion • Machinery transportation cost reduction • Labour transportation reduction
	Quality	• Controlled manufacturing facility • Automated machinery • Less exposure to the elements while in production
Disadvantages	Planning	• More project planning is required • Hard to make changes later
	Transportation	• Module's dimension constraints • Long-distance transportation • Requires permits when producing oversized components
	Site restrains	• Site accessibility • Requiring cranes access on-site • Labour availability in the area

(Ma et al., 2021) investigated the mechanical properties of a modular connection with superimposed beams. The study was conducted experimentally and numerically to assess the mechanical behaviours of the proposed connection within modular units, as shown in Figure 2.23. The connection focuses on connecting modular units to columns in both vertical and horizontal directions using an in-build component. The connection can utilize the floor beam of the upper units and the ceiling beam of the bottom units into an integrated system, with the advantages of easy installation without on-site welding, as shown in Figure 2.24.

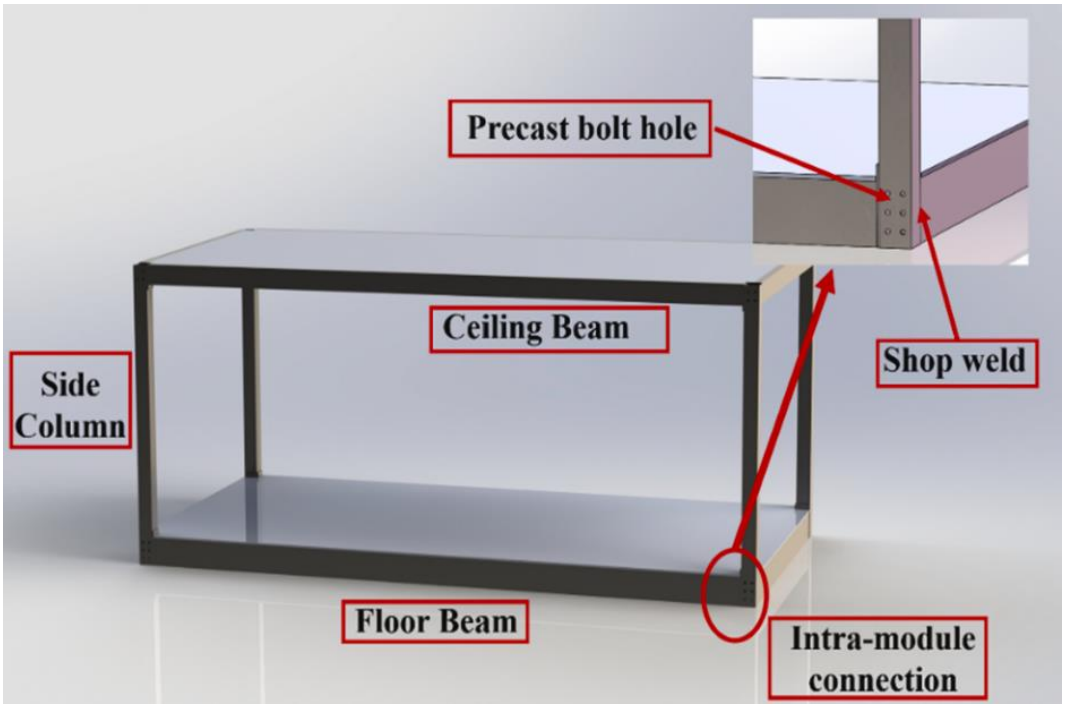

Figure 2.23 Single modular unit (Ma et al., 2021)

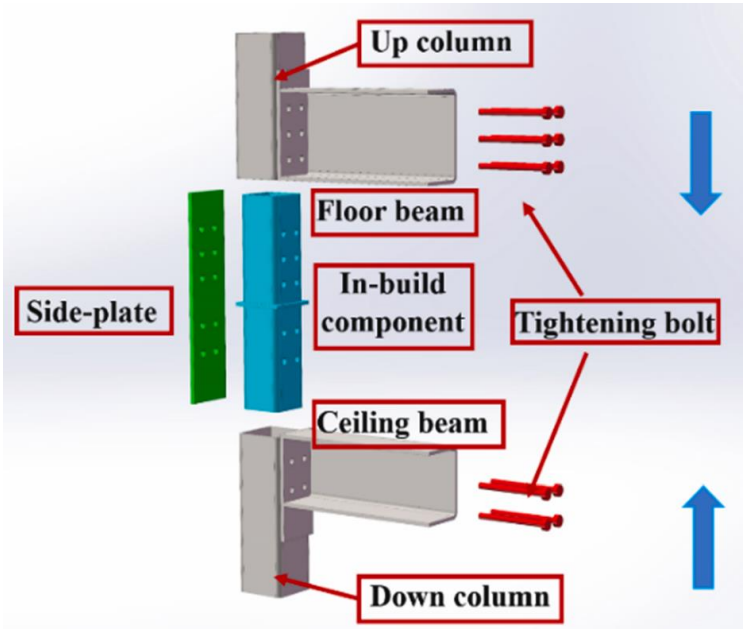

Figure 2.24 Proposed Type-A modular connection (Ma et al., 2021)

The study found that the proposed connection could allow the twin beams to rotate identically, ensuring the combined action of twin beams in the modular structure. At the same time, the main factors impacting the design of such connections are the twin beams' flexural stiffness ratio and the gap between the in-build component and column.

2.4 Summary

This chapter has discussed various aspects to consider when designing modular structures for healthcare applications. The first aspect to consider is the design of the ventilation system, which is done by utilizing the Lagrangian physics model to inject aerosols into the modular room and investigating the parameters impacting aerosols' destination, which will be presented in Chapter 3. Another aspect is the evaluation of wind load developed on different modules within a fishbone layout to identify the critical locations that experience higher load intensities, which will be adopted in Chapter 4. This chapter concludes with a previous study concerned with the design of modular structures, which highlights the need for accurate quantification of loads on modular structures, achieving better utilization for members and connections used in modular structures, and demonstrates the ability to create different modules grades that match different load intensities to optimize the modular structures in the healthcare applications.

Chapter 3 Ventilation System and Aerosols Simulation

3.1 Introduction

As the number of cases keeps on rising, the government of Canada has been working endlessly to limit the spread of the virus by implementing new laws and rules such as face mask requirements in public places and social distancing. Since hospitals are facing the challenge of the shortage of care beds, which in turn increases the number of mortalities, especially for people who suffer from other health conditions (Shoukat et al., 2020). Since the virus can be transmitted within indoor enclosures, it is vital to be able to track mouth-generated aerosols in an air-conditioned indoor environment such as hospital wards since they do not experience any increased temperatures that can lead to the evaporation of the medium carrying the pathogens which is water. Therefore, accumulation of viral loads can occur on surfaces, and the drying out process will slow. To assess the performance of the ventilation system in place, different approaches can be adopted to achieve appropriate results. Methods such as: (i) full-scale measurement, (ii) wind-tunnel testing, and (iii) numerical modelling (e.g., computational fluid dynamics (CFD)). The full-scale approach relies on a real situation where the complexity of the problem is taken into account. However, it provides less control over boundary conditions and a finite number of measuring points and can also be challenged by the limitations of the equipment used (i.e., the use of image processing to track particles), which can be very challenging if not conducted properly. As for the wind-tunnel approach, it provides control over the boundary conditions, although it can be costly to conduct, and the limitation lies in the number of points to be monitored. On the other hand, CFD provides full-scale numerical simulations, thus, providing comprehensive flow-field data of the investigated parameters while having the ability to alter the design without constructing a physical model. With the increasing number of applications, CFD has gained a lot of popularity in atmospheric and environmental processes, as the design methods advanced. CFD has been utilized in various wind engineering-related applications, including simulation of the flow field around structures (Elshaer et al., 2016; Tamura, 2008), pedestrian level wind(Adamek et al., 2017; Joerg, 2006), pollution dispersion (Tominaga and Stathopoulos, 2013), and assessing the viral contamination and air quality (Bhattacharyya et al., 2020; Szczepanik-Scislo and Schnotale, 2020), which is the focus of the current study. These latter applications rely on a Lagrangian approach, where a continuous phase (i.e., air) interacts with a discrete phase (i.e., water). The interaction does not include a reaction between the materials, but how they interact with each other in space. In many cases, CFD

can be used to understand certain behaviours and interactions between two phases (i.e., particle evaporation, break-up behaviour, and fluid film formation). This study utilizes CFD to understand the effect of the air ventilation rate on particles' destination, and the placement of the ventilation system to achieve an appropriate understanding of the mouth-generated aerosol propagation within a modular room. Many studies have adopted this approach to examine the effect of the surroundings on mouth-generated aerosols. For instance, (Blocken et al., 2020) conducted a study about the effect of mouth-generated aerosols while running outdoors with the social distancing of $1.5\ m$, and how the pattern of running and the distance between the leading person and tailing one can impact the exposure. It was found that as the distance between the leading and tailing person decreases, the exposure increases, which leads to the recommendation of running in a segregated side by side arrangement or keeping a larger distance to avoid the exposure.

The rate at which the volume of air being exchanged can impact the final position of aerosols in the ward (B. Zhang et al., 2020). In general, the health care system can be branched into three different components: (i) equipment, (ii) personnel, and (iii) space. As for the COVID-19 pandemic, the required equipment may include ventilators, which have been a major challenge to secure during the surge of this pandemic. Accordingly, there was a race to purchase and produce more ventilator units to respond to this critical need (Center for Devices and Radiological Health, 2021). As for personnel, retired doctors and nurses were asked to provide their service in addition to recruiting doctors from other specialties to cover COVID-19 wards (Zhou et al., 2020). While for the space challenge, modular buildings can be the solution as it has the advantage of being able to be quickly transported and rapidly deployed in targeted regions. However, they need an appropriate assessment of their performance in terms of room layout and achieving proper infection control by altering the ventilation rate (i.e., ACH) of the room, and the placement of the system inlet and outlet (Curry, 1990). When it comes to construction, structural performance, sustainability, and economic and social costs are important factors that aid decision-makers in proceeding with a design and comparing it with the conventional equivalent. Building construction relies on the extensive consumption of natural resources, leading to increased environmental emissions (Apuzzo and Kirkpatrick, 2020). Modular construction is an efficient building technique that utilizes pre-engineered building modules mainly volumetric units that represent structural elements of a building (typically produced off-site) that are assembled on-site to form different types of structures as shown in Figure 3.1 (a), including houses, tall buildings, and bridges. This

enables the use of a wider range of materials (e.g., timber, steel, concrete, and composites) and design techniques while maintaining higher quality control on the produced structures (Zhou et al., 2020). Since components are produced off-site in factories and transported to the site destination for assembly, that helps improve the reduction in waste material, improve safety, and minimize the building time (Innella et al., 2019; N.Usefi et al., 2021). Moreover, using hybrid cold-formed steel modular structures can aid in increasing sustainability and structural performance while reducing cost (Smith et al., 2010). The global market size of modular construction in 2018 was valued at 112.3 billion USD (Innella et al., 2019). MC provides flexibility in design and the ability to comply with different design requirements. MC can be characterized by three principles: standardization, dimensional coordination, and prefabrication. This enables construction to move from craft base to manufacturing base (Innella et al., 2019; N.Usefi et al., 2021). MC structures can be categorized into three main types: (i) componentized which allows for the greatest degree of design modification, however, the increasing number of components on a construction site can lead to added complexity in the design, as they require more joints, connections which increase the chance of misalignment, thus reducing the quality of the structure. (ii) Panelized (two-dimensional) which offers the capability of using a panel's cavity for the distribution of services such as plumbing, and electrical. They also offer a better-finished product than componentized as they are less likely to have visible marking where the joints are located. (iii) Modularized (three-dimensional) 95% of the work is completed in the factory, in the case of shipping three-dimensional volumetric units that can be joined on-site, since the assembly is mostly done at the manufacturing facility (N.Usefi et al., 2021). While MC can be used to form structures for different purposes and uses (i.e., residential, schools, hospitals); it also provides the capability of forming a high-rise structure, such as the building of Clement Canopy in Singapore, which sets an example for one of the tallest buildings that adopted the concept of MC. The building was made using prefabricated pre-finished volumetric construction (PPVC) system. Walls, floors, and ceilings are prefabricated and erected on-site, while the majority of the construction was done off-site. The structure consists of 1,866 modules, assembled as two 40-story towers (Zerndt, 2017). Bradford Royal Infirmary hospital is another example of a healthcare facility that utilized MC as the main construction method in one of its buildings. The energy efficiency and summertime overheating of the MC building have been investigated by Fifield et al. to determine the energy demand, internal temperatures, and ventilation performance. The building was airtight, unshaded,

lightweight, and well-insulated. It was found that MC provides an energy-efficient and convenient solution to the increasing demand in the healthcare systems while improving the performance of the building; better design of the architectural form and mechanical systems is needed to provide a safe and comfortable summertime environment for patients and clinical staff (Fifield et al., 2018). MC methods have been numerously used after the COVID-19 outbreak. A remarkable example of that is Huoshenshan Hospital in Wuhan, which was aimed to provide 1,000 hospital beds with an area of 34,000 m2. The design and construction were completed in only ten days and were done using rapid construction and MC (Zhou et al., 2020). Container units were assembled on-site or shipped as volumetric units. The structural build-up is shown in Figure 3.1 (b).

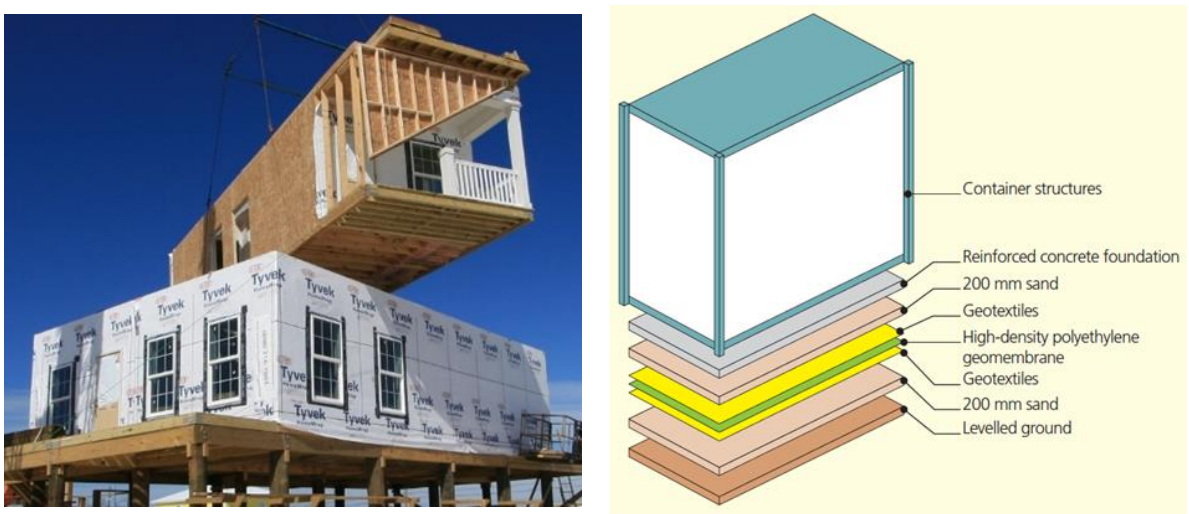

(**a**) (**b**)

Figure 3.1 (a) modular timber residential building (Modular Home Builders Association, 2021) and (b) A typical structural build-up (Zhou et al., 2021)

To further maximize the use of MC for sustainable healthcare applications, an efficient assessment and prediction tool is required to be developed for simulating the airflow and tracking the respiratory droplet transfer inside a modularly designed room. This can be enabled using high-fidelity computational fluid dynamics (CFD)-based modelling, which allows the assessment of the infection control abilities in the developed system. As discussed earlier, assessment of particle transmission within a health care facility is crucial for ensuring the safety of patients. Accordingly, the current study aims at designing a modular solution for expanding the capacity of available hospitals by providing pre-engineered units that can be deployed promptly while ensuring

adequate infection control within the designed facilities. The study examines the effect of changing the ventilation system efficiency by examining different levels of ACH. In addition, different locations for the ventilation units (i.e., inlets and outlets) are assessed to improve the flow circulation within the designed room. The chapter is divided into five sections. Section 3.1 (this section) reviews COVID-19 and its impact on the healthcare system while providing a comprehensive literature review about MC. Section 3.2 focuses on the numerical model details and provides the assessment method used in this study. Details about the validation of the adopted numerical model are provided in section 3.3. In contrast, section 3.4 focuses on a case study that involves the assessment of a modular room using multiphase Lagrangian CFD modelling. Finally, section 3.5 summarizes the chapter.

3.2 Numerical Model Details

To perform the study of aerosol transport and propagation in an air-conditioned space, a three-dimensional, transient, turbulent multiphase CFD model was developed. The numerical simulations were conducted using Simcenter STAR-CCM+ 2020.2 (15.04.008-R8), which was provided by Siemens. The simulations were performed on SHARCNET, which provides supercomputers that are efficient in performing different numerical simulations. The adopted numerical characteristics followed the study by (B. Zhang et al., 2020). To numerically model the injection of saliva particles, a Lagrangian model was used to model the flow of liquid droplets within the airflow field, which lasted for 1.0 seconds (i.e., cough duration). A discrete phase model was used to inject saliva into the domain, as for the enclosure of the room, it was modelled using the continuous air continuum. The gas continuum consisted of air with a density of $1.18\ kg/m^3$ at a static temperature of $18°C$, while the discrete phase of the droplets consisted of a liquid with a density of $1028.89\ kg/m^3$ at a static temperature of $37°C$ (i.e., typical human core temperature). The saliva consists of water, glycerin, and sodium with mass ratios of $1000:76:12$, respectively (B. Zhang et al., 2020). Since the particles generated from the mouth are typical of two main sizes (i.e., coarse and fine), two circular injectors with an area of $500\ mm^2$ are placed in front of the mouth boundary condition. These two injectors would eliminate the uncertainty added from the break-up behaviour, or have particles collide with each other upon injection if one injector was used. One injector is used to produce fine particles with a constant diameter of $5.0\ \mu m$. In contrast, the other is used to inject coarse particles following Rosin-Rammler distribution (Rosin and Rammler, 1933) with an average diameter of $170\ \mu m$, a minimum diameter of $77\ \mu m$ and a

maximum diameter of $737\ \mu m$. Both injectors are set to be at $37°C$ (i.e., typical human core temperature) with a flow rate of $5\ mg/s$. Since the gravity model is enabled, particle size will impact the destination of the particles. To model human breath, a function simulating tidal breathing was used and is represented as shown in Equation 1.

$$v(m/s) = 2.9sin(1.28t) \quad \text{Equation 1}$$

This function is time-dependent to account for inhaling and exhaling. Except during the cough, as the mouth velocity becomes $10\ m/s$ for one second (B. Zhang et al., 2020). The room inlet and outlet boundary conditions vary across the studied simulations depending on the ACH rate, the room geometry, and the vent sizes of the system. The simulation duration is 80 seconds, where the first 20 seconds are discretized into 0.1 seconds since the cough has not been introduced to the computational domain. After this, the remaining 60 seconds utilize a time-step of 0.005 seconds to satisfy the Courant-Friederichs-Lewy (CFL) number below 1.0 (Courant et al., 1928) to ensure the convergence of the solution.

3.3 Validation Model

To validate the numerical models used to simulate the propagation of mouth-generated aerosol in a modular room, a study conducted by (B. Zhang et al., 2020) involving a comprehensive comparison between a full-scale experimental system and CFD simulation of an air-conditioned chamber, was used to assess the transport and the trajectory of cough-induced aerosol. The chamber geometry is $2.9\ m$ long, $2.3\ m$ wide and $2.0\ m$ high, which includes four manikins sitting on chairs to simulate a gathering, as shown in Figure 3.2.

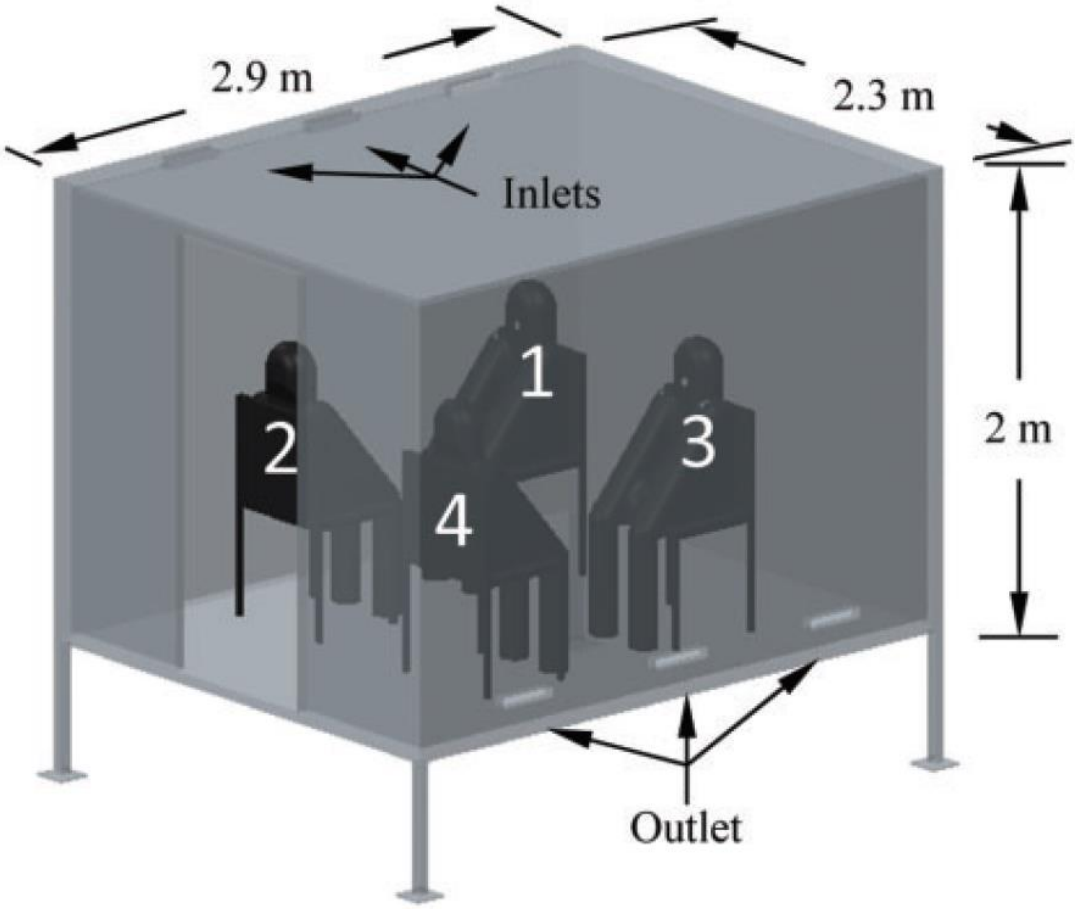

Figure 3.2 Geometric details of the validation model (Zhang et al. 2020)

Following (B. Zhang et al., 2020), The study was conducted under different ACH rates (i.e., 10, 20 and 40), which reflects the quality of air ventilation of the room. The simulation included two scenarios where mouth-generated aerosols were assumed to be initiated by either manikin 1 or manikin 3 under the same ACH rates. This has been designed to examine the impact of the boundary conditions on aerosol propagation and how being near the inlet or the outlet changes the destination of the aerosols. Six models were constructed using CFD, three models involving manikin 1, as seen in Figure 3.2, coughing under different ACH rates. In comparison, the other three models involved manikin 3, as seen in Figure 3.2, coughing under different ACH rates. It was determined that as the ACH increases, the stronger air movement would prevent direct aerosol inhalation under various coughing conditions. It was apparent that the mouth-generated aerosols from manikin 1 caused more aerosols inhalation under 10, 20, and 40 ACH as it is located near

the inlet, with percentages inhaled of 1.96%, 0.36%, and 0.2%, respectively. While the mouth-generated aerosols from manikin 3 caused aerosols inhalation of 0.86%, 0.76%, and 0.69%, respectively. It was also observed that as the ACH rate increases, more aerosols get carried back into the recirculation system. For instance, mouth-generated aerosols from manikin 1 caused fewer aerosols to be carried out of the outlet back into the ventilation system recirculation with percentages of 4.5%, 5.8%, and 22.9%. While mouth-generated aerosols from manikin 3 were significantly more at 8.5%, 10.3%, and 32.7%, respectively, due to it being closer to the outlet. Figure 3.3 demonstrates the differences between aerosol percentages at different rates for both mouth-generated aerosols from manikin 1 and 3.

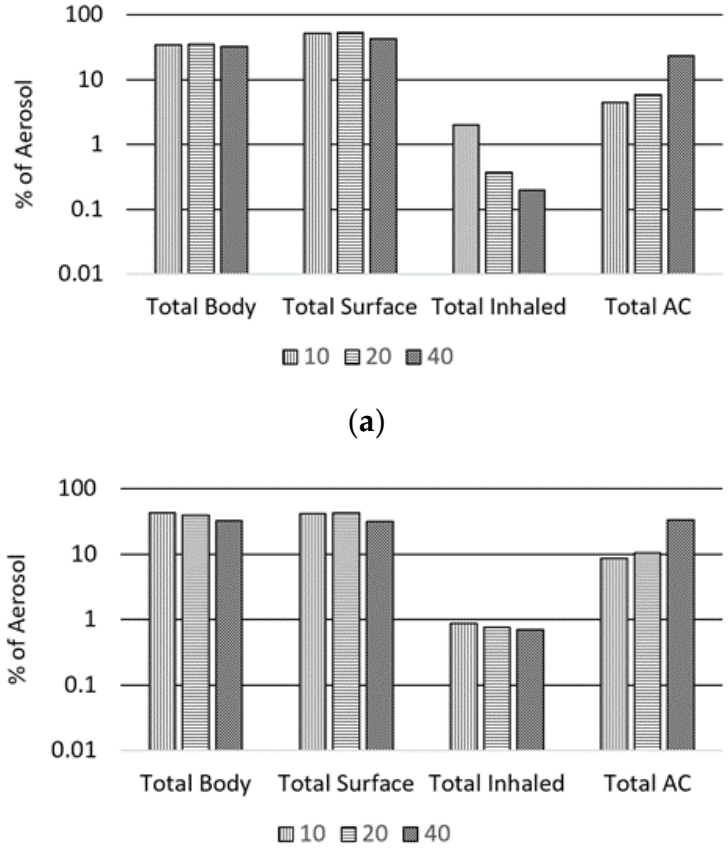

(**a**)

(**b**)

Figure 3.3 Summary of aerosol destination of (a) Manikin 1 and (b) Manikin 3 (adopted from Zhang et al. 2020)

Based on these results, a similar room configuration was modelled, and boundary conditions were set as shown in Figure 3.4, using the flow characteristics described in section 3.2 to validate the adopted numerical simulation using the reported experimental values.

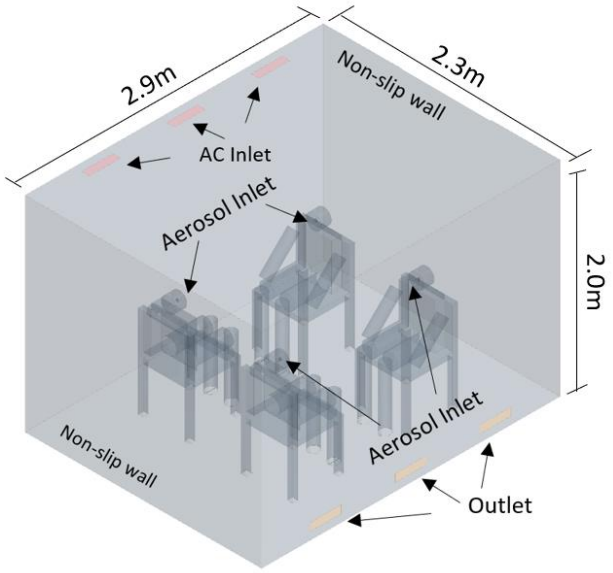

(**a**)

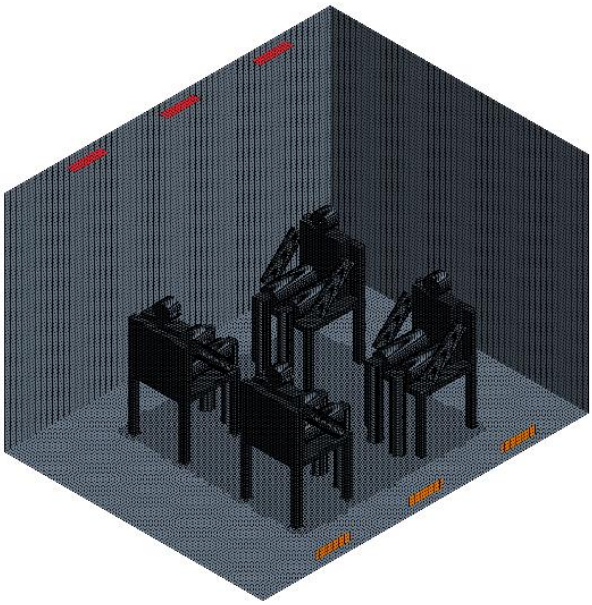

(**b**)

Figure 3.4 (a) Boundary conditions and (b) grid resolution used in the validation model

In the validation model, the mesh adopted was based on a mesh sensitivity analysis conducted by Zhang et al. (2020), based on four different mesh densities of 1 million, 1.5 million, 2 million, and 2.7 million. It was observed that for a total cell count of 2 million, the solution field tends to stay stable. Thus, the computational domain was spatially discretized into hexahedral meshes of $25\ mm$ and was further refined at the area near the aerosol injection to meshes of $10\ mm$, which yielded a total number of 2.5 M cells. Figure 3.5 shows the aerosol destination percentages calculated as the ratio between the mass of the particles passing through a boundary to the summation of the mass of the particles going through all other boundaries. Figure 3.6 shows a visual propagation of the mouth-generated aerosol with time. After running the validation models, it was observed that as the ACH rate increases, a similar trend was observed as fewer particles are being inhaled due to the influence of the AC. Under 10, 20, and 40 ACH, the percent inhaled for the mouth-generated aerosols from manikin 1 was 3.13%, 2.01%, and 1.9%, respectively, while the cough from manikin 3 was 2.84%, 2.9%, and 2.34%, respectively. This variation in following a similar trend is attributed to the ability of the numerical model to monitor smaller particle sizes compared to the experimental setup, which physically measures the collected particles at the receiver's end, in addition to the potential difference in the adopted geometry between the experimental and the numerical results. It is also worth mentioning that the quantity of aerosol collected at the outlet was observed to increase with the increase in the ACH for both the aerosol injection from Manikin 1 and 3. However, it is noted that the increase in exiting aerosols in the case of Manikin 1 compared to Manikin 3 is attributed to being nearer to the inlet of the ventilation system, which can be noticed in Figure 3.5.

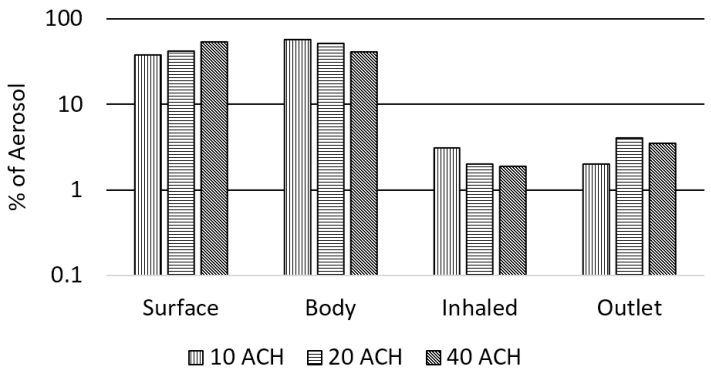

(**a**)

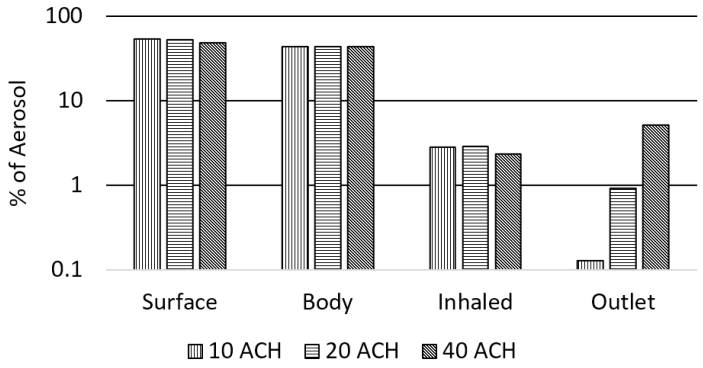

(**b**)

Figure 3.5 Summary of aerosol destination percentage of (a) Manikin 1 and (b) Manikin 3

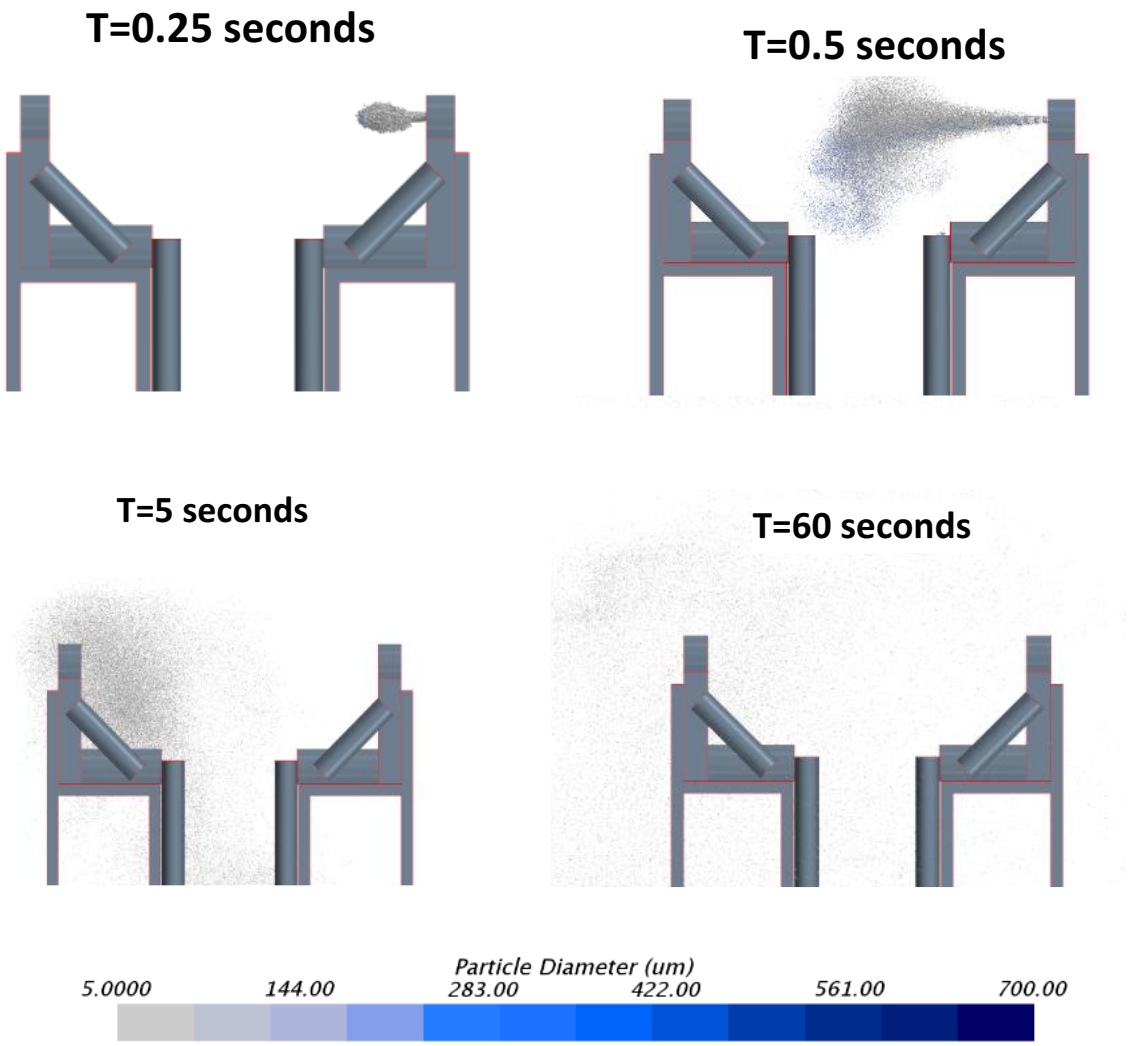

Figure 3.6 Propagation of aerosol particles in the validation model with time

To further understand the validation process, error quantification was done based on twelve different boundary conditions and configurations adopted in the validation. The overall average error calculated based on the percentage of aerosols was found to be 2.66%. Figure 3.7 shows the difference between the validation obtained in this study compared to (B. Zhang et al., 2020) for different ACH rates and cough injecting Manican.

While the validation model yielded similar trends to the case study done by (B. Zhang et al., 2020), it is essential to note that this variation can be due to different factors (i.e., the Manikin model used, humidity in the room). Since the focus of this study is on the distribution of mouth-generated

aerosols within a modular room, the humidity was not considered, as it can increase the coagulation, thus increasing the size of aerosols, which can lead aerosols to land on near surfaces.

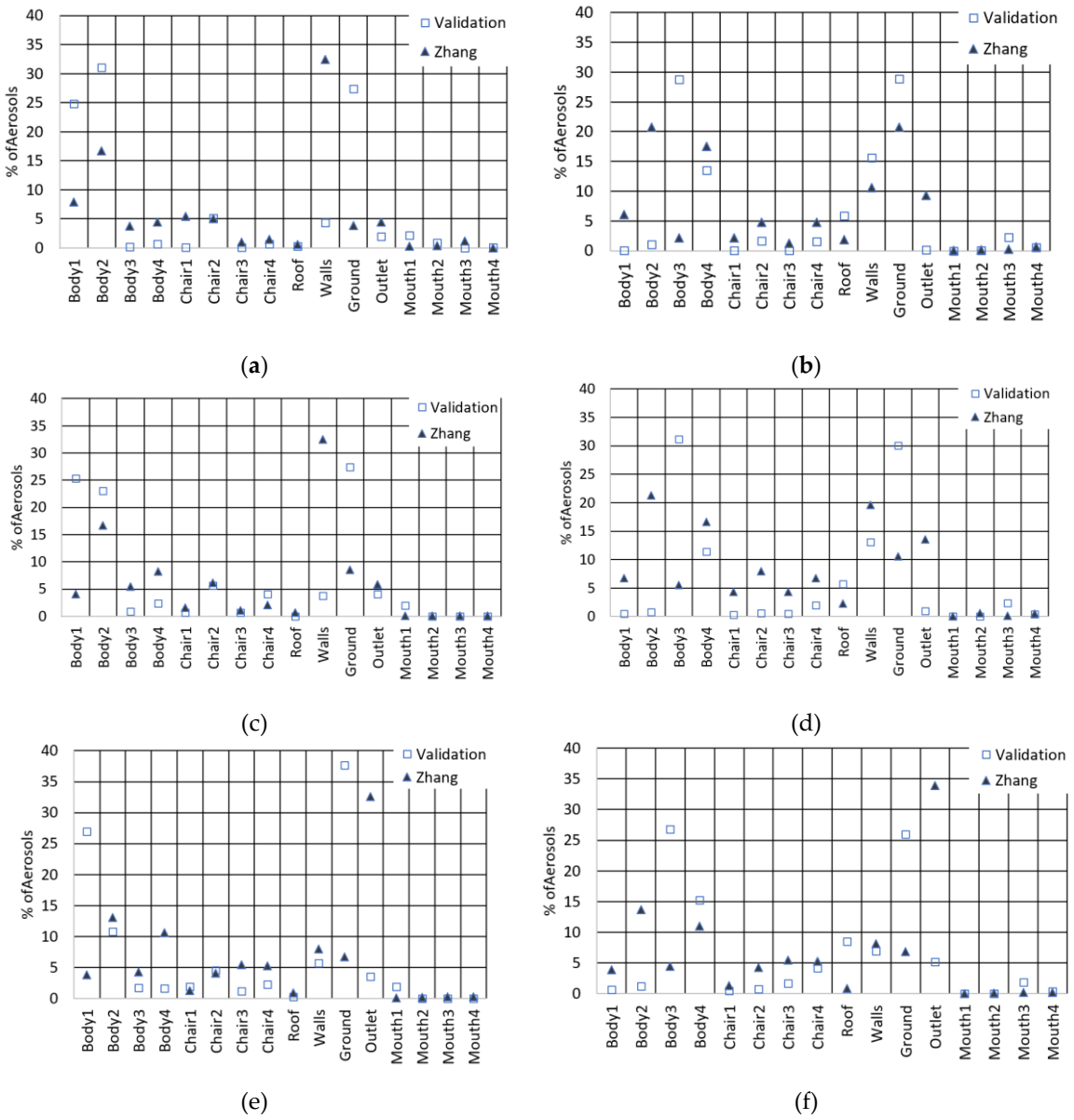

Figure 3.7 (a) Manikin 1 under 10 ACH (b) Manikin 3 under 10 ACH (c) Manikin 1 under 20 ACH (d) Manikin 3 under 20 ACH (e) Manikin 1 under 40 ACH (f) Manikin 3 under 40 ACH

3.4 Case Study and Discussion

3.4.1 Effects of Changing the Ventilation Rate

The geometry of a health care room is a governing aspect when assessing infection control as it dictates the required ventilation system parameters (i.e., inlet and outlet geometries and their flow characteristics). After designing the MC room, the dimensions were set to be $6.1\ m$ long by $2.5\ m$ wide and $3.0\ m$ high. The room represents the computational domain in the simulation, as the droplet transfer takes place inside the room. Figure 3.8 describes the room dimensions and the boundary conditions of the computational domain.

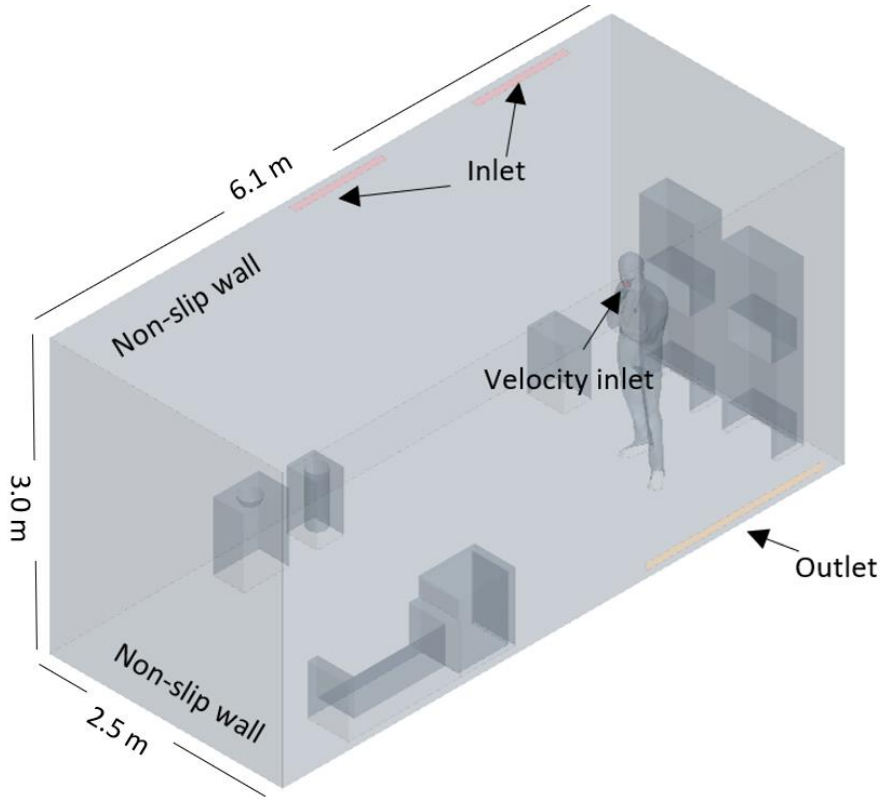

Figure 3.8 Layout for the modular construction room and its boundary numerical conditions

Based on the validation model and the adopted mesh sensitivity analysis, the computational domain was discretized into three zones according to the mesh sizes, as shown in Figure 3.9. Since Zone 1 is the closest to the injecting mouth, it adopted a mesh size of $10\ mm$, which has maintained

a similar refinement to that of the validation model. While Zone 2 and 3 have adopted courser mesh sizes of 30 mm and 75 mm, respectively since they have less influence on the flow while maintaining the satisfaction of Courant number (Courant et al., 1928) below unity.

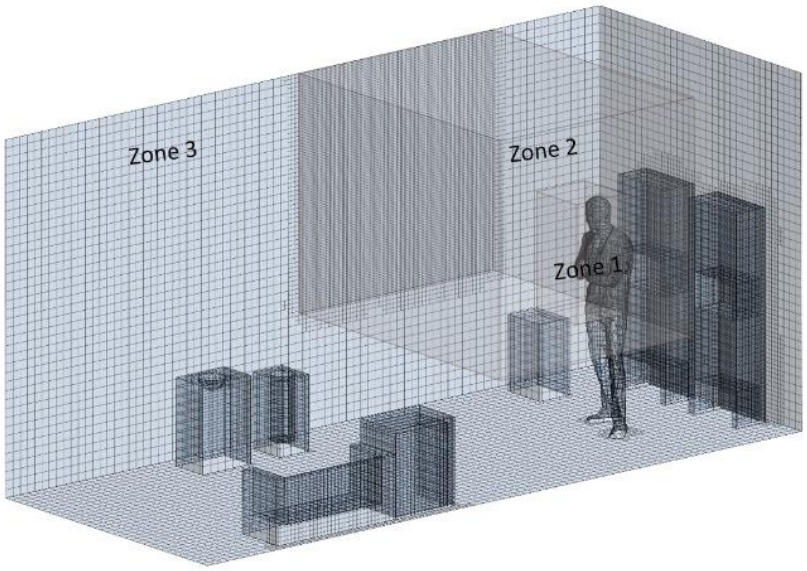

(**a**)

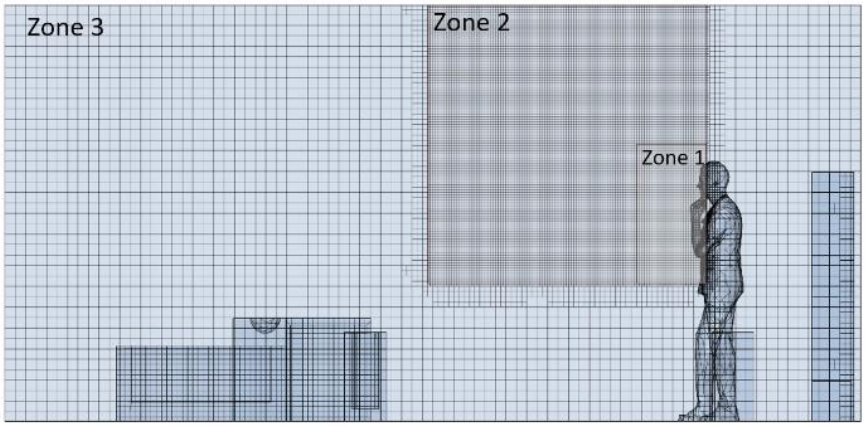

(**b**)

Figure 3.9 A volumetric representation of the finer mesh details (a) a representation of 30 mm mesh zone (b) a representation of 10 mm mesh zone

A mesh independent analysis was conducted to ensure the appropriate use of mesh sizes adopted in the simulations. Two simulations of the typical room were used with an ACH rate of 40 to

perform the mesh sensitivity analysis. The first simulation represented coarse mesh with a base size of 75 mm; as for the fine zone, only one zone was adopted near the subject to ensure an appropriate mouth opening consistent with the original simulation. This yielded a total number of 460,000 mesh cells. As for the finer mesh adopted, the base size used was 60 mm with two finer zones of 20 mm and 10 mm near the subject. This yielded a total of 3,860,000 cells. After processing the results, it was apparent that the mesh size adopted in the original simulation was adequate, as shown in Figure 3.10 below. Boundary conditions across the simulation remained consistent, except for walls, ground, and outlet; this can be attributed to the mesh size being too fine or too coarse, which could cause the particles to cell skip as that violates the Courant-Friederichs-Lewy value, which ultimately alters their final position. Since the time-step remained the same across the simulation. The method of quantifying the particles near the boundary conditions depends on a surface integral function that is also linked directly to the time-step to track particles on boundary conditions. Mesh 1 represents the mesh utilized in this study, Mesh 2 represents the coarser mesh, and Mesh 3 represents the finer mesh.

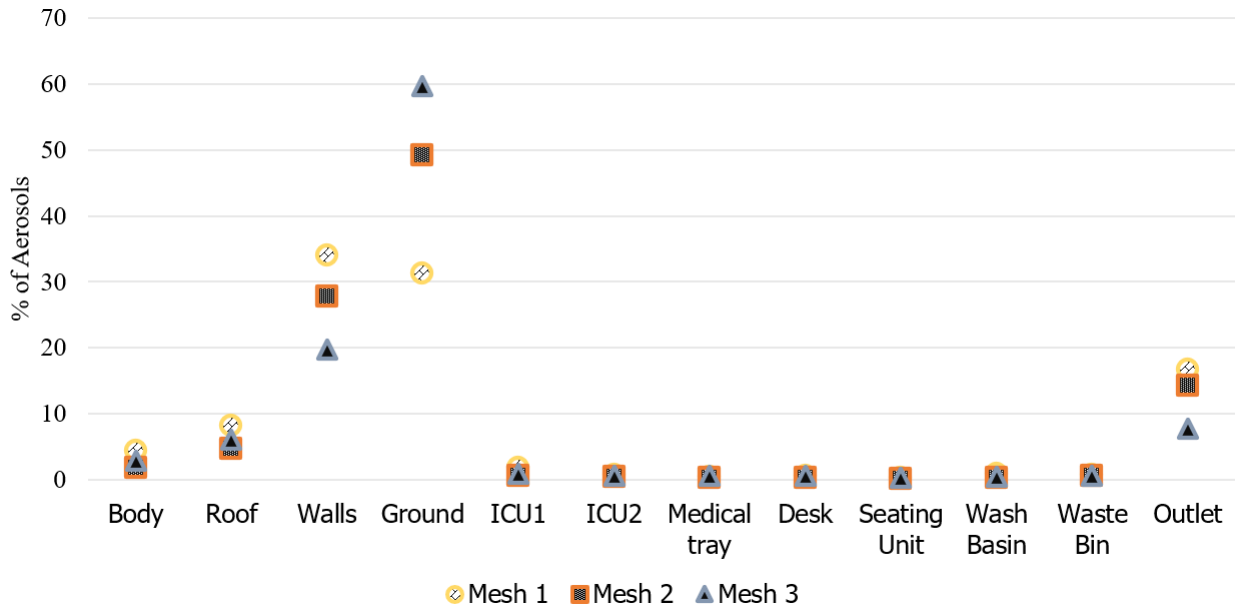

Figure 3.10 Mesh sensitivity analysis results

There are three governing boundary conditions of concern in this simulation, which are: the mouth, the system inlet, and the system outlet. The remaining boundary conditions are set to non-slip wall

conditions, as demonstrated in Figure 3.8. The ventilation system inlet is located on the roof of the room with two openings with dimensions of $1{,}000\ mm \times 64\ mm$ located $80\ mm$ away from the left wall and $610\ mm$ away from the back wall. Openings are placed $1{,}000\ mm$ apart from edge to edge. The velocity of the system inlet was calculated based on the ACH rate. In this case, 10, 20, and 40 ACH required velocities of $1.02\ m/s$, $2.04\ m/s$, and $4.08\ m/s$, respectively. The inlet was adjusted to be inclined downward at an angle of 30° from the horizontal plane. The ventilation system outlet is located on the right wall with dimensions of $2{,}000\ mm \times 64\ mm$ and placed $80\ mm$ away from the floor and $190\ mm$ away from the back wall. The outlet boundary condition was set as a pressure outlet with negative pressure calculated using the inlet velocity and the air density of the room to maintain constant air mass within the room. The suction pressure at the outlets was set to $-0.62\ Pa$, $-2.47\ Pa$, and $-9.88\ Pa$ for 10, 20, and 40 ACH, respectively. Figure 3.11 illustrates the distribution of the particles and their propagation over time for the ventilation case of 40 ACH.

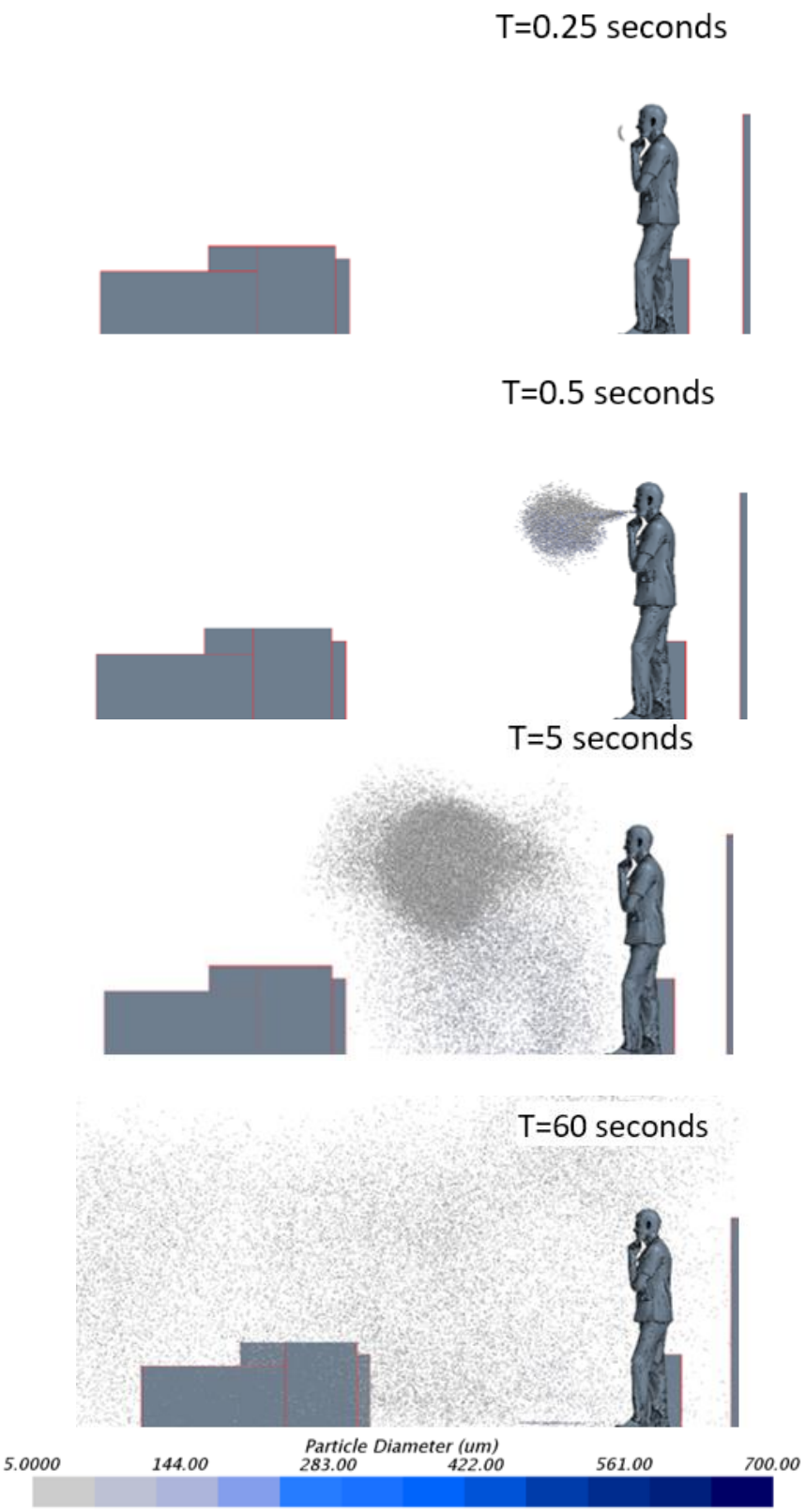

Figure 3.11 Propagation of aerosol particles in the modular room with time (10 ACH)

Figure 3.12 illustrates the impact of the ACH rate on the destination of aerosols within the computational domain. It was apparent that more particle count is exiting the outlet with higher ACH rates. The rate at which particles were exiting through the outlet increased by 41% by increasing the ACH from 10 to 20. While increasing the rate to 40 ACH yielded a 137% increase in particles leaving the outlet compared to 10 ACH. On the other hand, particles landing on equipment decreased by 19% by increasing the ACH rate from 10 to 20; also, it decreased by 25% when the rate was increased from 10 to 40 ACH.

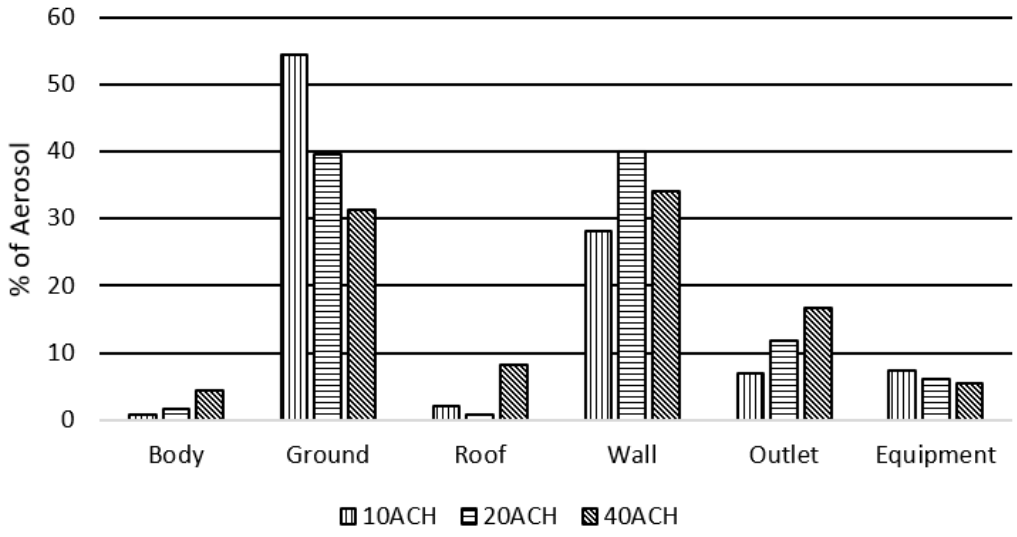

Figure 3.12 Aerosol distribution across the hospital room

3.4.2 Effect of Changing the Location of Ventilation Units

To determine the impact of changing the inlet location in the modular room, two cases of the same outlet position are to be investigated while changing the inlet position. Two ACH rates are used (i.e., 20 and 40 ACH) to enable the assessment of the performance of the placement of the vents. As recommended by the Centers for Disease Control and Prevention (CDC, 2020), the airflow within the room should be directed from the cleaner area toward the more contaminated area. It also recommended that the minimum required ACH rate for ICU to be 12. Since the facility is meant to be occupied by patients who are diagnosed with COVID-19, the focus of the study is to identify the room configuration that provides higher efficiency in contaminants removal by

altering the flow field. Accordingly, an ideal ventilation system for a hospital room is having an inlet near the front of the room. This is done to reduce the chances of having contaminants leaving the room. In the current parametric study, two configurations are demonstrated, as shown in Figure 3.13, where the first case examines the inlet to be located at the bottom of the front wall. In contrast, the second case examines an inlet located at the ceiling.

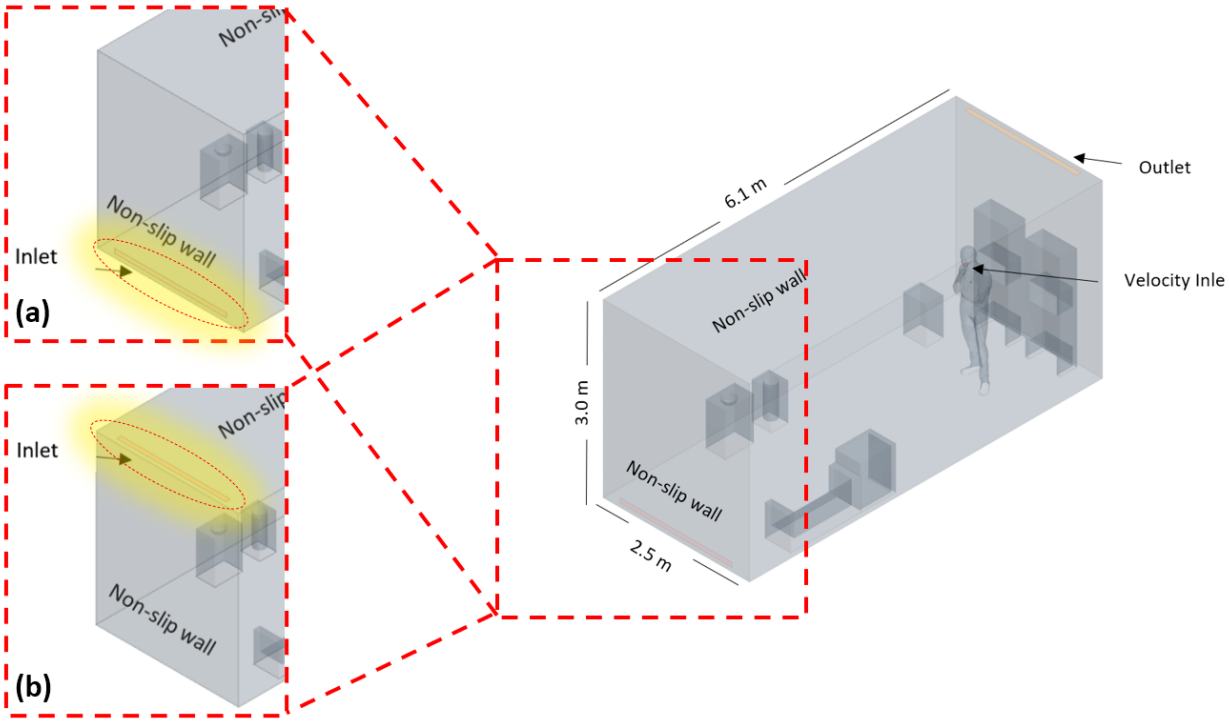

Figure 3.13 Boundary conditions of the parametric study where (a) represent the front wall inlet, and (b) represents the roof inlet

In the first case (a), the inlet is located on the roof of the modular room at 80 mm away from the front wall and shaped as a rectangular vent of dimensions 2,000 mm × 64 mm. In contrast, the outlet is of the same dimension and is 80 mm away from the back wall. In the other case (Case b), the inlet is located at the front wall and consists of 2,000 mm × 64 mm and 80 mm above the floor, while the outlet remains at the same position. Both cases involve the study of the effect of the ACH rate on contaminants removal.

After running the models, the model with the inlet at the ceiling performed the worst due to having less impact on the particles, as less than 1% of particles ended at the outlet in both the 20 and 40 ACH cases. 5.7% fewer particles landed on the ground when the ACH rate changed from 20 to 40 due to the increased suction. And since particles are required to travel further in this orientation, fewer particles were removed from the system. While the case of having the inlet at the front wall yielded the removal of at least 11% in both 20 and 40 ACH, and a 22.8% reduction in particles landing on the ground when the ACH rate increased from 20 to 40, as demonstrated in Figure 3.14, and this can be attributed to the location of the inlet, as it can directly impact the aerosols lifting them away from the ground towards the outlet. As for the overall performance of the different configurations studied, the typical room performed the best in terms of particles exiting the domain with the removal of 11.8%, and 16.7% of aerosols through the outlet in the cases of 20 and 40 ACH, respectively. As for particles landing on the walls, the typical room was observed to have decreased from 40% to 34% in the cases of 20 and 40 ACH, respectively, unlike the other configurations, where increasing the ACH rate yielded increased aerosols on walls. This can be due to having aerosols travel further in the domain, which increases the chance of particles landing on other surfaces between the inlet and the outlet.

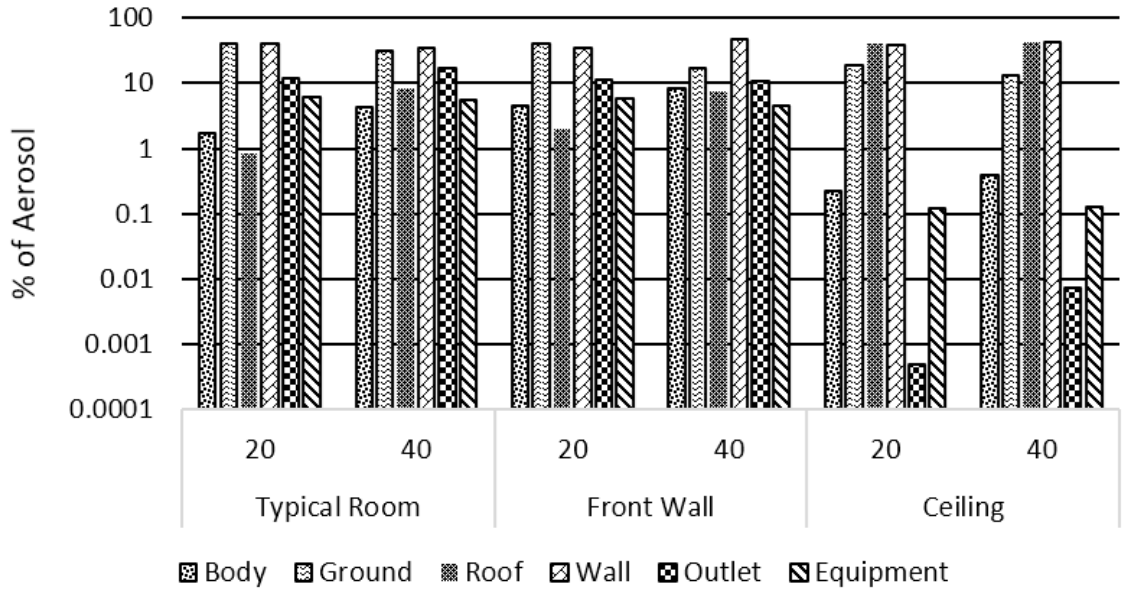

Figure 3.14 Aerosol distribution within the modular room under different ACH rates and different inlet locations

3.5 Summary

The current study examines the effect of different ventilation levels (i.e., 10, 20 and 40 ACH) in a modularly constructed hospital room by tracking the mouth-generated aerosol. It was found that as ACH increases from 20 to 40 ACH, the ability of the ventilation system to eliminate more suspended aerosol increases. In contrast, a typical room design yielded the removal of 11.8% compared to 16.7% under 40 ACH, which results in less viral load inhaled by other patients and health workers. It was also found that most of the aerosol accumulates over wall and ground surfaces, which emphasizes the importance of continuous disinfection of these surfaces. As for altering the inlet and outlet positions also impacts the aerosol destination; when having the inlet on the ceiling, the outlet performed less than 1% removal, therefore deeming the placement as ineffective. On the other hand, having the inlet at the front wall yielded as good of a performance as the typical room configuration discussed earlier; while that is true in the case of the 20 ACH rate, it is not when it comes to the 40 ACH rate, as particles have to travel less in the domain in the typical room design; therefore more particles will be exiting, as the typical room at 40 ACH achieved the removal of at least 16% of the total particles that landed on surfaces. The overall recommendation is that a typical design would be sufficient in terms of the particle's removal, there needs to be continuous disinfection. As for having the inlet at the front wall, it yielded 16% of particles landing on the ground, which is significantly higher than other configurations. Since altering the inlet position can impact the destination of the aerosols in the domain, it is recommended to have a flow field that has a shorter path so that particles can travel less, and also an appropriate ACH rate to achieve the desired contaminants removal. Higher ACH can yield better performance in general, although it strongly depends on inlet and outlet placement, as the results suggest.

Chapter 4 Wind Simulation and Modular Structures

4.1 Introduction

Modular structures have been attracting significant attention from the construction industry. They provide many advantages over conventional structures due to their speedy delivery, safer construction process, less material wastage and sustainability (Smith et al., 2010). Modular construction is a technique that involves the prefabrication of major structural components in an off-site location, then transported and assembled on-site to form various types of structures. This helps improve the efficiency of the construction process and ensures the quality of structures (Z. Chen et al., 2021; Gatheeshgar et al., 2021; Smith et al., 2010; Z. Zhang et al., 2020). Different materials can be utilized to form different structures highlighting their adaptability to the project scope. When it comes to modular buildings, three different types can be utilized depending on the project, which are componentized, panelized, and volumetric modules. In general, all building projects are typically constrained by cost limitations, which is reflected in the decisions of designers and construction professionals. The cost has three main aspects, which are material, labour, and time, whereas prefabricated buildings provide a reduction in all three. With the increasing demand for hospital beds due to COVID-19, modular buildings can be a suitable solution. They can be deployed rapidly and provide the healthcare system with the space needed to serve patients. A recent case where this technology has been adopted is Wuhan Thunder God Mountain hospital. (Z. Chen et al., 2021) reviewed the accelerated design and construction methods utilized in the hospital's construction. The hospital consists of modular composite buildings finished product to reduce the workload of field operations and save time, which in turn provided a capacity of 1,500 beds for COVID-19 patients, with the project taking a little more than ten days to complete. The project adopted a volumetric light steel structure skeleton and steel composite panels, with the mainframe beams and columns made of cold-formed steel welding. Many studies have focused on the structural aspect of modular buildings covering materials, connections (inter and intra), and types of modules. For instance, (Peng et al., 2021) performed numerical analyses of corner-supported modular buildings under wind actions using concrete-filled steel tubular columns, laminated double beams, and integrated concrete slabs in a 12-storey modular building. The study determined that this type of composite modular building can effectively improve the structural performance of modular buildings with an average increase of 21% in elastic stiffness and 33% in the maximum capacity under lateral load compared to hollow

steel sections. Another study conducted by (J. F. Zhang et al., 2020) focused on the mechanical property tests on full-scale assembled light steel modular buildings consisting of the bottom frame and top frame connected with columns and high-strength bolts. In the vertical capacity test, the modular unit failed due to the excessive flexural-torsional buckling of the four columns, which is the typical primary buckling mode. As for the bottom frame, it remained in the elastic stage indicating good deformation capacity and weak rigidity. Another example is the study conducted by (Wang et al., 2021), which aimed to test the seismic performance of the assembled light steel modular building based on joint stiffness analysis. The study was carried out through quasi-static loading using the finite element to perform stiffness analysis of the intra-modular and inter-modular connections. The study determined through the quasi-static test that the weld fractures at the connection between the ceiling beam and the corner fitting near the loading end decrease the bearing capacity, highlighting the importance of the connection quality. As for the ductility and energy dissipation for temporary buildings, capacity can be guaranteed; as for permanent modular structures, the performance is less. (Gatheeshgar et al., 2021) studied the development of affordable steel-framed modular units focusing on the enhancements of healthcare, structural and fire performance. The study focused on weight optimization for cold-formed steel joists in varying shapes, with results showing weight per unit length reduction of up to 24% without compromising the structural capacity. As for their intra connection, a novel cut and bend method was introduced to improve the faster jointing method. Strap bracing is also used for lateral stability. As for healthcare performance improvement, modular breathing panels are utilized in the corner post modules as sidewalls to improve indoor air quality. As for fire improvement, cold-formed steel joists can be utilized to control the heat transfer through the panels by increasing the heat insulation of the material. In another related aspect, a study conducted by (Gbadamosi et al., 2020) focused on isolation space creation for COVID-19 patients. Different spaces are analyzed in this case, including self-isolation at home, isolation at regular hospitals, epidemic hospitals, retrofitted buildings, temporary mobile cabins, and newly constructed temporary hospitals for COVID-19. The study is based on a mixed-method approach, which involves the analysis of secondary quantitative data and the qualitative review of literature on COVID-19. The study's outcome determined that the most effective methods of controlling the spread are through isolation in temporary mobile cabins or isolation at newbuild COVID-19 hospitals. (Suleiman et al., 2021a, 2021b) conducted a study examining the propagation of mouth-generated aerosols within a

modular room. It was determined that the main factors impacting the aerosols' final destination within a modular room are the air changes per hour rate and the flow path between the inlet and the outlet. Based on the literature, the main factors for designing modular buildings for COVID-19 patients are cost, efficiency, and structural performance. As for the cost, different modules grades can be proposed to reduce the cost and material usage through a multi-unit modular building. These grades can be categorized based on the location within the multi-unit layout of the structure, which will, in return, impact the developed load on the modules. The current study provides a detailed analysis of a multi-unit layout based on the forces developed on different modules surfaces due to wind loads. Peak forces are then compared, based on their location within the layout, to provide an understanding of how the location can impact the force development on the modules. The results can be further used to design different grades of modules, thus reducing the cost and materials used. Section 1 of this chapter (this section) covered the literature review for the use of modular construction in various applications. In contrast, section 2 covers the numerical model details, including the validation model's details concerning the geometry and physics adopted. The multi modules layout is examined, and its geometrical details are presented in Section 3. Section 4 summarizes the results obtained after running the models highlighting the significant data, and finally, section 5 concludes the summary of this chapter.

4.2 Numerical Model Details

A study conducted by (Ho et al., 2005) involved a comprehensive quality check of data obtained through experimental wind-tunnel testing compared to full-scale models. Parameters such as roof slope, building height, and building plan dimension are examined for different wind angles of attack. Mean pressure coefficient (Cp) and root mean square (RMS) pressure coefficient values obtained through wind-tunnel testing are compared to the corresponding numerical models. A validation simulation of CFD techniques is performed to assess the fidelity and accuracy of the numerical technique covered in section 2.2 of this chapter. As for the procedure, it starts with extracting the force-time history for each module within the layout, then identifying the critical forces within each force-time history obtained, followed by picking the most critical force within different wind angles of attack, and categorizing modules based on the critical wind forces, as shown in Figure 4.1.

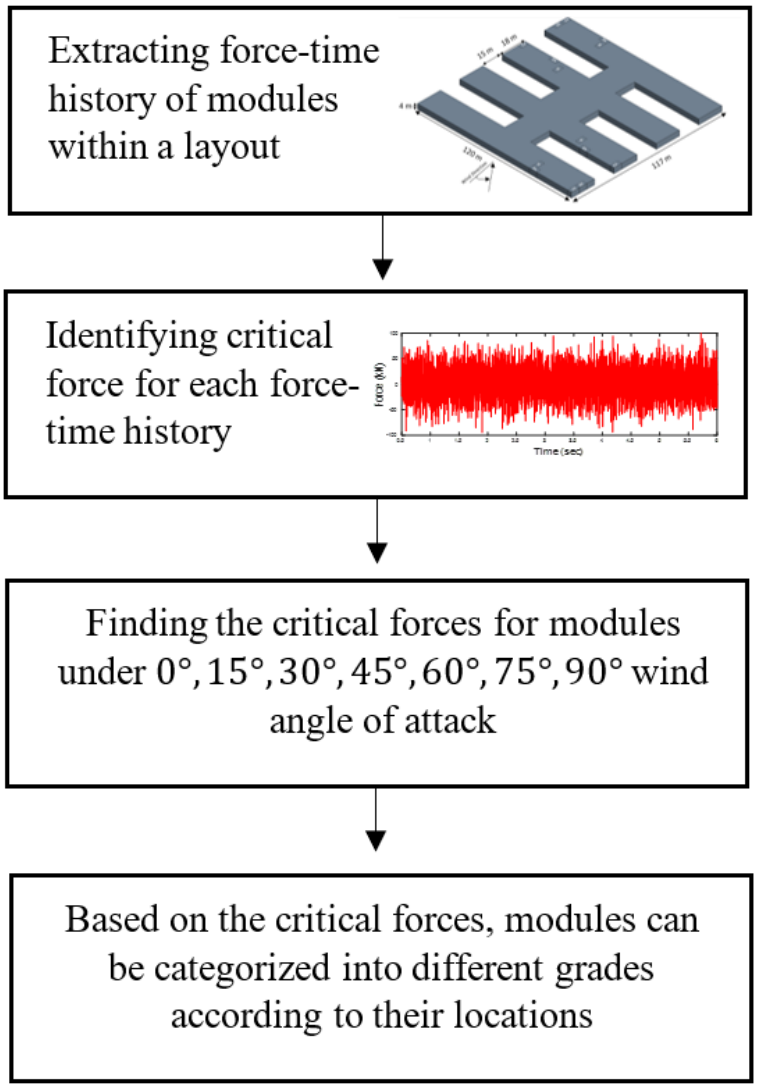

Figure 4.1 Procedure for obtaining critical forces on modules

4.2.1 Building Geometry and Details Adopted in the Validation

A gable roof building with a roof slope of 1: 12 and plan dimensions of 38.1 m × 24.4 m with a roof reference height of 7.32 m in full-scale using a wind angle of attack of 270° is used in the validation of the numerical model. As for the probes where the mean Cp and RMS Cp are collected, they are located across the roof, and they consist of 14 probes distributed on the roof surface, as shown in Figure 4.2. The mean velocity and turbulence intensity profiles are generated to match an open-terrain exposure with a roughness height (Z_o) of 30 mm with a reference velocity of 37.6 m/s at the height of 10 m in full-scale. The wind tunnel experimental study

adopted a length-scale and timescale of 1: 100 and 1: 25, respectively. The velocity and intensity profiles used in the case study matched with the wind tunnel experimental using Equation 2 for the mean wind velocity and Equation 3 for the wind turbulence intensity in the longitudinal direction.

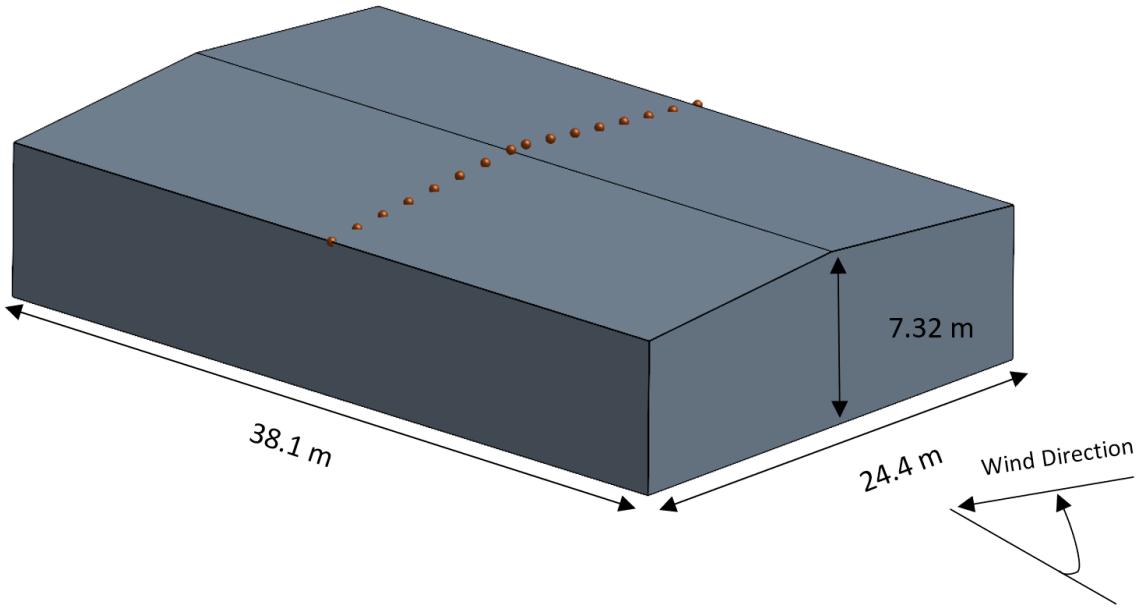

Figure 4.2 Full-scale geometric details of the validation model

$$\bar{U}(z) = \bar{U}_{ref}\left(\frac{z}{z_{ref}}\right)^{\frac{1}{\alpha}} \quad \text{Equation 2}$$

$$I_u = c_u\left(\frac{z_{ref}}{z}\right)^{bu} \quad \text{Equation 3}$$

The constants of the equations are obtained through parameters optimization, where the value of $\frac{1}{\alpha}$ which represents the exposure type is determined to be 0.13; as for the $\bar{U}_{ref}$ which is the velocity at the reference height is obtained from (Ho et al., 2005), and it is 37.6 m/s in full-scale at reference height (z_{ref}) of 10 m. As for the intensity profile, a known intensity at a select height is used as a reference to obtain the values of b_u and c_u. The adjustment parameters are optimized to minimize the overall error in matching the target profile. The values obtained for the c_u and b_u

are 0.183 and 0.17, respectively, yielding an overall error of 3.64%. The profiles are matched as shown in Figure 4.3 (a) and (b), respectively.

(a)

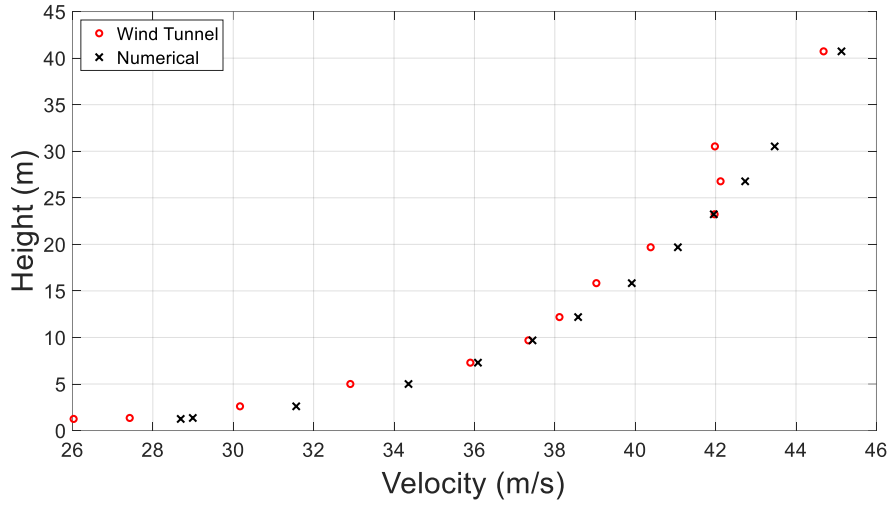

(b)

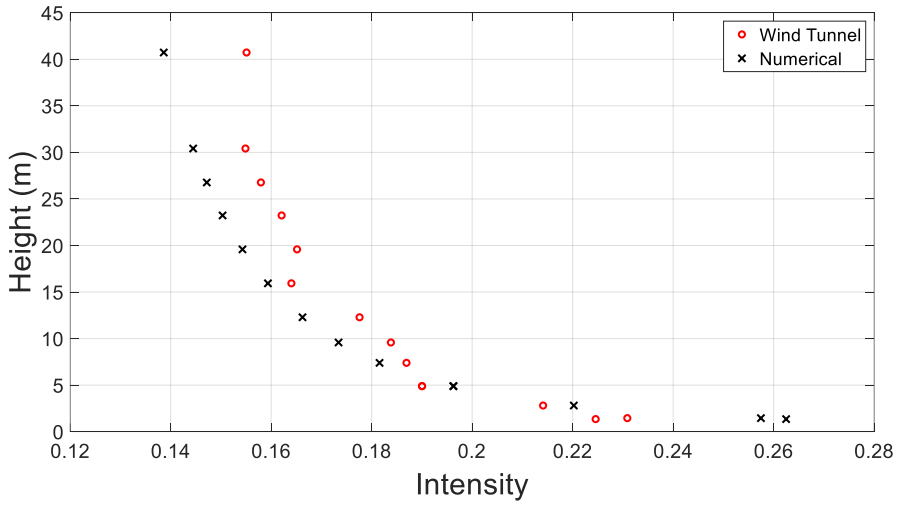

Figure 4.3(a) mean wind velocity profile adopted in the wind-tunnel experiment compared to numerical and (b) wind turbulence intensity profile adopted in wind-tunnel experiment compared to numerical

4.2.2 Numerical Details of the Validation Model

Based on the geometry explained in the previous section, STAR-CCM+ 2020.2 (15.04.008-R8) is used to perform a wind simulation following the Large Eddy Simulation (LES) turbulence modelling. Consistent discrete random flow generation (CDRFG), developed by (Aboshosha et al., 2015), is used to generate the inflow turbulence following the procedure described in (Elshaer et al., 2017, 2016). A computational domain of dimensions of $2.1\,m \times 3.5\,m \times 0.5\,m$ (in model scale) is used to perform the simulation, as shown in Figure 4.4. The building is placed $0.6\,m$ away from the inlet, and results collection started after $1{,}000$ time-steps to ensure the flow stabilization. As for the boundary conditions, the front wall is assigned as a velocity inlet, while the back wall is an outlet, sides and the roof of the computational domain are assigned as symmetry plane, as for the ground, it is set as a no-slip wall, as shown in Figure 4.4 (a). The computational domain is discretized into two zones based on the hexahedral mesh cell. Zone 1 adopted a base mesh size of $15\,mm$, while zone 2 had dimensions of $0.5\,m \times 0.95\,m \times 0.25\,m$, adopted a mesh size of $7.5\,mm$ yielding 1.36 M cells, as shown in Figure 4.4 (b).

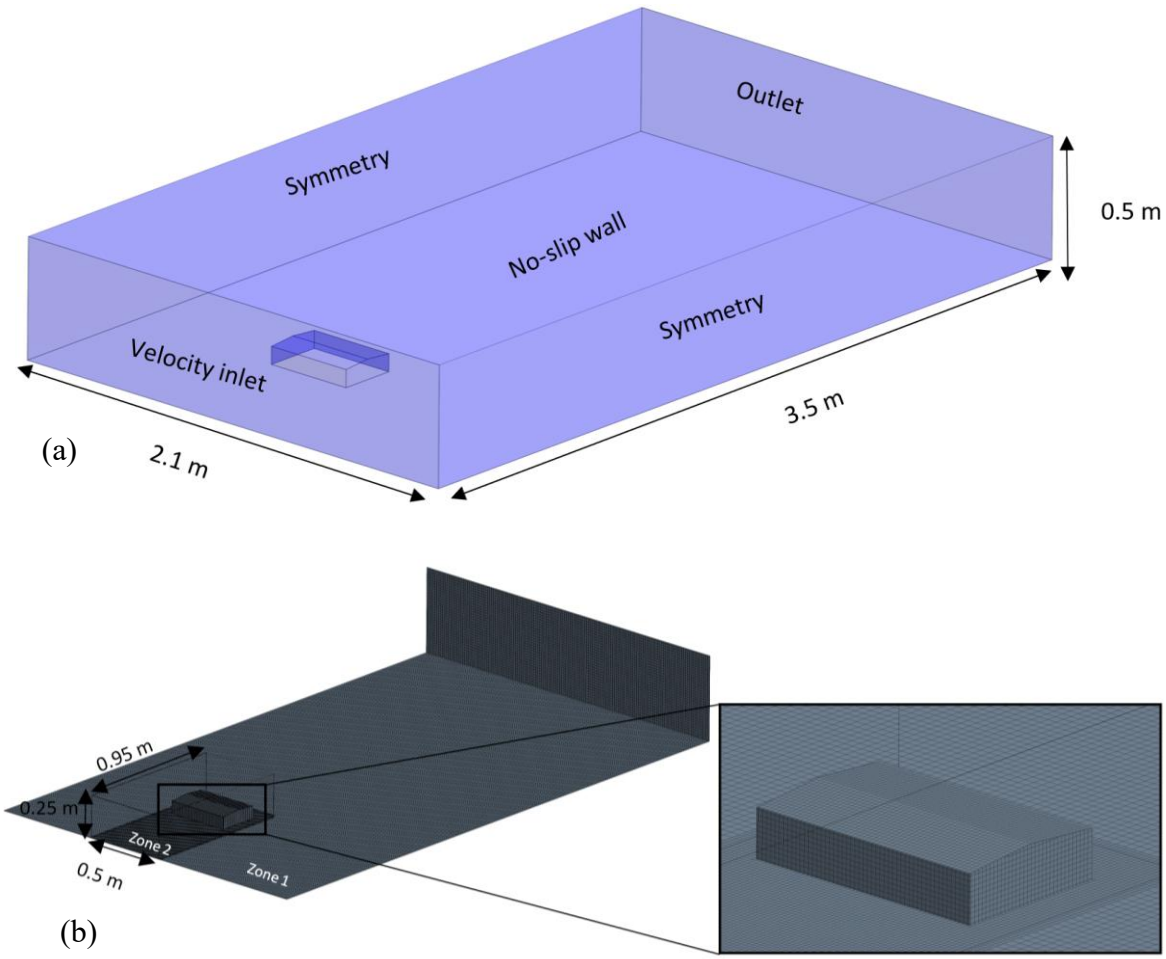

Figure 4.4 (a) Computational domain and boundary conditions adopted in the validation and (b) mesh discretization of the validation model

The simulation duration used is 10 seconds (in model scale) with a time-step of 0.5 milli-seconds with total time-steps of 20,000. The time-step is selected based on the velocity scale and the minimum cell size to satisfy the Courant-Friederichs-Lewy (CFL) number below unity to ensure the solution convergence (Courant et al., 1928). As for the reference pressure used to calculate Cp, a pitot tube probe is placed in the domain at the midpoint of the inlet before the building at the height of $0.48\,m$. After running the validation model, the mean Cp and RMS Cp across the ridgeline are compared, as shown in Figure 4.5 (a) and (b), respectively. The validation model results show a good agreement between the reading of Cp in the wind tunnel and the numerical method utilized in this chapter. Mean Cp results showed an error of 6.91%, as for the RMS Cp, it demonstrated an error of 17.32%.

(a)

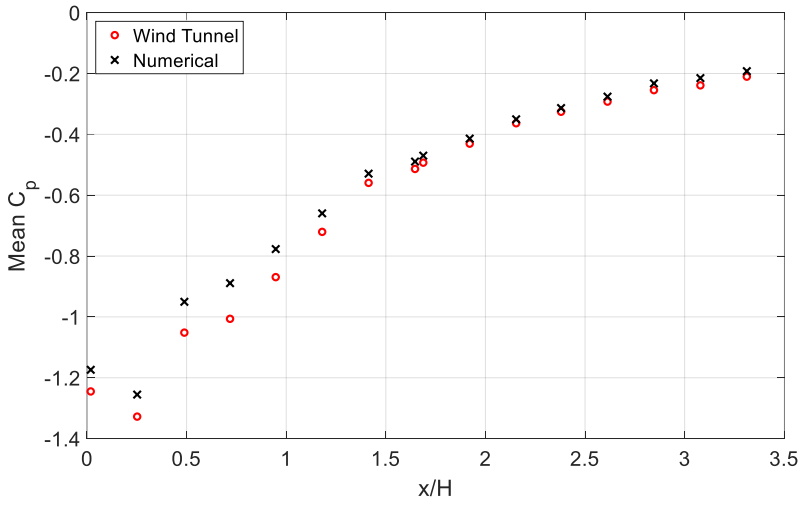

(b)

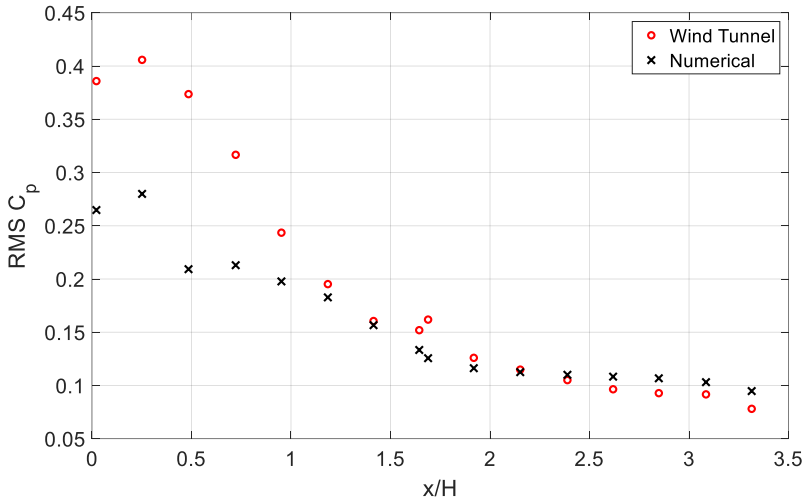

Figure 4.5 Comparison of (a) mean Cp and (b) RMS Cp using CFD and wind tunnel experimental testing

4.3 Case Study

This section utilizes the same physics adopted in the validation section to be used with a fishbone-like building layout of modular buildings adopted in Wuhan Thunder God Mountain hospital as discussed by (L. K. Chen et al., 2021) to obtain forces developed on their surfaces. Results can be further utilized to design different grades of modules to be adopted in the locations tested. Seven wind angles of attack are considered, which are $0°$,$15°$,$30°$,$45°$,$60°$,$75°$ and $90°$. Since multi modules building consists of single modules with a footprint of $3.0\ m\ \times\ 6.0\ m$ with $4.0\ m$ height as shown in Figure 4.6 (a), a fishbone layout is to be examined in CFD to determine the wind

forces developed on different surfaces distributed at select locations as shown in Figure 4.6 (b). Four corner modules, four internal modules, and six edge modules are examined.

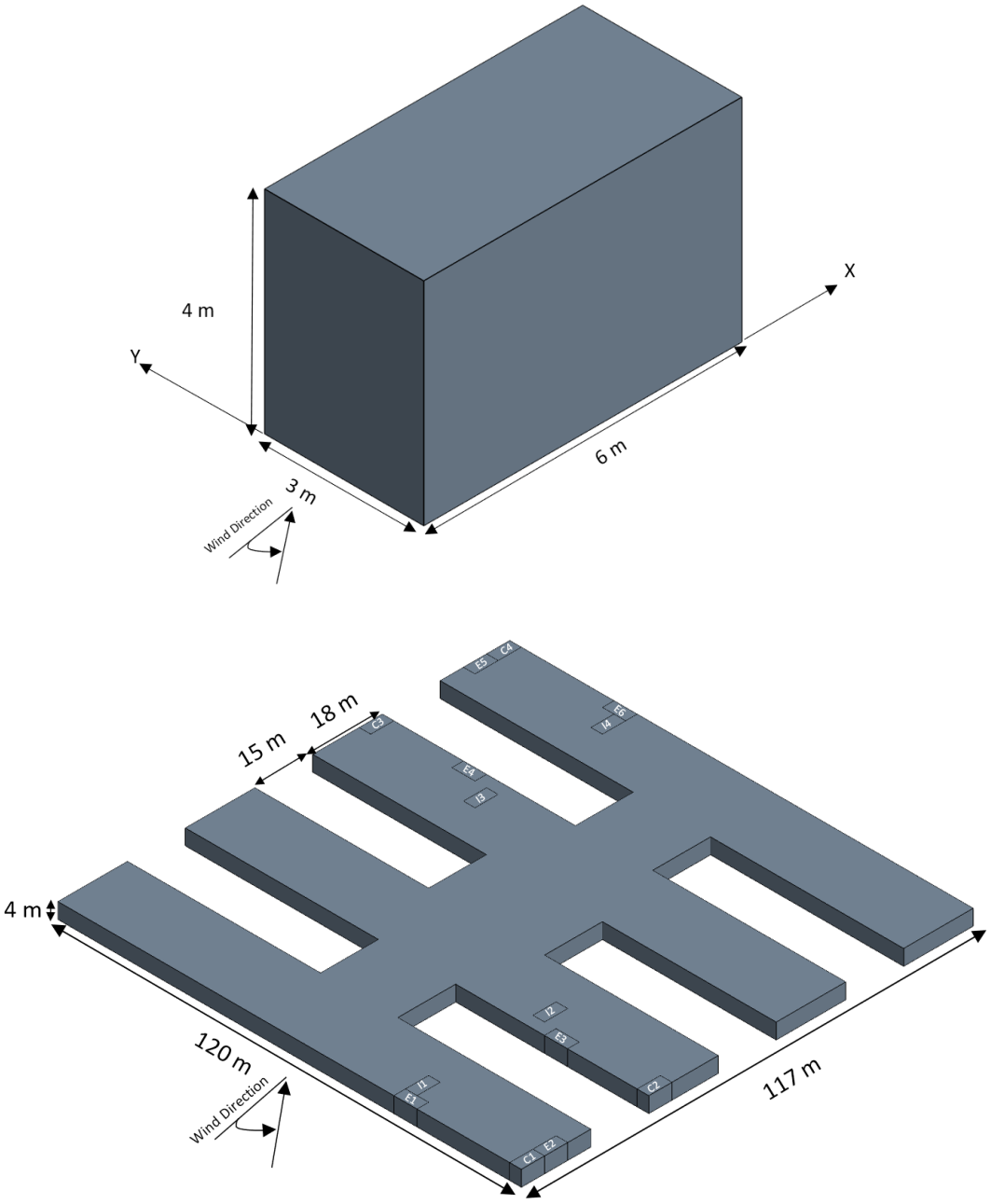

Figure 4.6 (a) Full-scale geometric details of a single module (b) full-scale geometric details of multi modules building

As for the computational domain for the multi modules building adopted in the numerical model, a rectangular block of size $3\,m \times 5\,m \times 0.5\,m$ is used to perform the simulation. The building is placed $0.8\,m$ away from the inlet, and data collection starts after $2{,}000$ time-step to ensure flow stabilization. The front wall is assigned as a velocity inlet, while the back wall is an outlet, the sides of the computational domain and the roof are assigned as symmetry plane, as for the ground, it is set as a no-slip wall, as shown in Figure 4.7.

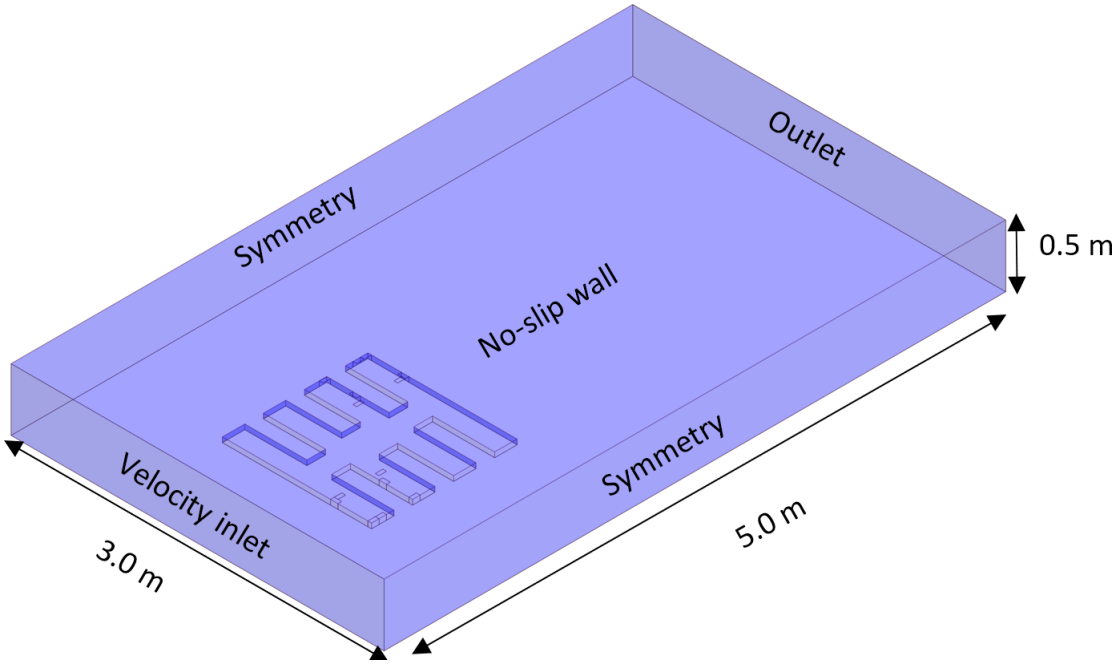

Figure 4.7 Computational domain and boundary conditions multi modules building

The computational domain of the multi modules building is discretized into three zones based on the hexahedral mesh cell. Zone 1 adopted a base mesh size of $50\,mm$, while zone 2, with dimensions of $1.9\,m \times 2.5\,m \times 0.3\,m$ adopted a mesh size of $30\,mm$. Zone 3 consists of the building itself with a mesh size of $2.5\,mm$ yielding 0.9 M cells, as shown in Figure 4.8. The simulation duration is 6 seconds, with a time-step of 0.25 milli-second, with three inner iterations, and a total of $24{,}000$ time steps. Data collection of forces starts after $2{,}000$ time steps to establish flow stabilization. The time-step is selected based on the velocity scale and the minimum cell size

to satisfy the Courant-Friederichs-Lewy (CFL) number below unity to ensure the solution convergence (Courant et al., 1928).

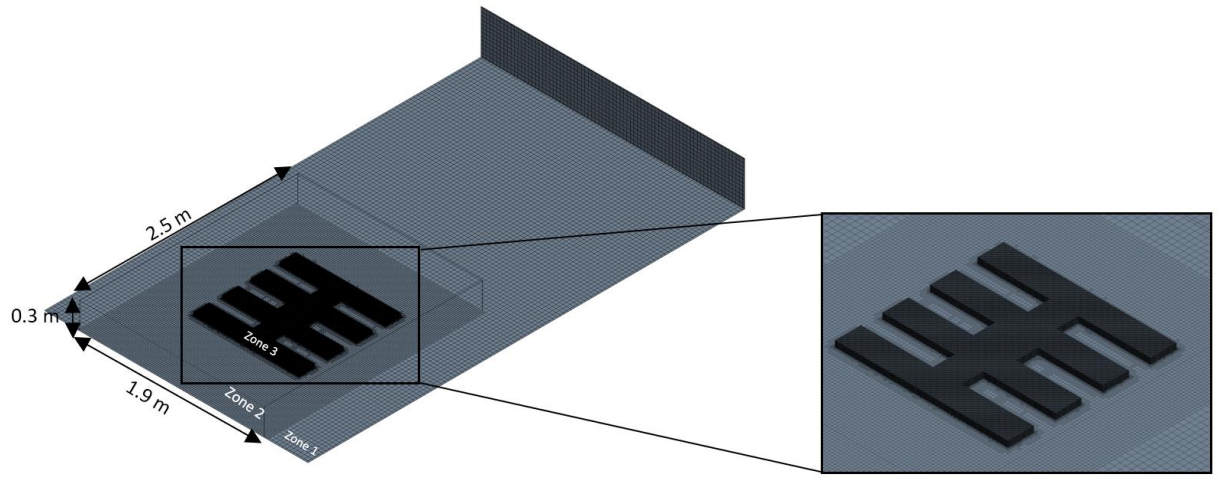

Figure 4.8 Mesh discretization of multi modules buildings

4.4 Results and Discussion

After running all the models, the force-time history of each module within the layout is extracted to find the critical forces developed on its surfaces. Since different wind angles of attacks are examined, the most critical force is selected as a peak design force for each direction (i.e., X, Y and Z). The X-direction is chosen to be in the longer span direction, while the Y-direction is in the shorter direction, as shown in Figure 4.6 (a). As for the wind angle of attack 0° and 90°, the force values are the resultant on those surfaces, thus making them the values experienced by the modules. Unlike when the wind angle of attack is 15°,30°,45°,60° and 75°, in these cases, the only force that can be utilized from the force-time history is the force in the Z-direction. As for the forces in the X-direction, and Y-direction, the resultant forces are found by resolving the forces reported in those directions. Force-time histories are reported in model-scale; to convert them to full-scale, forces are multiplied by a force scale of 160,000. Figure 4.9 shows a time history for module C4 in the X-direction from the wind angle of attack of 30° from 0.5 seconds to 6 seconds.

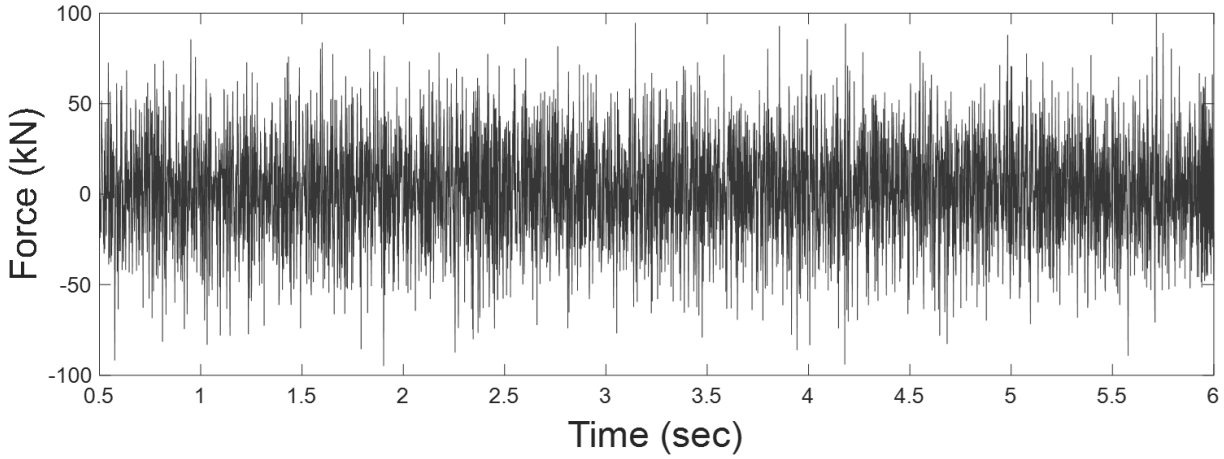

Figure 4.9 Force-time history of module C4 in the X-direction with a wind angle of attack of 30°

Since there are four corner modules, six edge modules, and four interior modules, the developed wind-induced loads are expected to be more critical in those corner and edge modules. As for the internal modules, the critical forces are expected to occur in the Z-direction. The results summarized in Figure 4.10 show the forces in the X, Y, and Z directions. To categorize the grades of the modules, a comparison between the corner modules is conducted to determine the most critical to be used at corner locations. As for the edge modules, forces developed on them are compared to the corner ones. The critical loads can be used at all edge locations in the layout. As for the internal ones, the only comparison is in the Z-direction to the corner and edge modules since they experience little to no force in the X and Y wind directions. Based on the results, corner modules experience higher forces in X and Y wind directions. This can be attributed to the larger area of flow separation corner modules experience. For example, module C4 experienced the most significant X-direction wind force of $100\ kN$ compared to the corner modules under all different wind angles of attacks. As for the most significant Y-direction wind force, it was developed on module C1 with a value of $103\ kN$. As for the Z-direction for the corner modules, the most significant force was experienced by module C4 with a value of $74\ kN$, and this is the largest Z-direction force experienced by any modules tested. As for the edge modules, the module that experienced the largest force in the X wind direction is module E2, with a value of $96\ kN$, which is 4% less than the largest force developed on corner modules. As for the Y-direction wind experienced by edge modules, the largest force developed on module E1 with a value of $93\ kN$,

which is 10% less than the largest force developed on corner modules. Based on these findings, modules located at corners can be further reinforced against the straining actions caused by increased surface exposure, as they experience the most critical forces in the X-wind and the Y-wind directions. As for the edge modules, they tend to experience weaker forces than corner modules due to having less exposure to wind pressure. Thus, their design forces can be reduced to reduce the material used. As for internal modules, their design can be reduced further since they experience critical forces in Z-direction mainly. These observations can be further investigated by examining a single module under wind load to obtain forces developed on its surfaces. They can then be compared to the different module locations to determine the impact of the location on the module's design force.

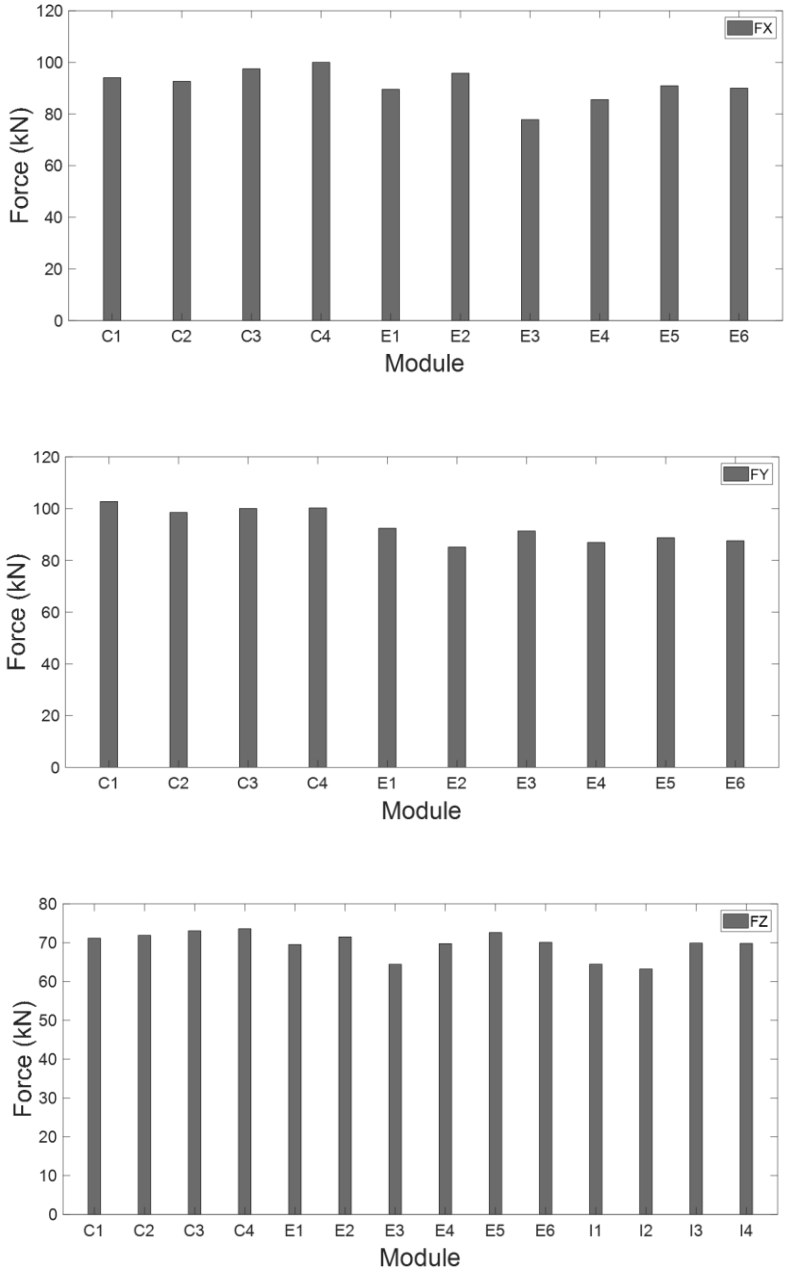

Figure 4.10 Forces developed on modules in a multi-module layout

4.5 Summary

The modular construction technique is an effective solution to the conventional construction challenges when it comes to healthcare space. There have been many studies concerning the structural optimization of the modular structure, but further studies are needed to investigate the impact of the lateral load (e.g., wind load) on modular structures. Based on the challenges proposed, a case study is conducted on a multi modules building with a fishbone layout, including seven wind angles of attack, to obtain force-time history acting on the modules' surfaces. Peak forces developed on surfaces are extracted to get the design forces. Based on the results, it is determined that corner modules experienced the largest peak forces in all wind directions (X, Y, and Z). Edge modules experienced 5% and 10% less force than the corner module in the X and Y direction, respectively. The results highlight the importance of obtaining peak forces on modular buildings since the pressure distribution can be hard to predict, especially within complex layouts, since the layout can consist of a large number of modules, thus highlighting the importance of categorizing the modules based on grades. The forces obtained can then be used to design modules with different grades based on the module location within the studied layout.

Chapter 5 Conclusion and Future Work

5.1 General

This thesis presented a summary of the past experiments and numerical research performed to investigate the different aspects of modular buildings for COVID-19. Through the literature review, gaps in the research are identified. It aims to provide comprehensive planning for the ventilation systems to be adopted in modular buildings for the use of healthcare systems, by investigating different ACH rates and ventilation system placements within a modular hospital room. In addition, the thesis examines different modules within a hospital layout examined to monitor forces developed on their surfaces. Six edge modules, four corner modules, and four internal modules were monitored to investigate how the module location impacts the load developed. The studies of these aspects are performed using CFD and were validated with experimental and wind tunnel tests.

5.2 Core Contributions

The outcome of this research work is expected to open the gate for further concern in the planning of modular structures for healthcare systems. The core contributions of this thesis are:

- Development of CFD models to match the behaviour of the spread of aerosols using Lagrangian models to simulate mouth-generated particles.
- Identifying different factors impacting the propagation of mouth-generated aerosols within a modular room.
- Development of a validated CFD model to predict wind loads developed on different modules within a fishbone layout.
- The use of different grades of modules based on their locations within the layout studied.

5.3 Conclusion

5.3.1 Propagation of Mouth-Generated Aerosols Within a Modular Hospital Room

This part of the thesis explored vital factors impacting the propagation of mouth-generated aerosols within a modular room to assess the ventilation system's performance. A modular room with a geometry of $6.1\,m$ long by $2.5\,m$ wide and $3.0\,m$ high, has been examined by using the Lagrangian model to inject aerosols in the domain to assess the ventilation system performance through two distinct parameters, the ventilation system rate, and the inlet and outlet placements. Based on the results, the following conclusions can be drawn:

- As the ACH rate increases, the ability to eliminate suspended aerosols also increases, which results in less viral load inhalation by room occupants. The rate at which particles were exiting through the outlet increased by 41% by increasing the ACH from 10 to 20. While increasing the rate to 40 ACH yielded a 137% increase in particles leaving the outlet compared to 10 ACH.

- It was found that continuous disinfection is necessary based on the accumulation of particles on different surfaces within the room. As aerosols landing on equipment almost reached 10%.

- The aerosol removal rate is highly dependent on the ACH rate and the flow field between the inlet and the outlet. As demonstrated by the different placements investigated in Chapter 3, where the best performing placement was when there was a direct flow field between the inlet and the outlet.

- Room geometry is a factor to consider when placing the inlet and the outlet as the destination between the inlet and the outlet increases, the aerosol removal rate decreases, which is attributed to the increased aerosol travel distance as demonstrated in Chapter 3, where the best performing configuration is when the inlet is located at the roof, and outlet on the sidewall (e.g., shorter path).

5.3.2 Wind Load Evaluation on a Modular Building

This part of the thesis highlights the variation of wind load intensities on modules within the modular structure's layout adopted from the literature. A fishbone layout was investigated to identify critical locations where load intensities vary, to quantify the loads, and provide quantitative results to further improve the design of the layout and the modules considered. Based on the results, the following main conclusions were found:

- Module location within a layout impacts the magnitudes of the developed wind loads. It was found that corner modules within the studied layout experienced the most significant wind loads in X, Y, and Z directions, highlighting the need to assess the layout performance and design according to the peak forces. As opposed to edge modules, which experienced 5% and 10% less force in the X and Y direction, respectively.

- With varying modules studied, the need to categorize the modules based on the wind load they experience is essential, especially when considering a large project that adopts a large number of modules.

- Categorizing the modules based on the load they experience can help reduce the materials used, thus reducing the structure's cost and making it more sustainable.

5.4 Recommendations for Future Works

This thesis aims to study the deployment of modular buildings to combat the COVID-19 crisis, highlighting the need to evaluate the ventilation systems and the wind loads they experience. Different methods can be used to assess these aspects, such as full-scale experimental testing (for the ventilation system) and wind tunnel tests (for the wind loads evaluation). The present research highlights different aspects impacting these parameters and suggests the need to focus on critical factors influencing them. With the different ACH rates studied, and the configurations of the ventilation systems, it was clear that they are the main factors impacting the translation of the mouth-generated aerosols within a modular room. As for the wind load evaluation, the main factor studied in this thesis is the layout of the modular building. The layout plays a critical role when it comes to the wind load distribution on the structure. Thus, the following recommendations are proposed for future work:

- The utilization of optimization techniques to optimize the ventilation system placement within a modular room, based on location and openings sizes.

- Further assessing the modular building ventilation performance to understand how to control the spread within a modular building by implementing specific measures (i.e., negative pressure systems).

- Implementing different physics models (i.e., particles break-up and fluid film formation) to accurately assess the viral load on various surfaces within the modular room, which requires further understanding of the COVID-19 virus.

- Assessing the potential source of the cough within the room to optimize the ventilation system further and account for various possible locations.

- Assessing different layouts to optimize the selection based on the geographical location and climate where the placement of the modular structure will take place.

- Considering the utilization of roof modifications (e.g., parapets) to alter the flow, to study their impact on load developed on modules.

- Considering a different structural design of modules (i.e., stacked).

References

Aboshosha, H., Elshaer, A., Bitsuamlak, G.T., El Damatty, A., 2015. Consistent inflow turbulence generator for LES evaluation of wind-induced responses for tall buildings. J. Wind Eng. Ind. Aerodyn. 142, 198–216. https://doi.org/10.1016/j.jweia.2015.04.004

Adamek, K., Vasan, N., Elshaer, A., English, E., Bitsuamlak, G., 2017. Pedestrian level wind assessment through city development: A study of the financial district in Toronto. Sustain. Cities Soc. 35, 178–190. https://doi.org/10.1016/j.scs.2017.06.004

Ahmadzadeh, M., Farokhi, E., Shams, M., 2020. Since January 2020 Elsevier has created a COVID-19 resource centre with free information in English and Mandarin on the novel coronavirus COVID- 19 . The COVID-19 resource centre is hosted on Elsevier Connect , the company ' s public news and information .

Aliabadi, A.A., 2013. Dispersion of Expiratory Airborne Droplets in a Model Single Patient Hospital Recovery Room with Stratified Ventilation.

Anghel, L., St, C., Sasc, R., Verdes, M., 2020. Impact of HVAC-Systems on the Dispersion of Infectious Aerosols in a Cardiac Intensive Care Unit.

Apuzzo, M., Kirkpatrick, D., 2020. Covid-19 Changed How the World Does Science, Together

Beggs, C.B., Kerr, K.G., Noakes, C.J., Hathway, E.A., Sleigh, P.A., 2008. The ventilation of multiple-bed hospital wards: Review and analysis. Am. J. Infect. Control 36, 250–259. https://doi.org/10.1016/j.ajic.2007.07.012

Bhattacharyya, S., Dey, K., Paul, A.R., Biswas, R., 2020. A novel CFD analysis to minimize the spread of COVID-19 virus in hospital isolation room. Chaos, Solitons and Fractals 139, 110294. https://doi.org/10.1016/j.chaos.2020.110294

Blocken, B., Malizia, F., van Druenen, T., Marchal, T., 2020. Towards aerodynamically equivalent COVID19 1.5 m social distancing for walking and running. Urban Phys. 11.

CDC, 2020. Interim clinical guidance for management of patients with confirmed coronavirus disease (COVID-19).

Center for Devices and Radiological Health, 2021. Medical Device Shortages During the COVID-19 Public Health Emergency

Chen, L.K., Yuan, R.P., Ji, X.J., Lu, X.Y., Xiao, J., Tao, J.B., Kang, X., Li, X., He, Z.H., Quan, S., Jiang, L.Z., 2021. Modular composite building in urgent emergency engineering projects: A case study of accelerated design and construction of Wuhan Thunder God Mountain/Leishenshan hospital to COVID-19 pandemic. Autom. Constr. 124. https://doi.org/10.1016/j.autcon.2021.103555

Chen, Z., Khan, K., Khan, A., Javed, K., Liu, J., 2021. Exploration of the multidirectional stability

and response of prefabricated volumetric modular steel structures. J. Constr. Steel Res. 184, 106826. https://doi.org/10.1016/j.jcsr.2021.106826

Courant, R., Friedrichs, K., Lewy, H., 1928. Über die partiellen Differenzengleichungen der mathematischen Physik. Kurt Otto Friedrichs 53–95. https://doi.org/10.1007/978-1-4612-5385-3_7

Curry, F., 1990. Isolation rooms. Filtr. Sep. 27, 164. https://doi.org/10.1016/0015-1882(90)80038-m

Elshaer, A., Aboshosha, H., Bitsuamlak, G., El Damatty, A., Dagnew, A., 2016. LES evaluation of wind-induced responses for an isolated and a surrounded tall building. Eng. Struct. 115, 179–195. https://doi.org/10.1016/j.engstruct.2016.02.026

Elshaer, A., Gairola, A., Adamek, K., Bitsuamlak, G., 2017. Variations in wind load on tall buildings due to urban development. Sustain. Cities Soc. 34, 264–277. https://doi.org/10.1016/j.scs.2017.06.008

Fifield, L.J., Lomas, K.J., Giridharan, R., Allinson, D., 2018. Hospital wards and modular construction: Summertime overheating and energy efficiency. Build. Environ. 141, 28–44. https://doi.org/10.1016/j.buildenv.2018.05.041

Gatheeshgar, P., Poologanathan, K., Gunalan, S., Shyha, I., Sherlock, P., Rajanayagam, H., Nagaratnam, B., 2021. Development of affordable steel-framed modular buildings for emergency situations (Covid-19). Structures 31, 862–875. https://doi.org/10.1016/j.istruc.2021.02.004

Gatheeshgar, P., Poologanathan, K., Gunalan, S., Tsavdaridis, K.D., Nagaratnam, B., Iacovidou, E., 2020. Optimised cold-formed steel beams in modular building applications. J. Build. Eng. 32. https://doi.org/10.1016/j.jobe.2020.101607

Gbadamosi, A.Q., Oyedele, L., Olawale, O., Abioye, S., 2020. Offsite Construction for Emergencies: A focus on Isolation Space Creation (ISC) measures for the COVID-19 pandemic. Prog. Disaster Sci. 8. https://doi.org/10.1016/j.pdisas.2020.100130

Godbole, S., Lam, N., Mafas, M., Fernando, S., Gad, E., Hashemi, J., 2018. Dynamic loading on a prefabricated modular unit of a building during road transportation. J. Build. Eng. 18, 260–269. https://doi.org/10.1016/j.jobe.2018.03.017

Government of Canada, 2022. Interactive data visualizations of COVID-19 [WWW Document]. URL https://health-infobase.canada.ca/covid-19/?stat=num&measure=total&map=pt#a2

Gupta, J.K., Lin, C.H., Chen, Q., 2009. Flow dynamics and characterization of a cough. Indoor Air 19, 517–525. https://doi.org/10.1111/j.1600-0668.2009.00619.x

Ho, E., Surry, D., Davenport, A.G., 1992. Low building load variability with applications to wind

codes. J. Wind Eng. Ind. Aerodyn. 43, 1814–1815. https://doi.org/10.1016/0167-6105(92)90597-4

Ho, T.C.E., Surry, D., Morrish, D., Kopp, G.A., 2005. The UWO contribution to the NIST aerodynamic database for wind loads on low buildings: Part 1. Archiving format and basic aerodynamic data. J. Wind Eng. Ind. Aerodyn. 93, 1–30. https://doi.org/10.1016/j.jweia.2004.07.006

Hwan Doh, J., Ho, N.M., Miller, D., Peters, T., Carlson, D., Lai, P., 2017. Steel Bracket Connection on Modular Buildings. J. Steel Struct. Constr. 02. https://doi.org/10.4172/2472-0437.1000121

Hyttinen, M., Rautio, A., Pasanen, P., Reponen, T., Earnest, G.S., Streifel, A., Kalliokoski, P., 2011. Airborne infection isolation rooms - A review of experimental studies. Indoor Built Environ. 20, 584–594. https://doi.org/10.1177/1420326X11409452

Innella, F., Arashpour, M., Bai, Y., 2019. Lean Methodologies and Techniques for Modular Construction: Chronological and Critical Review. J. Constr. Eng. Manag. 145, 04019076. https://doi.org/10.1061/(asce)co.1943-7862.0001712

Joerg, F., 2006. Recommendations of the COST action C14 on the use of CFD in predicting pedestrian wind environment. Fourth Int. Symp. Comput. Wind Eng. 529–532.

Kamali, M., Hewage, K., 2016. Life cycle performance of modular buildings: A critical review. Renew. Sustain. Energy Rev. 62, 1171–1183. https://doi.org/10.1016/j.rser.2016.05.031

Lacey, A., Chen, W., Hao, H., Bi, K., 2018. Numerical study of the structural response to wind loading: modular building case study. 13th Int. Conf. Steel, Sp. Compos. Struct. 1–10.

Lawson, P.M., Byfield, M.P., Popo-Ola, S.O., Grubb, P.J., 2008. Robustness of light steel frames and modular construction. Proc. Inst. Civ. Eng. Struct. Build. 161, 3–16. https://doi.org/10.1680/stbu.2008.161.1.3

Lindsley, W.G., Pearce, T.A., Hudnall, J.B., Davis, K.A., Davis, S.M., Fisher, M.A., Khakoo, R., Palmer, J.E., Clark, K.E., Celik, I., Coffey, C.C., Blachere, F.M., Beezhold, D.H., 2012. Quantity and size distribution of cough-generated aerosol particles produced by influenza patients during and after illness. J. Occup. Environ. Hyg. 9, 443–449. https://doi.org/10.1080/15459624.2012.684582

Lopez, D., Froese, T.M., 2016. Analysis of Costs and Benefits of Panelized and Modular Prefabricated Homes. Procedia Eng. 145, 1291–1297. https://doi.org/10.1016/j.proeng.2016.04.166

Ma, R., Xia, J., Chang, H., Xu, B., Zhang, L., 2021. Experimental and numerical investigation of mechanical properties on novel modular connections with superimposed beams. Eng. Struct. 232. https://doi.org/10.1016/j.engstruct.2021.111858

N.Usefi, Sharafi, P., Mortazavi, M., Ronagh, H., Samali, B., 2021. Structural performance and sustainability assessment of hybrid-cold formed modular steel frame. J. Build. Eng. 34. https://doi.org/10.1016/j.jobe.2020.101895

Peng, J., Hou, C., Shen, L., 2021. Numerical analysis of corner-supported composite modular buildings under wind actions. J. Constr. Steel Res. 187. https://doi.org/10.1016/j.jcsr.2021.106942

Ren, J., Wang, Y., Liu, Q., Liu, Y., 2021. Numerical Study of Three Ventilation Strategies in a prefabricated COVID-19 inpatient ward. Build. Environ. 188, 107467. https://doi.org/10.1016/j.buildenv.2020.107467

Ricci, M., Patruno, L., de Miranda, S., 2017. Wind loads and structural response: Benchmarking LES on a low-rise building. Eng. Struct. 144, 26–42. https://doi.org/10.1016/j.engstruct.2017.04.027

Rosin, P., Rammler, E., 1933. The laws of governing the fineness of powdered coal.

Shoukat, A., Wells, C.R., Langley, J.M., Singer, B.H., Galvani, A.P., Moghadas, S.M., 2020. Projecting demand for critical care beds during COVID-19 outbreaks in Canada. Cmaj 192, E489–E496. https://doi.org/10.1503/cmaj.200457

Smith, R.E., Timberlake, J., Smith, F., 2010. PREFAB ARCHITECTURE.

Suleiman, M., Elshaer, A., Billah, M., 2021a. COVID-19 MODULAR CONSTRUCTION.

Suleiman, M., Elshaer, A., Billah, M., Bassuony, M., 2021b. Propagation of mouth-generated aerosols in a modularly constructed hospital room. Sustain. 13. https://doi.org/10.3390/su132111968

Szczepanik-Scislo, N., Schnotale, J., 2020. An air terminal device with a changing geometry to improve indoor air quality for VAV ventilation systems. Energies 13. https://doi.org/10.3390/en13184947

Tamura, T., 2008. Towards practical use of LES in wind engineering. J. Wind Eng. Ind. Aerodyn. 96, 1451–1471. https://doi.org/10.1016/j.jweia.2008.02.034

Tominaga, Y., Stathopoulos, T., 2013. CFD simulation of near-field pollutant dispersion in the urban environment: A review of current modeling techniques. Atmos. Environ. 79, 716–730. https://doi.org/10.1016/j.atmosenv.2013.07.028

Wang, X., Su, P., Liu, J., Zhao, S., 2021. Seismic performance of ATLS modular house based on joint stiffness analysis. J. Constr. Steel Res. 183. https://doi.org/10.1016/j.jcsr.2021.106770

WHO, 2020. Coronavirus. URL https://www.who.int/health-topics/coronavirus#tab=tab_1

Zerndt, Z., 2017. The Clement Canopy, Singapore.

Zhang, B., Guo, G., Zhu, C., Ji, Z., Lin, C.H., 2020. Transport and trajectory of cough-induced bimodal aerosol in an air-conditioned space. Indoor Built Environ. https://doi.org/10.1177/1420326X20941166

Zhang, J.F., Zhao, J.J., Yang, D.Y., Deng, E.F., Wang, H., Pang, S.Y., Cai, L.M., Gao, S.C., 2020. Mechanical-property tests on assembled-type light steel modular house. J. Constr. Steel Res. 168. https://doi.org/10.1016/j.jcsr.2020.105981

Zhang, Z., Pan, W., Zheng, Z., 2020. Fighting Covid-19 through fast delivery of a modular quarantine camp with smart construction. Proc. Inst. Civ. Eng. Civ. Eng. 174, 89–96. https://doi.org/10.1680/jcien.20.00025

Zhou, M., Su, X., Chen, Y., An, L., 2020. Rapid construction and advanced technology for a Covid-19 field hospital in Wuhan, China. Proc. Inst. Civ. Eng. Civ. Eng. 174, 29–34. https://doi.org/10.1680/jcien.20.00024

Zhu, S.W., Kato, S., Yang, J.H., 2006. Study on transport characteristics of saliva droplets produced by coughing in a calm indoor environment. Build. Environ. 41, 1691–1702. https://doi.org/10.1016/j.buildenv.2005.06.024